Moment capacity of cold-formed stainless steel channel sections with edge-stiffened web holes, unstiffened web holes and plain webs

Vivekanandan Sivaji

A thesis submitted in fulfilment of the requirements

for the degree of Master of Engineering

Supervised by

Dr Zhiyuan (Arthur) Fang, Dr Krishanu Roy and Prof James Lim

School of Engineering

The University of Waikato

New Zealand

THE UNIVERSITY OF
WAIKATO
Te Whare Wānanga o Waikato

2024

ABSTRACT

Stainless steels exhibit a unique combination of high corrosion resistance and excellent mechanical properties for structural applications like channel sections, angles, and hollow pipes that have been used for construction projects over the past few decades.

Recently, cold-formed stainless steel (CFSS) channel sections with edge-stiffened web holes as flexural members have been developed and widely used in the building industry for simplifying the installation of plumbing and electrical services. Previous research has shown that edge-stiffened web holes are about as strong as plain webs when it comes to moment capacity for cold-formed steel (CFS) channel sections. However, there is a notable lack of research on CFSS channel sections. This paper aims to address this gap by presenting a comprehensive numerical investigation.

A nonlinear elasto-plastic finite element (FE) model was developed and validated against test results from Chen et al. [2]. The developed FE models demonstrated reasonable agreement in terms of moment capacity, load-displacement curves, and failure behaviour.

A total of 888 finite element analyses (FEA) were conducted on the moment capacity of CFSS channel sections with plain webs, unstiffened web holes, and edge-stiffened web holes. The material properties of stainless-steel types, namely EN 1.4509 (ferritic), EN 1.4462 (duplex), and EN 1.4301 (austenitic), were obtained from the literature. Subsequently, a parametric study was conducted to investigate the effects of number of holes, web depth, hole diameter, and stiffener length on the moment capacity of CFSS channel sections.

To evaluate the performance and accuracy of current design guidelines, the FE results were compared against the design capacities predicted by the current design guidelines of the American Iron and Steel Institute (AISI 2016) and Australia/New Zealand (AS/NZ 2018). The comparison results show that the design capacities predicted by AISI (2016) and AS/NZS (2018) are conservative by 4.5% on average for edge-stiffened web holes and unreliable for calculating the capacity of CFSS channel sections. Consequently, new reduction factor design equations were proposed to predict the moment

capacity of CFSS channel sections with unstiffened and edge-stiffened web holes. Finally, a reliability analysis was conducted to ensure that the proposed equations could be reliable.

Keywords: Cold formed stainless steel, edge-stiffened web holes, finite-element model, parametric study, proposed design equation

PREFACE

This thesis is submitted to the University of Waikato, New Zealand, in fulfilment of the requirement for the master's degree in civil engineering. The work contained in this thesis has not been previously submitted for a degree or diploma at any other higher educational institution. To the best of my knowledge and belief, the thesis contains no material previously published or written by another person except where due reference is made.

ACKNOWLEDGEMENTS

Firstly, my sincere thanks to my main supervisor, Dr. Zhiyuan (Arthur) Fang, co-supervisors Dr. Krishanu Roy, and Professor James B.P. Lim, for their unwavering support throughout my research, whose constant guidance and contributions were integral to the successful submission of my journal papers, making me an independent researcher.

Heartfelt gratitude goes to Bikram Paul, Dinesh Lakshmanan Chandramohan and Kushal Gosh for their continuous support. I extend my sincere thanks to my well-wishers in New Zealand for shaping my thesis with invaluable encouragement.

I express my appreciation to my best friends in New Zealand, Shubham Tiwari, Gagan Sengundham Dinesh and Gowrava Mohanswamy for their year-round support. Special thanks to the University of Waikato, School of Engineering, for providing computing machines and research assistance.

Finally, I want to express my gratitude to my family, my father Sivaji S, my mother Jayanthi S and my fiancée Priya T for their unwavering support to pursue my masters.

TABLE OF CONTENTS

LIST OF FIGURES

LIST OF TABLES

CHAPTER 1. Introduction

1.1 General

Cold-formed stainless steel (CFSS) is an exceptionally strong and versatile material used in construction. It has characteristics such as ductility, impact resistance and formability and is suitable for use in a wide variety of architectural and structural applications [1]. The use of CFSS has emerged as a compelling material in the field of structural engineering, blending the cost-effectiveness and versatility of cold-formed steel with the exceptional properties of stainless steel. This combination offers a unique set of advantages, including corrosion resistance, durability, and aesthetic appeal, making CFSS a promising candidate for a wide range of structural applications. CFSS channel sections are often manufactured with web holes for the installation of building services, such as plumbing, electrical, and heating systems, in the walls and ceilings. It should be noted that traditional holes are normally flat punched without edge lips (i.e., with an unstiffened web hole), but here's the challenge that these web holes, in their typical form, aren't as strong as they are without web holes. The presence of web holes in CFSS channel sections will result in changes in the distribution of stress and consequently, there will be changes in the buckling characteristics and ultimate strength. To make these structures stronger, engineers have thought about reinforcing these web holes along the edges. The web holes are strengthened through a continuous lip around the perimeter of the hole (i.e., with an edge-stiffened web hole) [2]. The new design allows oversize web holes to be formed on the web and at the same time, the CFSS channel sections still provide satisfactory strength and performance. However, there is no research on CFSS channel sections with edge-stiffened web holes.

This study explores the flexural behavior of CFSS channel sections with plain webs, unstiffened web holes and edge-stiffened web holes. This study uses material properties for stainless-steel types EN 1.4509 (ferritic), EN 1.4462 (duplex), and EN 1.4301 (austenitic), obtained from the literature [3-6]. Two channel cross sections were considered, sections C200 and C300 [5]. All web holes have nominal diameters (a) as a ratio of hole depth to web depth, i.e., = 0.2, 0.4, and 0.6 and the

holes are placed at the mid-height of the sections. The nominal length of the edge-stiffener (q) is fixed at 5 mm, 7 mm, and 10 mm. However, there is no study reported in the literature to determine the moment capacity of CFSS channel sections. Furthermore, the American Society of Civil Engineers (ASCE) [7] does not offer guidelines for determining the moment capacity of CFSS channel sections with edge-stiffened web holes.

Figure 1-1 Structural stainless steel at Gent Sint Pieters railway station in Belgium. Photo: Patrick Lints [8].

Figure 1-2 Cold-formed steel sections as the primary load-carrying members [9].

Figure 1-3: The use of CFS members in the construction of buildings [10].

1.2 Manufacturing process

Cold-formed stainless-steel members are commonly manufactured using the cold-forming or cold-rolling technique. Cold forming is the process of shaping metal at a temperature that is lower than its recrystallization temperature, often done at room temperature. This procedure is often used for the production of various stainless-steel profiles, such as channels, angles, tubes, and other structural shapes, which is quite different from HRS members. For CFSS channel sections, web holes for the installation of services are punched at predetermined positions, which reduces the installation time. As shown in Figure 1–4, the manufacturing process involves forming the material by either press-braking or cold-roll forming to obtain the required shape [4].

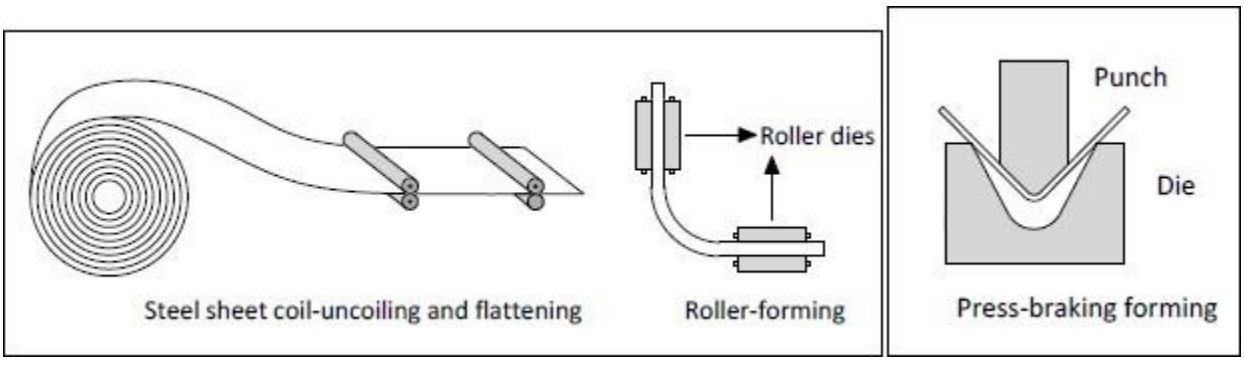

Figure 1-4: CFSS members manufacturing process [11].

1.3 Application of CFSS channel sections in building constructions

In recent years, the use of edge-stiffened holes in the webs of cold-formed steel channels (CFS) has become common in New Zealand to simplify the installation of plumbing and electrical services. CFSS channel sections are extensively used in various industries and construction projects due to their distinctive features and benefits. In building construction, they are integral for floor framing, roof systems, and wall studs due to their outstanding strength, corrosion resistance, and adaptability for various structural components. CFSS channel members are also used in many industries, such as infrastructure projects, including bridges, walkways and support structures for various installations, such as solar panel frames, equipment mounts, and platforms. Also used in architectural applications for creating aesthetically pleasing and structurally sound elements such as handrails, facades, and decorative trims. Transportation industrial applications like trailer frames, truck bodies, and railcar components. Also used in the energy sector for supporting components in power plants, as well as in the construction of wind turbine towers and solar panel structures. Due to their corrosion resistance, CFSS channel sections are employed in marine and offshore structures, including shipbuilding, offshore platforms, and port facilities. The stainless steel's ability to withstand saltwater exposure is a key advantage in these applications. CFSS channel sections are widely used in numerous industries due to their versatility, strength, and corrosion resistance, making them a popular choice for a diverse range of applications.

Two recent examples of structures that make substantial use of cold-formed stainless steel tubular elements are the Regents Place Pavilion in London [12] and the Helix Bridge in Singapore [13]. Figure 1–5 shows the Regents Place Pavilion in London, UK, which opened to the public in 2009. The structure is made entirely of stainless steel, featuring 258 cold-formed rectangular hollow section columns, each 7.8 m long, supporting a roof plane. The 50 × 50 × 4 hollow sections are made of austenitic stainless-steel grade EN 1.4404. Figure 1–6 show the Helix pedestrian bridge in Marina Bay, Singapore, which was opened to the public in 2010. It is the world’s first double helix pedestrian

bridge, where two helices made of duplex stainless steel hollow sections spiral around each other to form the shell of the 280 m structures.

Figure 1-5 The Regents Place Pavilion [12].

Figure 1-6 The Helix pedestrian bridge [13].

Figure 1-7: Photo of CFS channel beams with edge-stiffened web holes in CFS concrete flooring system [10].

CHAPTER 2. Literature review

2.1 Introductory remarks

This chapter presents an extensive literature review on the behaviour of CFS and CFSS channel sections with edge-stiffened web holes, un-stiffened web holes, and plain webs, under different loading conditions such as bending, shear, and web crippling. The literature review comprises two primary components. No research has been found in the literature investigating that moment capacity of CFSS channel sections with edge-stiffened web holes.

2.2 Research on the CFSS channel sections

This chapter presents an extensive literature review on the behavior of CFS and CFSS channel sections with edge-stiffened web holes, un-stiffened web holes, and plain webs under different loading conditions such as bending, shear, and web crippling. The literature review comprises two primary components. No research has been found in the literature investigating the moment capacity of CFSS channel sections with edge-stiffened web holes.

The literature review on the structural behavior of CFSS channel sections provides a comprehensive overview of key studies conducted by various researchers. The study conducted by Yousefi et al. [1] primarily focuses on the web crippling failure of these specific cold-formed ferritic stainless steel sections with offset web holes and fastened flanges, providing a unified set of design equations. A total of 18 experimental tests and a parametric study including a total of 576 FE models results were reported. The experimental and FE results are compared against strengths predicted in accordance with the American Iron and Steel Institute (AISI) [14] and Australia and New Zealand Standard (AZ/NZS) [15] for cold-formed carbon steel plain-lipped channel sections, as well as the equations proposed by the previous researchers for stainless steel plain-lipped channel sections. It was found that design equations are unreliable and unconservative by 22% for cold-formed ferritic stainless steel unlipped channel sections. Therefore, based on the results of this study, two new reliable web crippling strength reduction factor equations were proposed.

(a) IOF Loading (b) EOF Loading

(c) ITF Loading (d) ETF Loading

Figure 2-1: Experimental setup used by Yousefi et al. [1] to conduct web crippling failure of cold-formed ferritic stainless steel channel sections.

Yousefi et al. [16] conducted a combination of experimental and FE analyses to investigate the web crippling strength of cold-formed ferritic stainless steel unlipped channel sections with fastened flanges under the end-two-flange loading condition. A total of 27 web crippling tests were presented: 9 tests conducted on channel sections without web holes and 18 tests conducted on channel sections with web holes. When conducting tests with web holes, the holes were located either at the centre or offset from the load and reaction plates. A parametric study was conducted using quasi-static finite element analysis. The strengths obtained from reduction factor equations are first

compared to those calculated from equations recently proposed for cold-formed stainless steel, which were unconservative by 10%, and the experimental investigation also shows that, for the case of unlipped channels without web holes, the European Standard (EN 1993-1-4) [17] and ASCE [7] are too conservative by 43% and 28%, respectively. So, based on the experimental and FE results, web crippling design equations are proposed for both sections, with and without web holes.

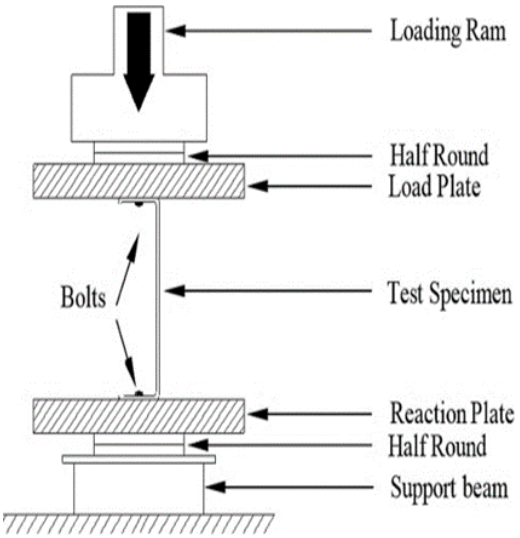

(a) Schematic end view of test set-up

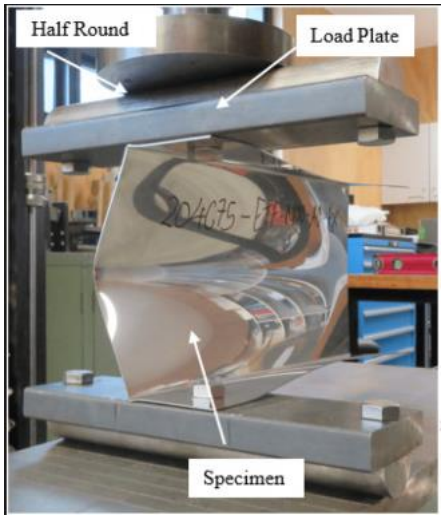

(b) Plain section

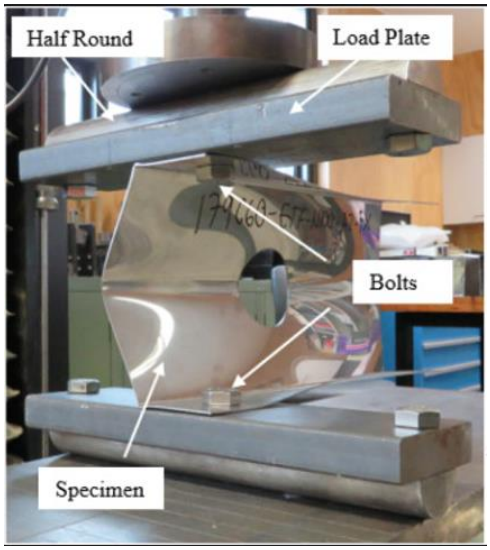

(c) Unstiffened web hole located at the centre of the span

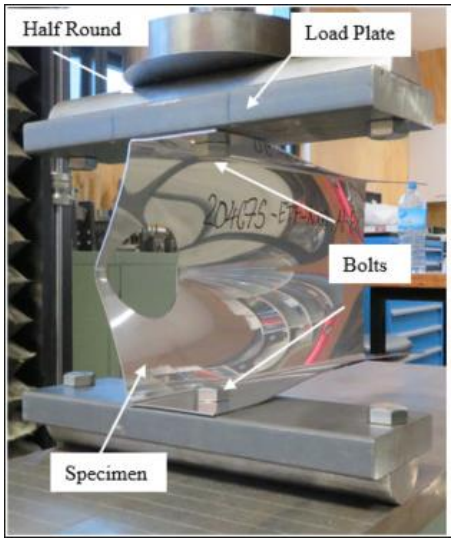

(d) Unstiffened web hole located at the offset to the reaction plates

Figure 2-2: Experimental test by Yousefi et al. [16] to investigate web crippling strength of cold-formed ferritic stainless steel unlipped channel sections under ETF Loading condition.

Yousefi et al. [3] also conducted a numerical investigation on the web crippling strength of cold-formed stainless steel lipped channel sections with web openings subjected to interior-one-flange loading conditions. A parametric study of 2218 was reported in the literature. Web holes were located at the centre beneath the bearing load. Three grades of stainless steel were considered: duplex EN1.4462, austenitic EN1.4404 and ferretic EN1.4003. Channel depths of 142 mm, 202 mm and 302 mm were chosen. Thickness of 1.27mm, 4.0 mm and 6.0 mm. Hole depth ratios of 0.2, 0.4, 0.6 and 0.8 were set as the parameters for the parametric study. To account for the influence of the circular web openings, strength reduction factor equations were determined and compared to recent equations proposed for cold-formed carbon steel. It was observed that for duplex grade, strength reduction factors are conservative by 2% and for austenitic and ferritic grades by around 9%. New web crippling strength reduction factor equations were proposed for both cases of flanges unfastened and flanges fastened to the bearing plates.

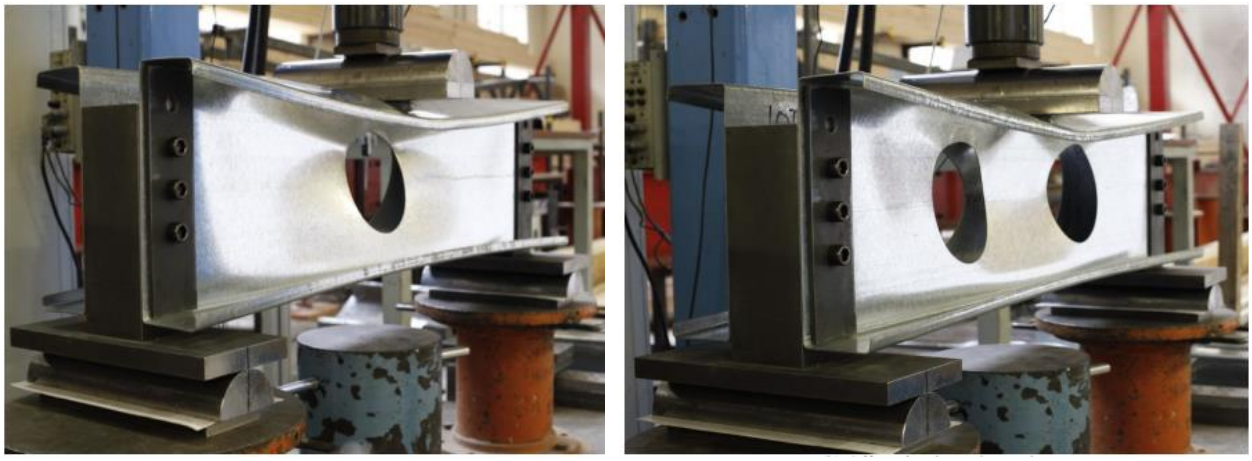

(a) Centred circular web opening (b) Offset circular web opening

Figure 2-3: Experimental of cold formed stainless steel lipped channel-sections under interior-one-flange (IOF) loading condition by Yousefi et al. [3].

Fang et al. [5] presented a finite element analysis on the web crippling strength of cold-formed stainless steel channel sections with circular web holes, subjected to end-one-flange loading conditions. Three grades of stainless steel, EN 1.4509 (ferritic), EN 1.4462 (duplex), and EN 1.4301 (austenitic), were considered. A total of 1728 FE models were performed. In the investigation, the

parameters that were chosen and varied were as follows: The depth of the web (b_w) ranged from 100 mm to 300 mm; the ratio of flange width to web height (b_f/b_w) ranged from 0.2 to 0.5; the ratio of lip width to flange width (b_l/b_f) ranged from 0.4 to 0.6; the ratio of hole diameter to web flat depth (a/h) ranged from 0.2 to 0.8; the ratio of hole distance to web flat depth (x/h) ranged from 0.04 to 0.98; and the ratio of bearing length to web flat depth (N/h) ranged from 0.17 to 1.14. The results of the parametric study were used to propose new web crippling strength equations and strength reduction factor equations that outperformed the equations of the ASCE [7], AISI [14], and the AS/NZS [15].

In the realm of shear behavior Yousefi et al. [6] conducted an experimental and numerical investigation for cold-formed ferritic stainless-steel channel sections with circular web holes. A total of 21 shear tests on pair channel sections loaded at mid-length with a span aspect ratio of 1.0 are presented. Web holes are placed either at the centre, mid-span, or offset from the applied load. The FE models were developed and validated against the experimental test results. The FE models are used for a parametric study to extend the test results for different web thicknesses (t) between 1.5 and 2.0 mm and the channel clear height to thickness ratios (h/t) are from 86.05 to 167.63. The channels were of three different cross-section heights: C175, C200, and C250. Although there are no specific guidelines regarding shear strength reduction factors for stainless steel and only the North American specifications AISI [14] and AS/NZS [15] for carbon steel members provide two equations for channels with centred openings, such equations are found to be unreliable and unconservative for ferritic stainless steel channel sections by 20%. Based on both experimental and numerical results, new reliable design equations in the form of shear strength reduction factors are proposed.

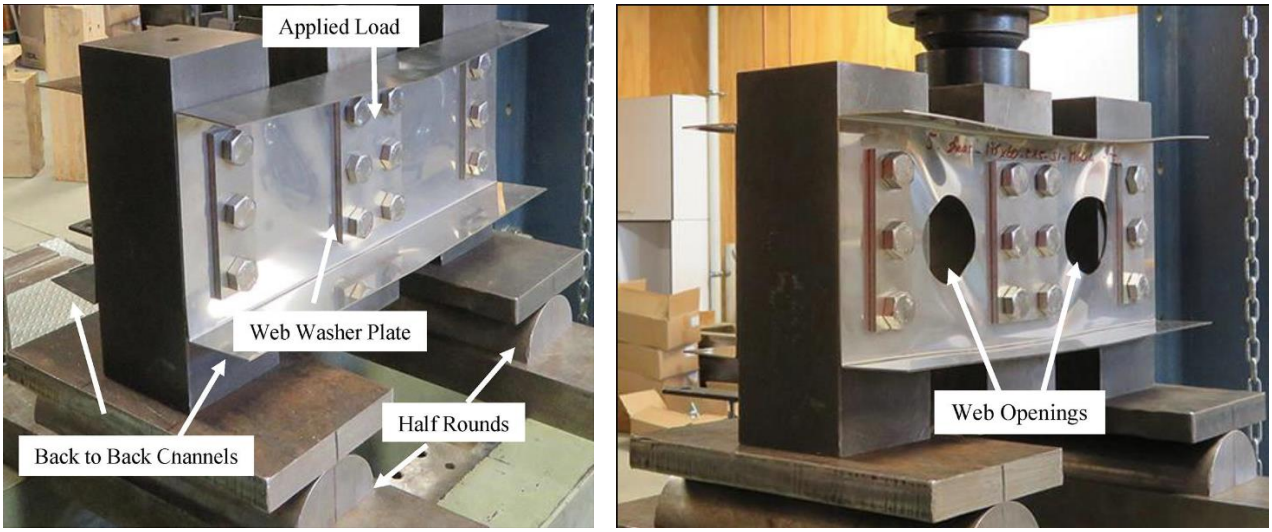

(a) Plain section (b) Centred circular web opening

Figure 2-4: Experimental analysis by Yousefi et al. [6] of cold-formed ferritic stainless steel under shear behavior.

Ishqy et al. [18] conducted a numerical investigation to determine the shear behavior of cold-formed stainless steel LCB sections with unstiffened circular web holes. A total of 180 FEA models were developed and a parametric study was carried out with austenitic and duplex types of stainless steel grades. Nine web hole depth to clear web height ratios (d_{wh}/d_1) ranging from 0.1 to 0.85 were considered. The FEA results were compared with the design rules presented in AS/NZS [15] for CFS design standards, which are either conservative or unsafe to use for the CFSS LCBs with circular openings. Therefore, three sets of equations with different approaches to predict the shear capacity of CFSS LCBs with circular web openings were proposed.

2.3 Research on the CFS channel sections

Several studies in the literature have investigated the structural behavior of CFS channel sections. The current study can benefit from the significant insights provided by the existing research on the moment capacity of cold-formed steel (CFS) channel sections. Boshan Chen [9] conducted a combination of both experimental and numerical analysis on the moment capacity of cold-formed channel beams with edge-stiffened web holes, un-stiffened web holes and plain webs. A total of 215 results, comprising 16 four-point bending tests and 199 FEA were reported. A parametric study was

conducted using the validated FE model to investigate the effects of beam length, hole diameter, stiffener length and fillet radius. It was found that in the case of a channel beam with five edge-stiffened web holes, the moment capacity increased by as much as 14.5% compared to that of a plain channel beam. For comparison, the same section with unstiffened web holes had a 13.6% reduction in moment capacity. Furthermore, the accuracy of current design guidelines in accordance with the AISI [14] and AS/NZS [15] standards was verified by comparing the tests and FEA results against the design strengths for moment capacity of CFS channel beams without web holes and it was found that the AISI [14] and AS/NZS [15] can closely predict the moment capacity of CFS channel beams without web holes. On the other hand, for CFS channel beams with web holes were compared against the moment capacity calculated from the design equations of Moen and Schafer [19]. The Moen and Schafer [19] design equations were found to be over-conservative by around 11% and 28% for the moment capacity of CFS channel beams with un-stiffened and edge-stiffened web holes, respectively.

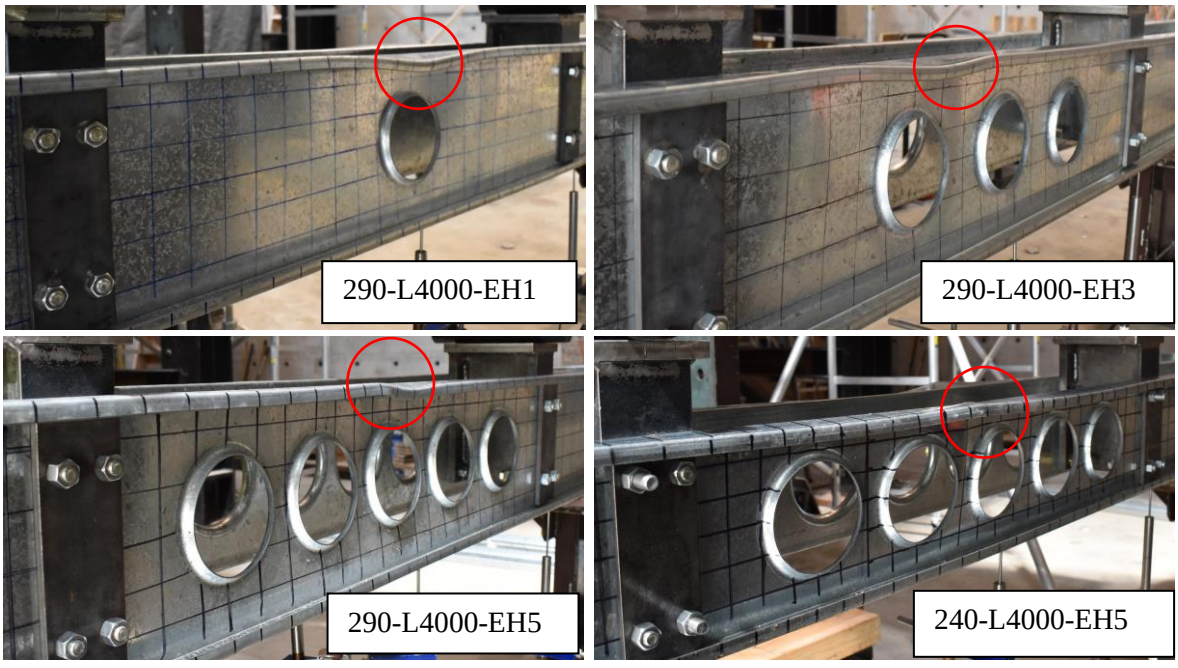

(a) Edge stiffened web holes

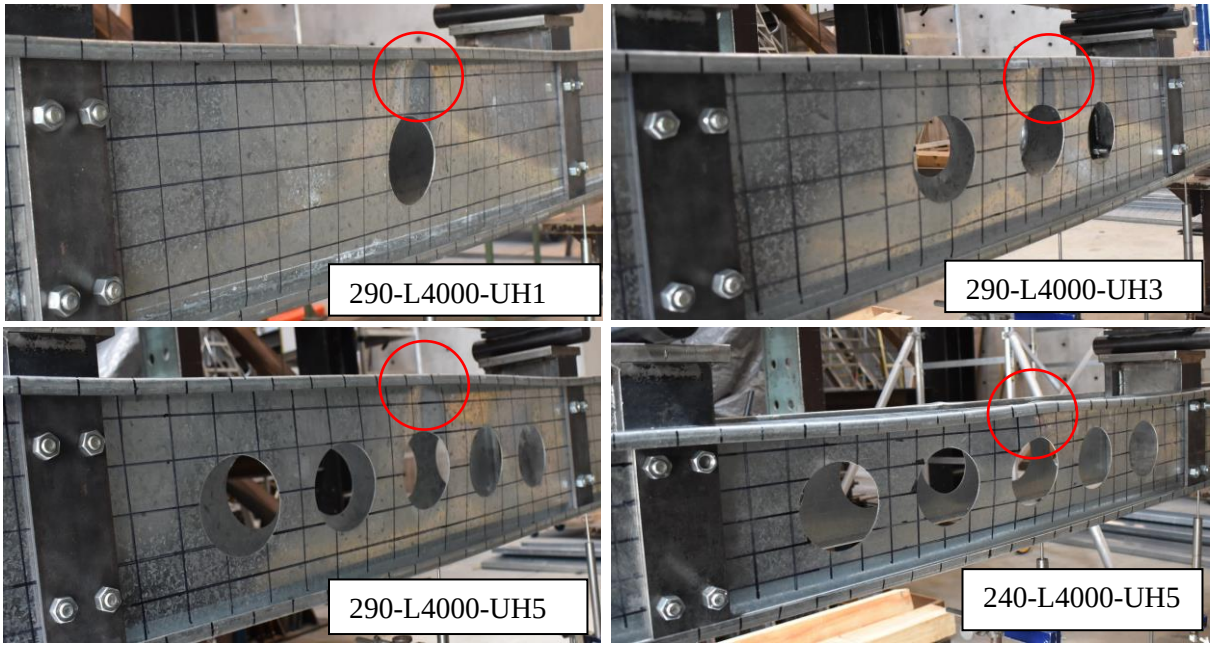

(b) Unstiffened web holes

Figure 2-5 Failure modes of CFS channel beams with holes under bending.

Researchers Moen et al. [19, 20], Zhao et al. [21], Yu et al. [22, 23], and Thirunavukarsu et al. [24] conducted both experimental and numerical studies. They proposed an approach based on the Direct Strength Method (DSM) to develop equations for determining the moment capacity. Their studies contribute foundational knowledge on the structural behavior of CFS channel sections with unstiffened circular web holes. Moreover, Degtyareva et al. [25, 26] expanded the scope of their research by investigating the influence of unstiffened slotted web holes on the moment capacity of CFS channel sections. Their work provides additional insights into the effects of different types of web holes on the structural performance of CFS channels.

While the literature comprehensively addresses CFS channel sections with unstiffened circular web holes. However, there is a significant lack of study on sections with edge-stiffened circular web holes under four-point bending. Chen et al. [27], Yu et al. [28], and Dai et al. [29] have contributed to this area by investigating the effect of edge-stiffened circular web holes through a combination of experimental and numerical methods. Notably, their findings indicate an enhanced moment capacity when compared to plain webs.

In addition, some studies investigated the effect of unstiffened and edge-stiffened circular web holes on CFS channel sections under shear [30–33], compression [34–38] and web crippling [39, 40]. However, despite the wealth of research on CFS channel sections with various types of web holes. The moment capacity and behavior of Cold-Formed Stainless Steel (CFSS) channel sections with both edge-stiffened and unstiffened web holes remain unexplored in the literature. This constitutes a critical research gap that the current thesis aims to address.

2.4 Aim and scope of this research.

The objective of this thesis is to investigate the capacity of CFSS channel sections with edge-stiffened web holes subjected to bending. The investigation will be performed based on the finite element analysis. Specific objectives of this work are listed below:

1. To establish nonlinear finite-element (FE) models to simulate the structural behavior of CFSS channel sections subjected to bending. The measured cross-section dimensions, material properties obtained from the literatures and geometric imperfections were also included in the FE models. The FE models will then be validated against the results obtained from the tests conducted by Chen et al. in terms of deformed shapes, moment capacity and stress-strain curves.
2. The validated FE models will be used to perform a parametric study involving 888 FE models to investigate the influence of different parameters on the capacity of such CFSS channel sections with edge-stiffened web holes under bending.
3. To evaluate the performance of current design guidelines while predicting the capacity of CFS channel sections with edge-stiffened web holes, FEA results will be compared against the design strengths predicted by the current design guidelines, such as AISI (2016) and AS/NZS (2018).
4. Based on the results obtained from the parametric study, suitable design reduction factor equations will be proposed for calculating the capacity of CSFS channel sections with edge-

stiffened web holes. A reliability analysis will also be carried out to evaluate the accuracy and reliability of the proposed reduction factor equations.

2.5 Outline of the thesis

This thesis is focused on the capacity of CFSS channel sections with edge-stiffened web holes subjected to bending. The thesis is structured into the following six chapters:

Chapter 1 Briefly introduces the background, problem statement, and outline of the thesis.

Chapter 2 Summaries the literature review on the behavior and design of both CFSS and CFS channel sections including the case channel sections with edge-stiffened web holes, un-stiffened web holes, and plain webs subjected to web crippling, bending, and shear.

Chapter 3 Describes the finite element modelling.

Chapter 4 Describes the numerical analysis work conducted in this study to assess the moment capacity of CFSS channel sections with edge-stiffened web holes, un-stiffened web holes, and plain webs.

Chapter 5 Provides Design recommendations in accordance with the American Iron and Steel Institute (AISI) [14] and Australia and New Zealand Standard (AZ/NZS) [15].

Chapter 6 Describes the proposed design reduction factor equation and the reliability of the proposed reduction factor equations for CFSS channel sections with unstiffened and edge-stiffened web holes.

Chapter 7 Provides conclusions including the limitations of the current study and recommendations for future researchers and practicing engineers.

CHAPTER 3. Description of finite element modelling

3.1 General

The moment capacity of CFSS channel sections, both with and without web holes, including edge-stiffened and un-stiffened configurations, was determined using a numerical model developed with finite element analysis (FEA) software in the ABAQUS manual [41]. The FE model developed in this study could closely predict the moment capacity of CFSS channel sections. In the finite element model, the centre line dimensions and non-linear material properties of the CFSS channel sections were used. Detailed modelling techniques are discussed in detail below.

3.2 Summary of experimental tests done by Chen et al. [9]

In their experimental investigation, Chen et al. [9] conducted tests on CFS channel sections featuring plain webs as well as those with unstiffened and edge-stiffened web holes. This study considered different parameters on their sections, such as web depths, web hole sizes, number of holes and stiffener length under four-point bending. The modelling techniques used by Chen et al. [9] were used to develop the FE model and the experimental results by Chen et al. [9] were used to validate the FE models of CFSS channel sections with plain webs, unstiffened web holes and edge-stiffened web holes. More details of the experimental setup and test results can be found in the literature [9].

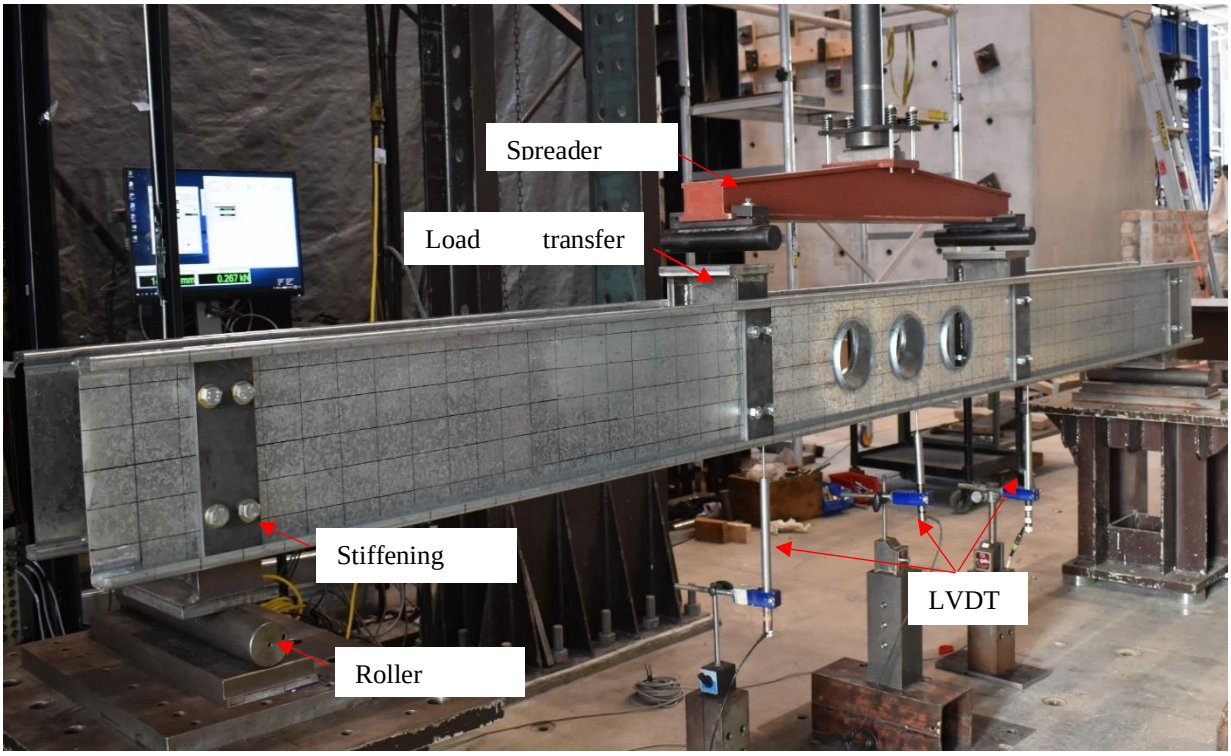

(a) Overall view of loading rig

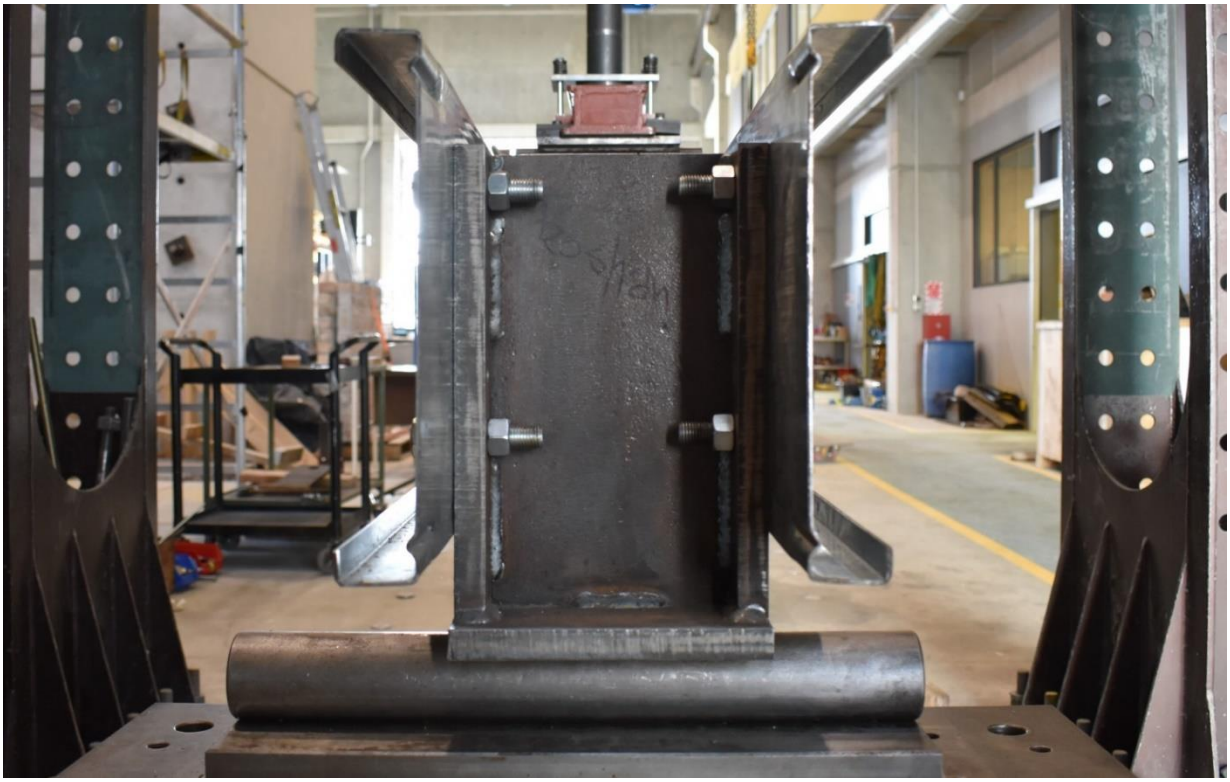

(b) Side view of loading rig

Figure 3-1: Experimental test conducted by Chen et al. [2] to determine the moment capacity of cold formed steel channel sections.

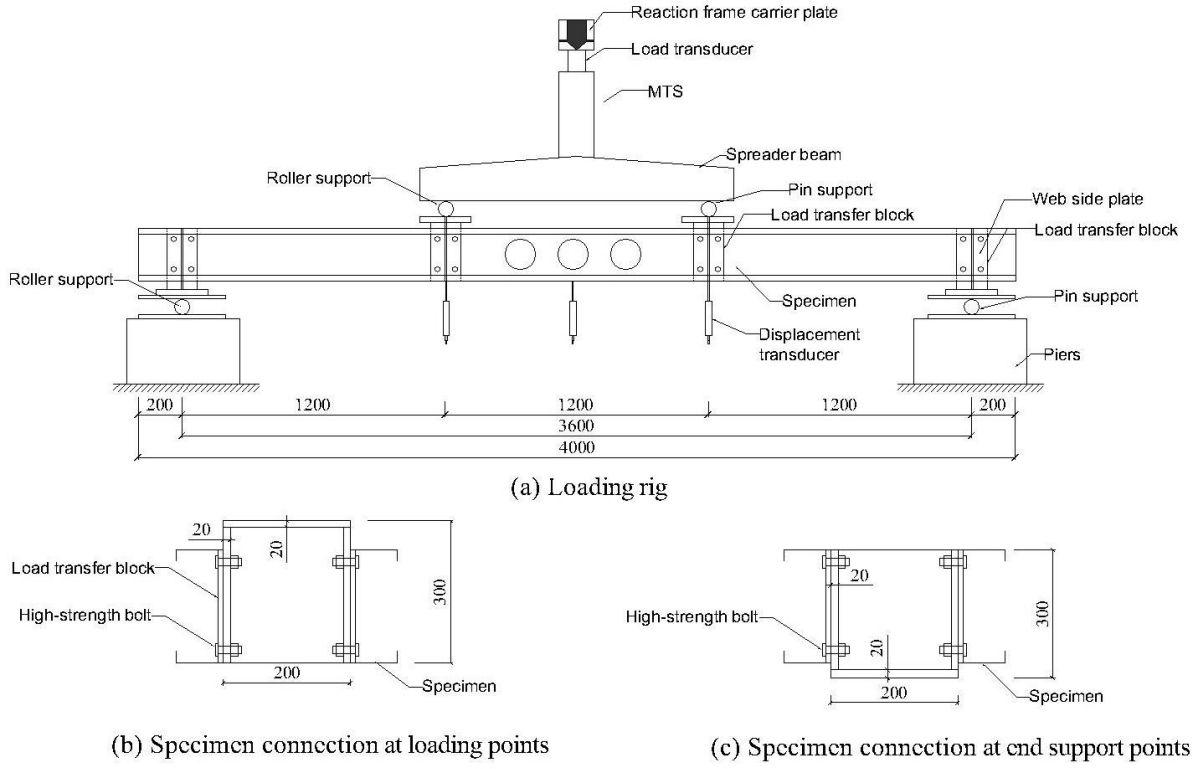

Figure 3-2: Schematic drawing of loading rig.

3.3 Geometry and material properties

An elastic-plastic model was used for modelling the overall geometry of the channel sections with plain channel sections, unstiffened, edge stiffened web holes. The geometrical dimensions and material properties for the CFSS sections for this study were taken from the literature [3-6] and the design manual for structural stainless steel, respectively.

As per the ABAQUS [41], the engineering material curve was converted into a true material curve by following the equations below:

$$\sigma_{true} = \sigma(1+\varepsilon) \tag{1}$$

$$\varepsilon_{true(pl)} = \ln(1+\varepsilon) - \frac{\sigma_{true}}{E} \tag{2}$$

where E is the Young's modulus, σ_{true} is the true stress, $\sigma_{\underline{u}}$ is the ultimate tensile strength, σ and $\varepsilon_{true(pl)}$ are the engineering stress and strain respectively in ABAQUS [41].

3.4 FE meshing

S4R shell elements were used to model the CFSS channel sections. To ensure the accuracy of the numerical simulations, a mesh sensitivity analysis was meticulously conducted to identify the optimal mesh size. The results of this analysis guided the selection of appropriate mesh dimensions, with the chosen sizes being 5mm x 5mm for CFSS channel sections and 10mm x 10mm for bearing plates, as depicted in Figure 3-3. Notably, a finer mesh size was specifically employed for areas featuring web holes and rounded corners. This finer mesh, illustrated in Figure 3-4, was chosen to capture potential stress concentrations around these critical regions, ensuring a detailed and accurate representation of the structural behavior of CFSS channel sections during the analysis.

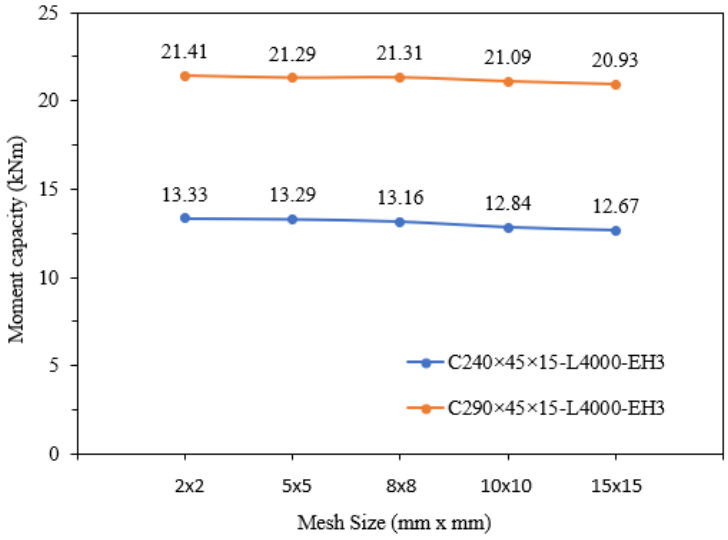

Figure 3-3 Graph for mesh sensitivity analysis.

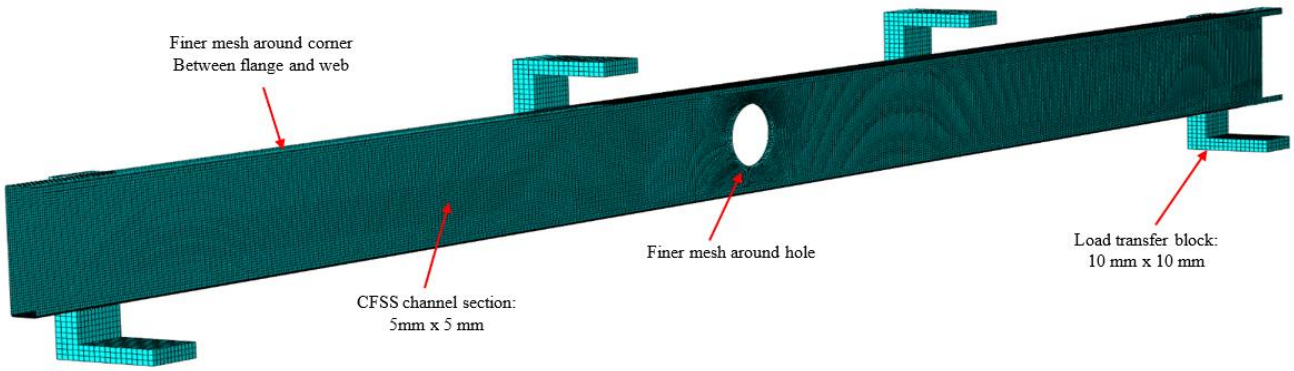

Figure 3-4 Details of meshing of the model.

3.5 Boundary conditions

In the FE model, surface-to-surface interaction was defined between the webs of each CFSS channel section and load transfer blocks. The reaction forces and concentrated loads were transferred from the L-shaped load transfer blocks to the specimen. The support and loading blocks with the higher stiffness were chosen as the master surface, and the web of the channel was selected as the slave surface. To model the link between the beams and the load transfer blocks, a multi-point constraint (MPC) beam connector element from the ABAQUS [41] library was employed.

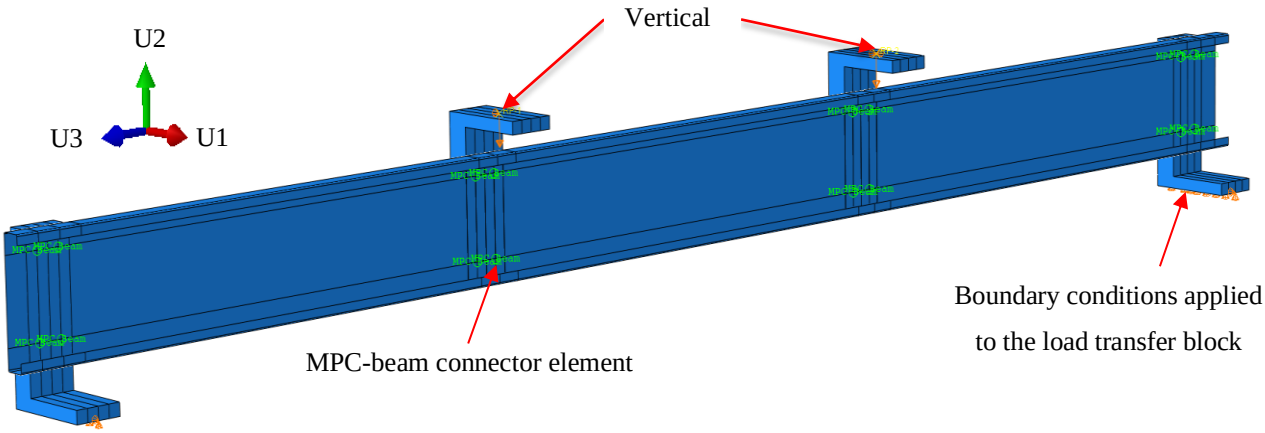

Figure 3-5 Details of FE model.

The supported boundary condition was modelled by releasing both the axial displacement along the specimen and the in-plane rotation at the roller support to replicate the experimental boundary conditions. The translations of U1 and U3 were fixed at two reference points that were set at the top of the load transfer block, and the loading was applied using a displacement control method by defining a vertical displacement along U2. Figure 3-5 specifies the boundary conditions used in the FE model.

3.6 Modelling of initial imperfections

In the FE modeling, initial geometrical imperfections were considered. Local and lateral-torsional geometric imperfections were also taken into account as per the methods used in [9, 29]. The magnitude of local imperfections was taken from the recommendations of AS/NZS [14]. The ABAQUS library's *IMPERFECTION option was used to model the imperfect initial geometries of

CFSS channel sections. Eigenvalue analysis was then performed, and the lowest buckling mode was considered as the critical buckling mode in the FE model to incorporate the imperfection magnitudes [9, 29].

3.7 Analysis procedure

Two different analysis methods, elastic buckling and dynamic implicit analysis, were used to model the CFS channel sections. Elastic buckling analysis was used to obtain the eigenvectors for modelling the initial geometric imperfections. The quasi-static response of CFS channel sections subjected to four-point bending was calculated using dynamic analysis with implicit time integration. It was found that using dynamic analysis in FE models can lead to better comparisons of the initial stiffness and post-buckling behavior of CFS sections when compared to test results. Therefore, in this study, dynamic analysis was preferred over static-risk analysis. The modelling techniques presented by Chen et al. [9] were applied in the present study.

3.8 Validation of the finite element model

The FE models on CFS channel sections were validated using the results published by Chen et al. [9]. Table 3 shows a comparison of the test results (MEXP) with the numerical results (MFEA) for sections 240 and 290. The MEXP/MFEA ratio has a mean value of 0.94. Table 3 compares the comparison moment capacity obtained from equations AS/NZS [15] with the numerical results (MFEA). The failure modes obtained from the FEA of the current study and the experimental results obtained from Chen et. al. [9] are shown in Figure 3–6. Figure 3-7 shows the moment versus displacement relationship obtained from both the FEA and the test. Overall, the model developed in this paper exhibited a good correlation with the experimental results.

There were no prior investigations into the moment behavior of CFSS channel sections, and the finite element (FE) modelling methods for CFS channel sections and CFSS channel sections are comparable; therefore, the current study will employ the same FE modelling techniques discussed in Section 3 to simulate the behavior of CFSS channel sections under bending. It is noted that the only difference between CFS and CFSS studies is the material property.

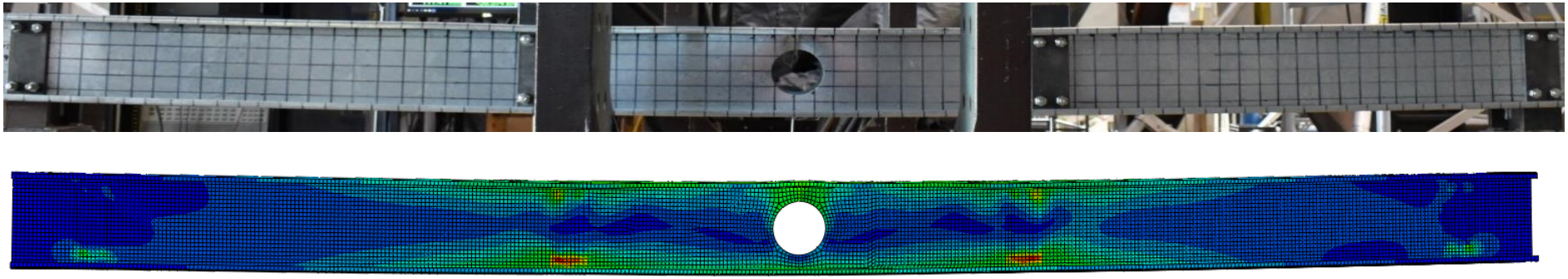

(a) C240-UH1

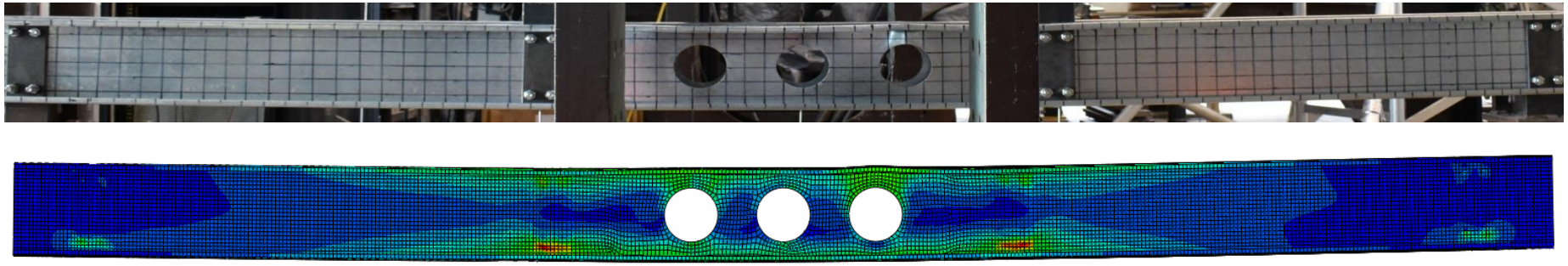

(b) C240-UH3

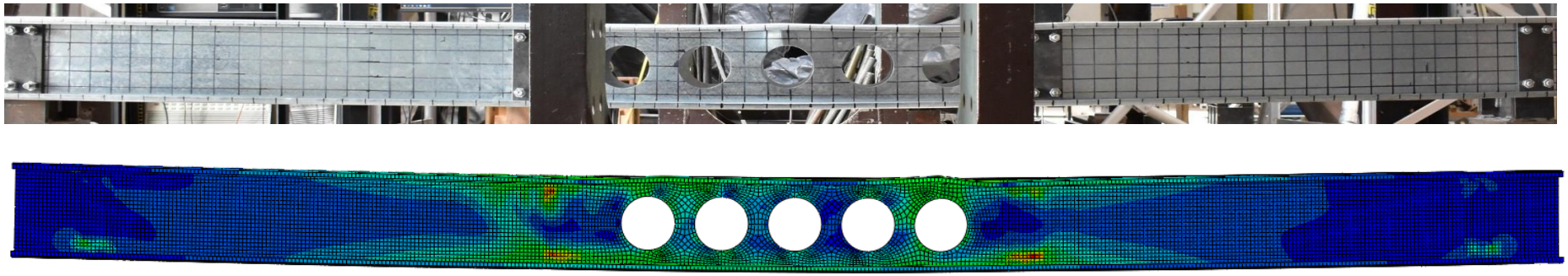

(c) C240-UH5

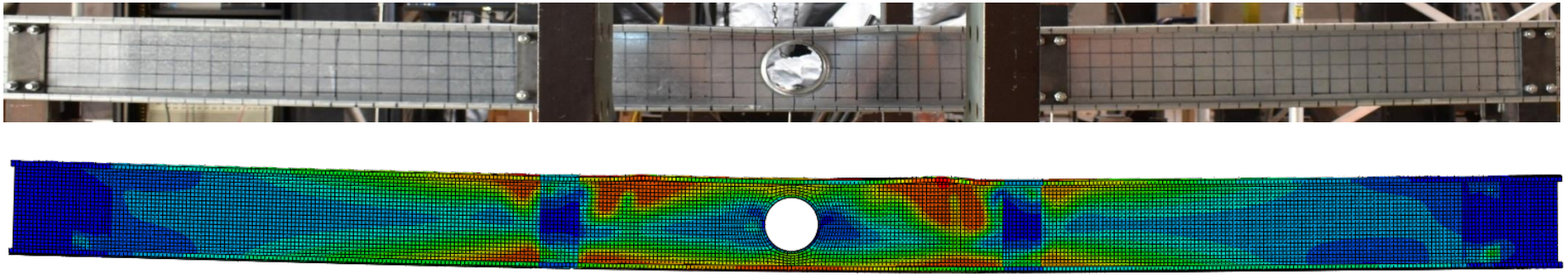

(d) C240-EH1

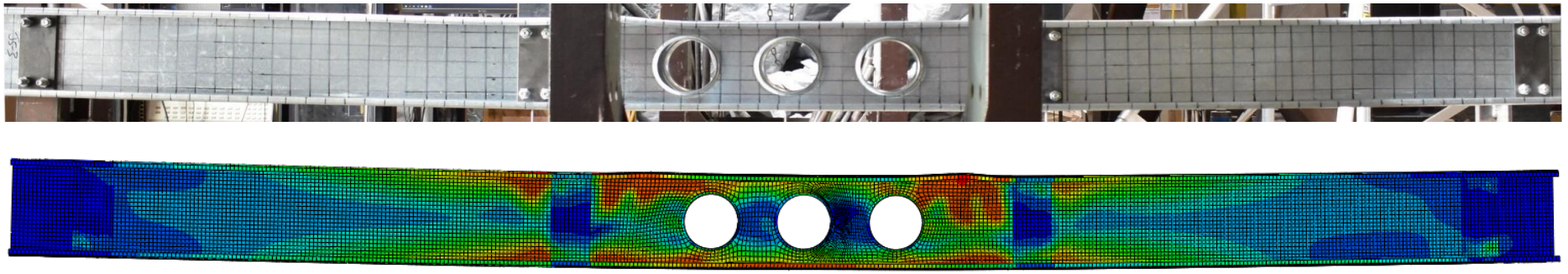

(e) C240-EH3

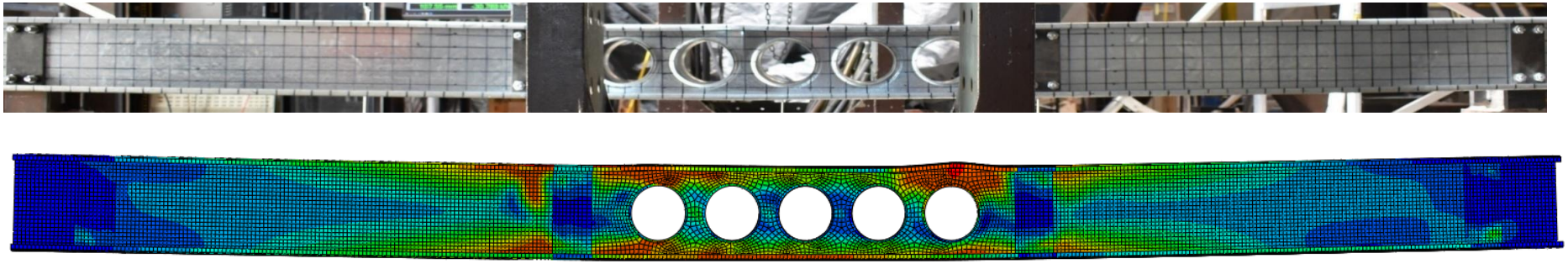

(f) C240-EH5

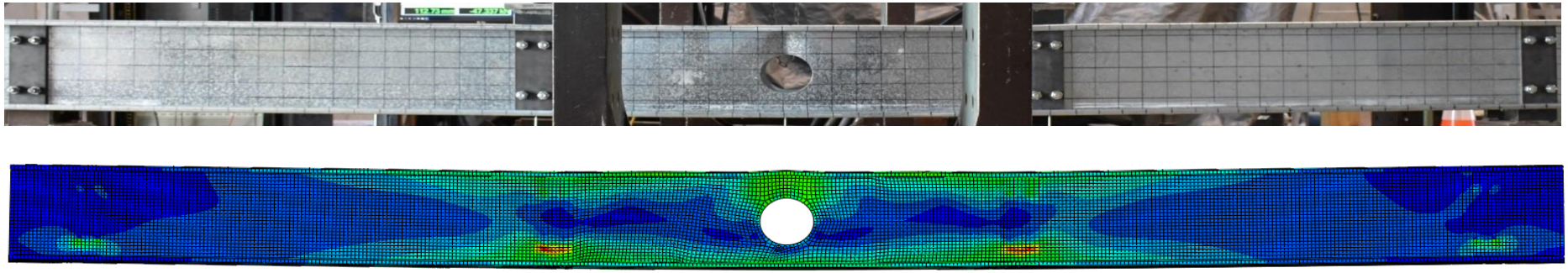

(g) C290-UH1

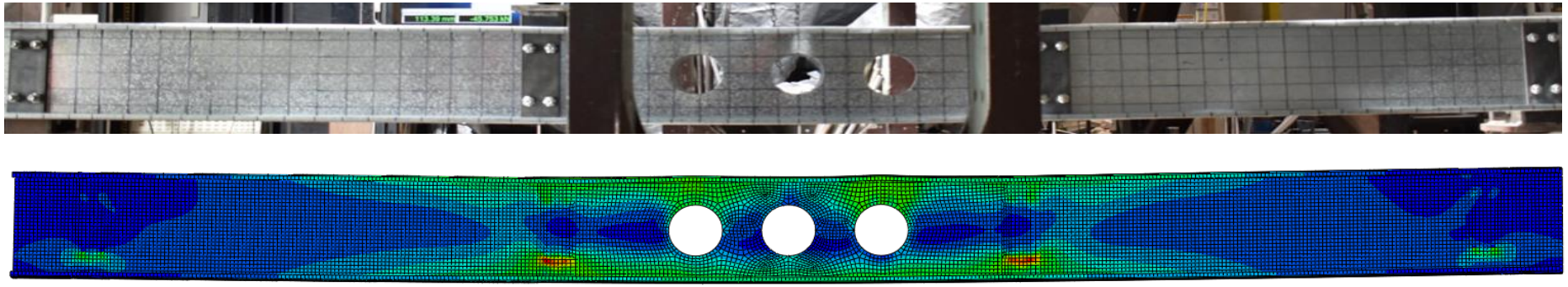

(h) C290-UH3

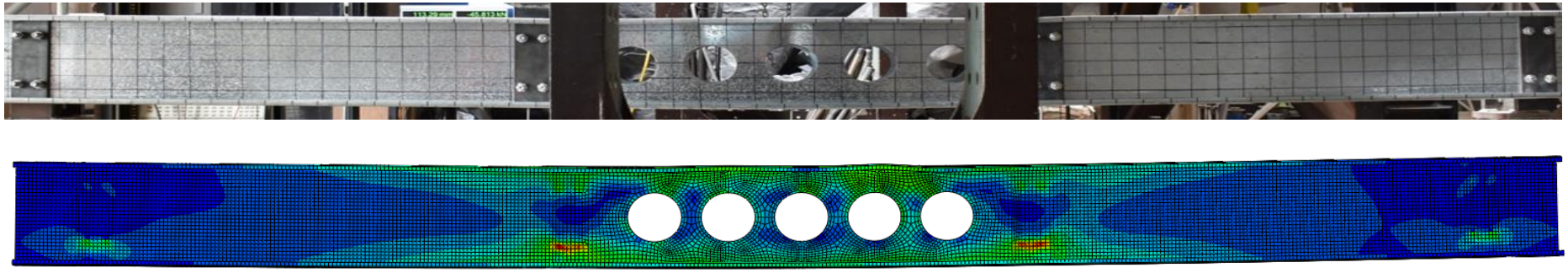

(i) C290-UH5

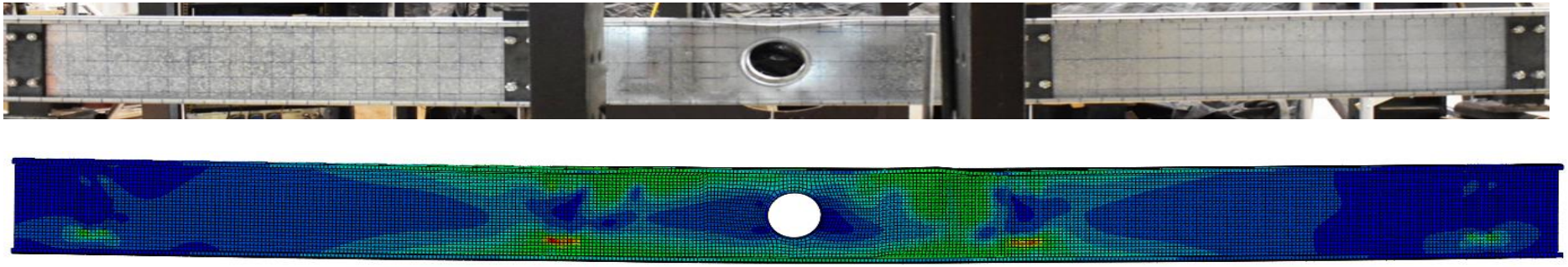

(j) C290-EH1

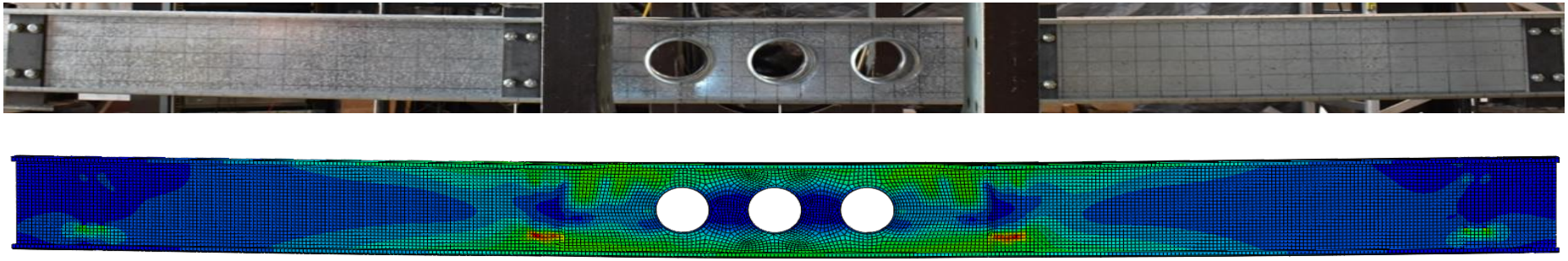

(k) C290-EH3

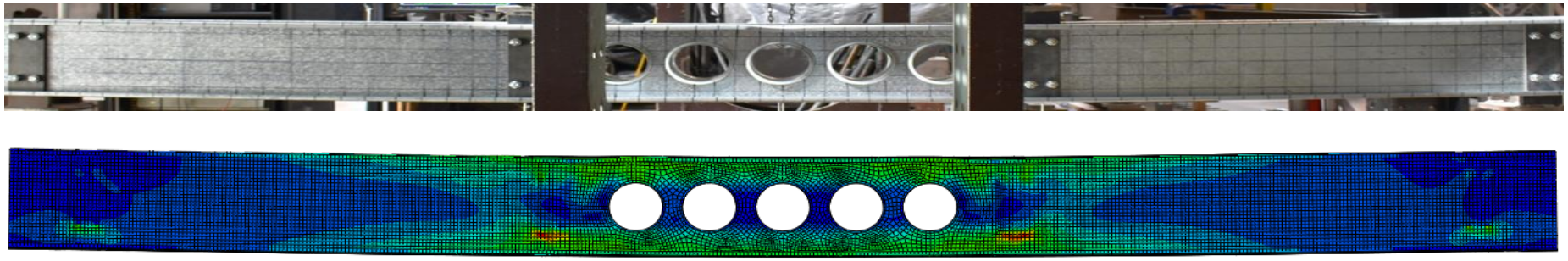

(l) C290-EH5

Figure 3-6: Deformed shapes at failure from experiments and FEA.

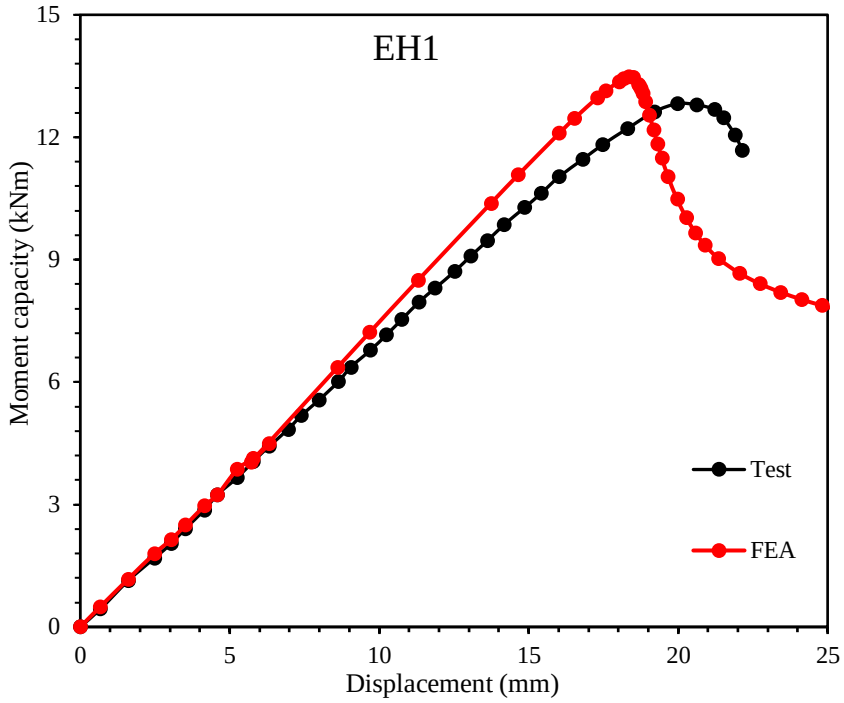

(a) C240-L4000-EH1

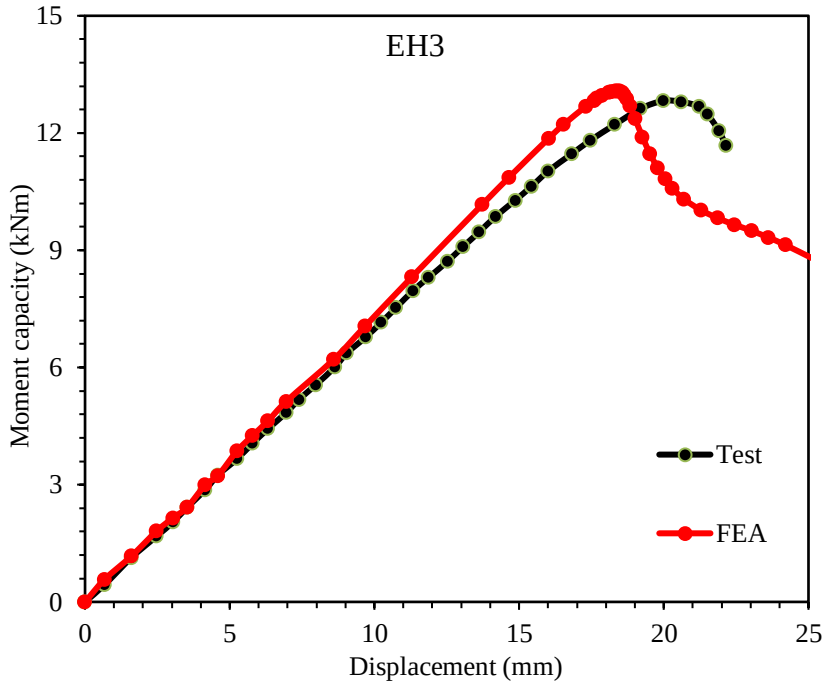

(b) C240-L4000-EH3

Figure. 3-7 Comparison of moment verses displacement curves of test [9] and FEA results for CFS channel sections with edge stiffened web holes.

CHAPTER 4. Parametric study

4.1 General

A parametric study considering 888 FE models was conducted on CFSS channel sections with plain webs, unstiffened web holes and edge-stiffened web holes using the validated FEA modelling techniques. In addition, Python scripting was used to generate all the FE models for the parametric study (see Appendix A). In the study, two channel cross sections were considered: C200x65x15 and C300x80x20, with thicknesses (*t*) varying from 1.5mm to 3 mm and with three different properties (austenitic, duplex and ferritic) grades of stainless-steel materials, as shown in Fig. 5. In order to study the effects of specimens with web holes, the following parameters were varied: the ratio of hole depth to web depth (*a/h*) from 0.2 to 0.6 and the stiffener length (*q*) of 5 mm, 7 mm and 10 mm. The moment capacity of CFSS channel sections with plain webs, unstiffened, and edge-stiffened web holes obtained from FEA is presented in Tables 4, 5 and 6 for austenitic, duplex and ferritic grades of stainless steel, respectively.

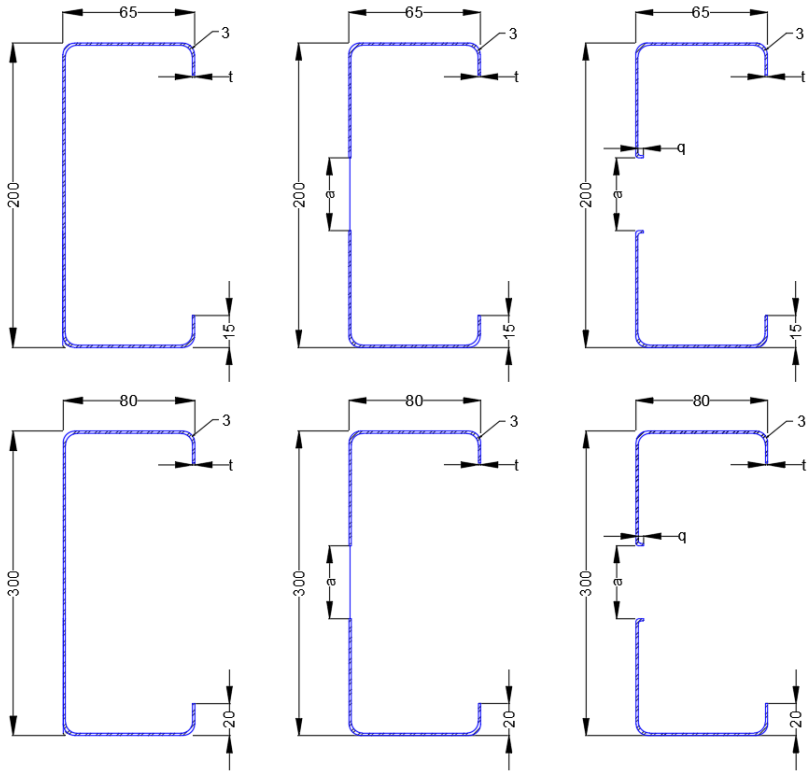

Figure 4-1: Cross sectional details (All dimensions are in mm)**.**

The specimens used for the parametric study were labelled such that the web depth, thickness, ratio of web hole to depth and stiffener length between the web and stiffener were defined. Figure 4-2 illustrates the labelling of the channel sections used in the parametric study. For example, the label "C200-T1.5-3EH-D0.4-Q7" can be explained as given below.

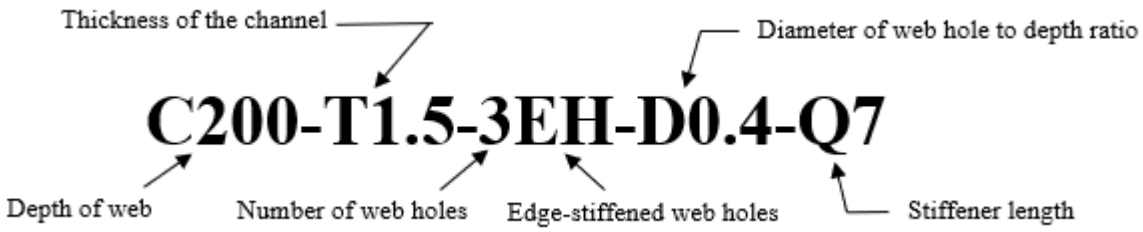

Figure 4-2: Labelling of specimen.

4.2 CFSS channel sections with plain webs

4.2.1 Effect of section thickness

Figure 4-3 shows the impact of thickness on the moment capacity of CFSS channel sections. In terms of austenitic stainless steel, when increasing the thickness from 1.5 mm to 2 mm, the average moment capacity increased by 45%. Similarly, for thicknesses of 2 mm to 2.5 mm and 2.5 mm to 3 mm, the moment capacity increased by 27.6% and 21.5%, respectively. In terms of duplex stainless steel, thickness variations from 1.5 mm to 2 mm resulted in a moment capacity increase of up to 67.6%, followed by 40.1% for 2 mm to 2.5 mm and 25.4% for 2.5 mm to 3 mm. In terms of ferritic stainless steel, the channel sections presented moment capacity increases of 45.5%, 29.2%, and 21.2% for these respective thickness variations.

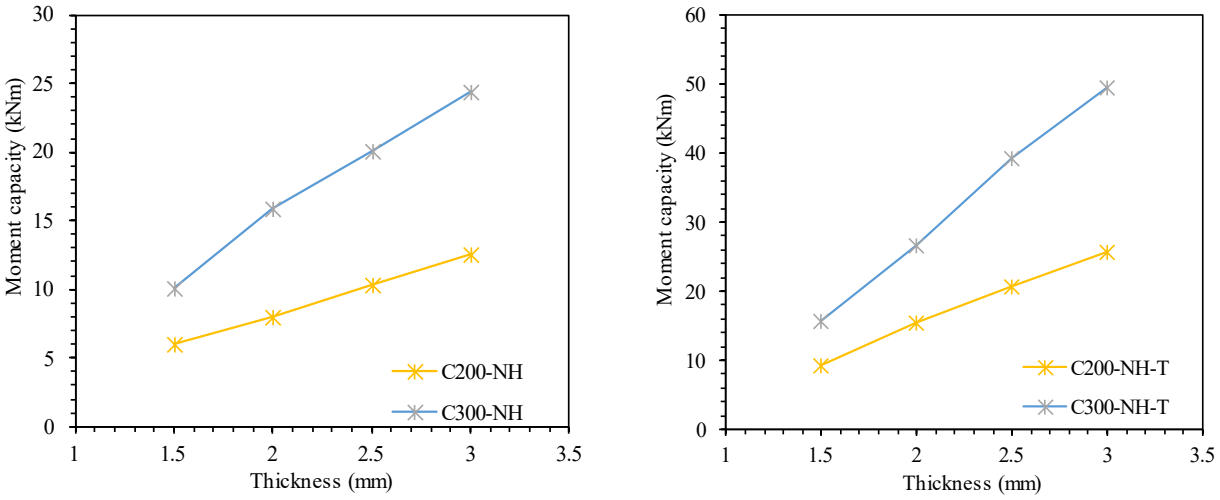

(a) Austenitic (b)Duplex

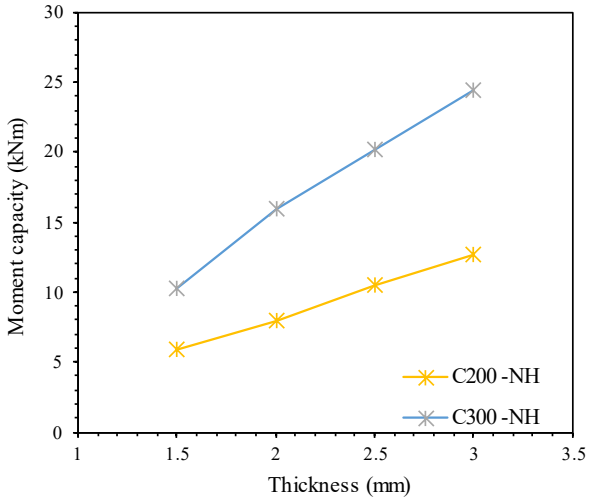

(C) Ferritic

Figure 4-3: Effect of thickness for CFSS channel section with plain webs.

4.2.2 Moment capacity of plain sections in austenitic, duplex, ferritic stainless-steel

Figure 4-4 illustrates the effects of various grades of CFSS channel sections on average moment capacity. As can be seen from Figure 4–4, the average increase in moment capacity was 84.8% when the grades of CFSS channels changed from austenitic to duplex. Similarly, an 84% increment in moment capacity can be seen when the grades of CFSS channel sections change from ferritic to duplex. Notably, despite having the same yield stress for austenitic and ferritic materials, the moment capacity decreases by 0.45% due to differences in Young's modulus, ultimate stress, and ultimate strain.

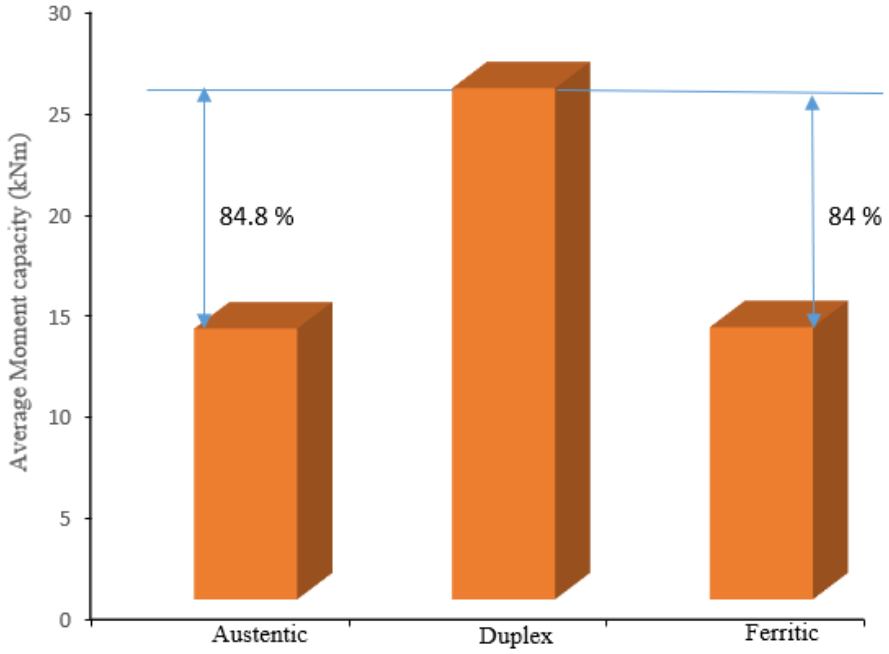

Figure 4-4: Effects of various grades of CFSS channel sections.

4.3 CFSS channel sections with unstiffened web holes

4.3.1 Effect of a/h ratio on moment capacity for CFSS channel section

The effects of the a/h ratio on the moment capacity of the CFSS channel section with unstiffened web holes are shown in Figure 4–5 and Tables 4, 5 and 6 for austenitic, duplex and ferritic grades of stainless steel, respectively. A decreasing trend can be observed in the moment capacity when the a/h ratio increases from 0.2 to 0.6. From the results of the parametric study, it was found that when the a/h ratio increased from 0.2 to 0.4, the moment capacity decreased by 2.65% for austenitic CFSS channel sections. Similarly, for duplex CFSS channel sections, the moment capacity decreased by 1.8%, and for ferritic CFSS channel sections, it decreased by 2.8%. Likewise, when comparing the a/h ratio from 0.2 to 0.6, for austenitic stainless steel, the moment capacity decreased by 9.1%, for duplex stainless steel, it decreased by 9.6%, and for ferritic stainless steel, it decreased by 9.9%. Similarly, when comparing the a/h ratio from 0.4 to 0.6, the moment capacity decreased by 6.6%, 7.9%, and 6.8% for austenitic, duplex, and ferritic stainless steel, respectively. It is important to note that the a/h ratio has a significant effect on moment capacity.

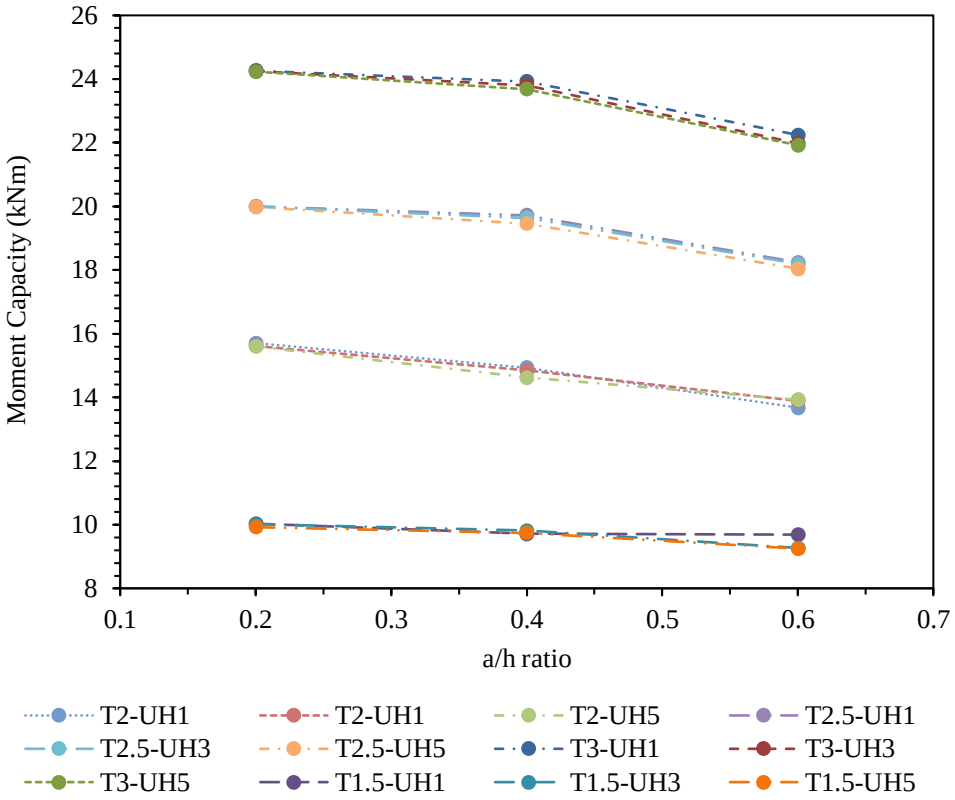

(a) Austenitic C300-L4000-T-UH-D

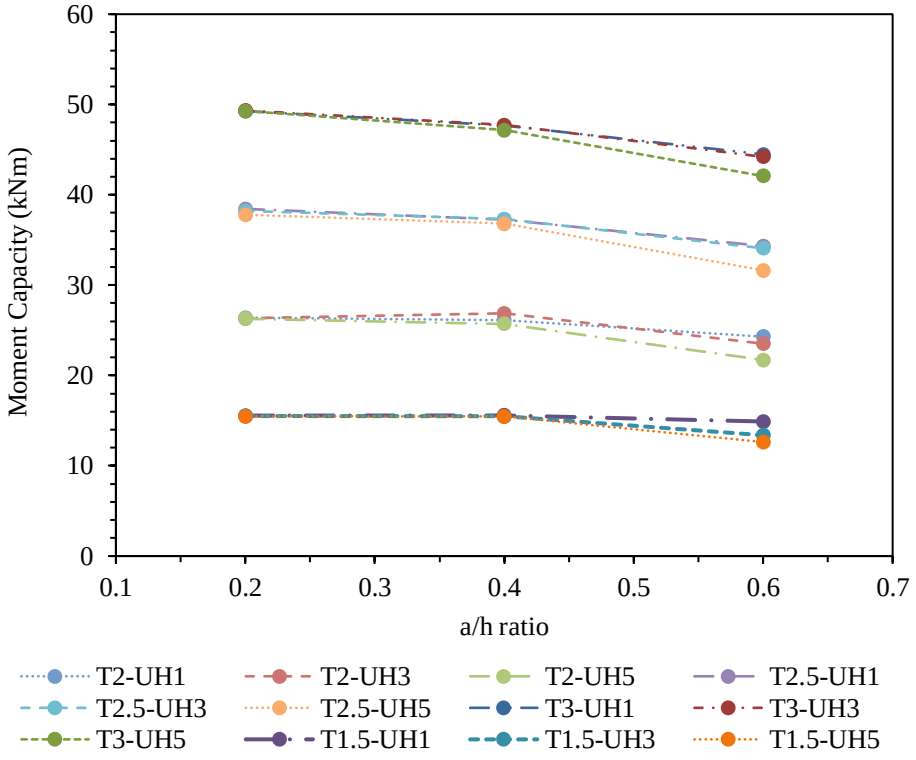

(b) Duplex C300-L4000-T-UH-D

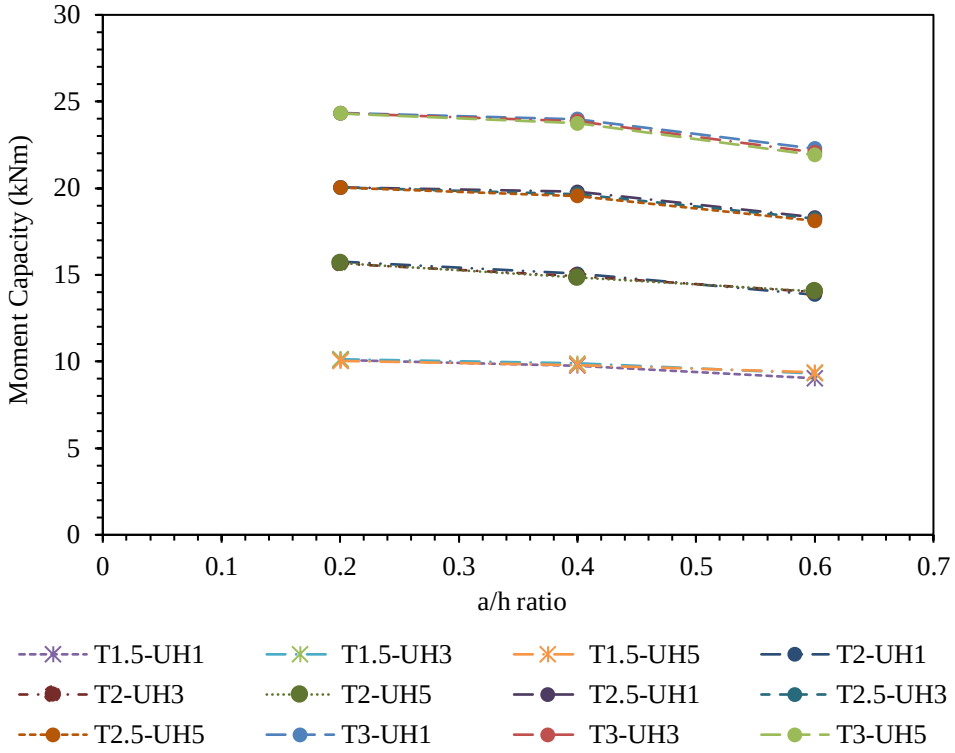

(C) Ferritic C300-L4000-T-UH-D

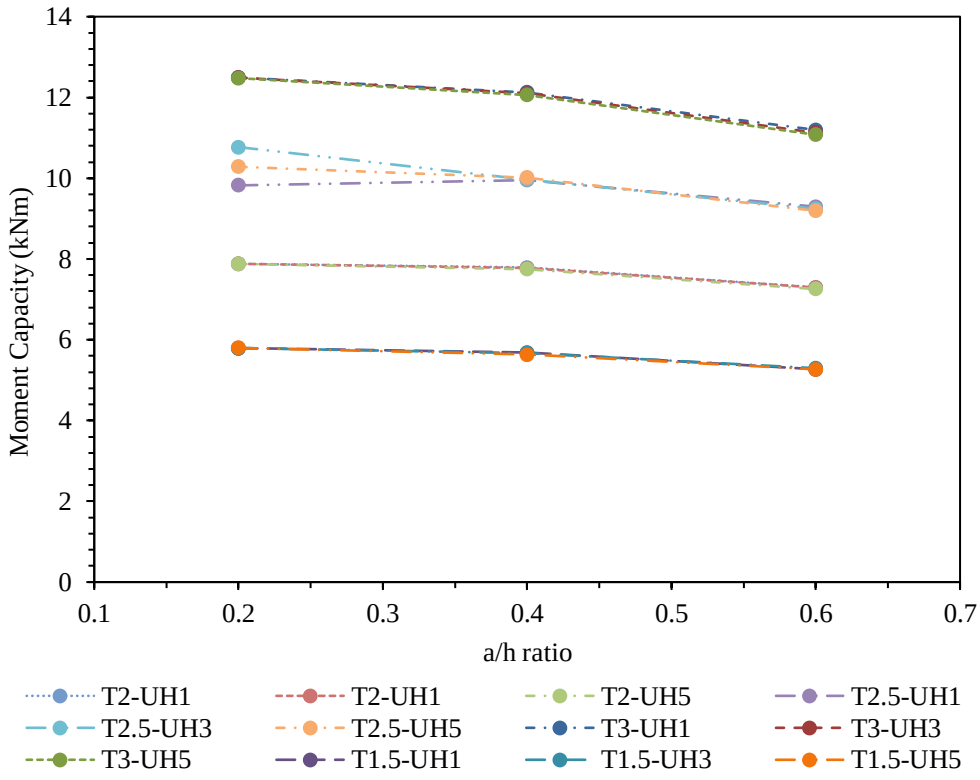

(d) Austenitic C200-L4000-T-UH-D

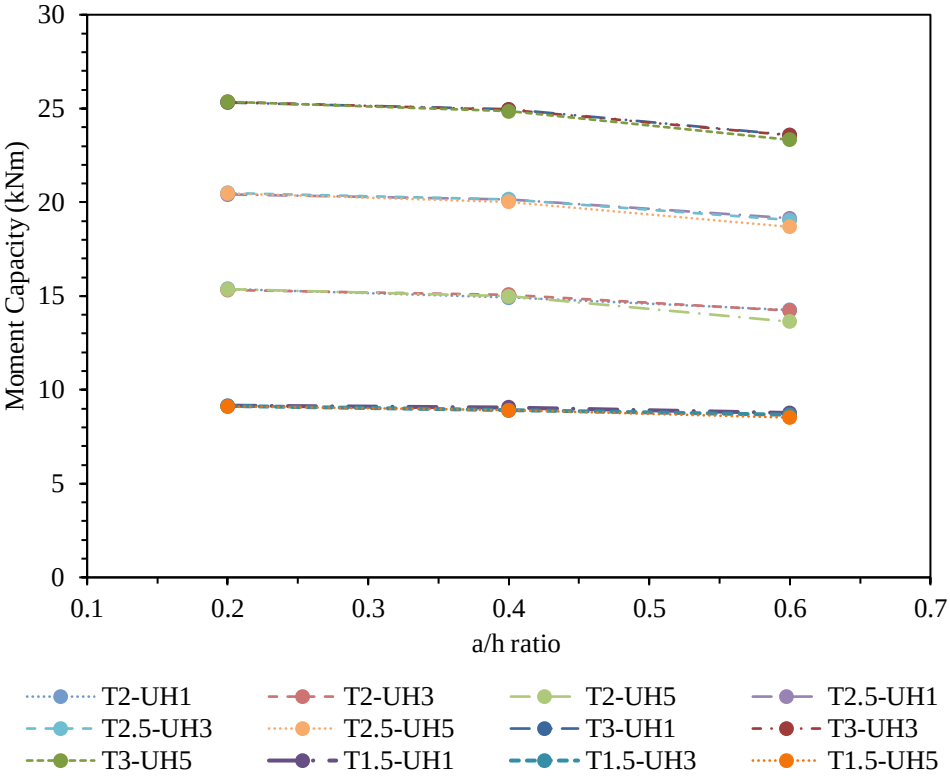

(e) Duplex C200-L4000-T-UH-D

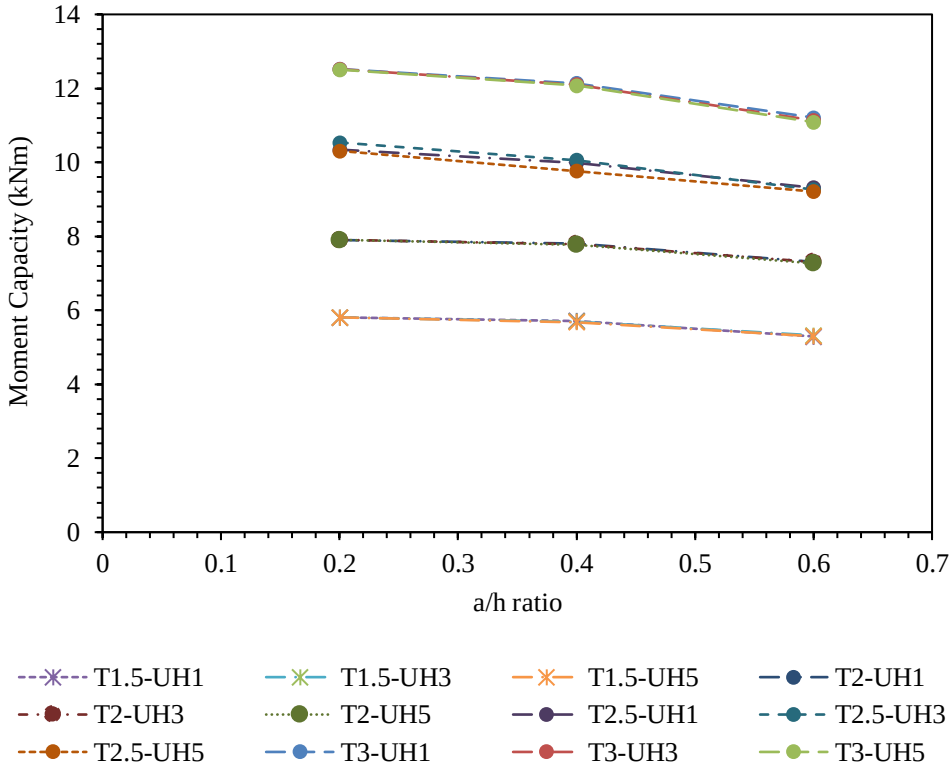

(f) Ferritic C200-L4000-T-UH-D

Figure 4-5: Effect of web hole diameter to web depth ratio for CFSS unstiffened channel sections.

4.3.2 Effect of number of holes on moment capacity for CFSS channel section

Figure 4–6 show the effect of the number of holes on the moment capacity of the CFSS channel sections with unstiffened web holes. When the number of holes increased from 1 to 3, the moment capacity decreased by 1.06%, 2.1% and 1.8% for austenitic, duplex, and ferritic stainless steel, respectively. Similarly, when the number of holes increased from 1 to 5, the moment capacity decreased by 7.5%, 8.7% and 8.4%, respectively.

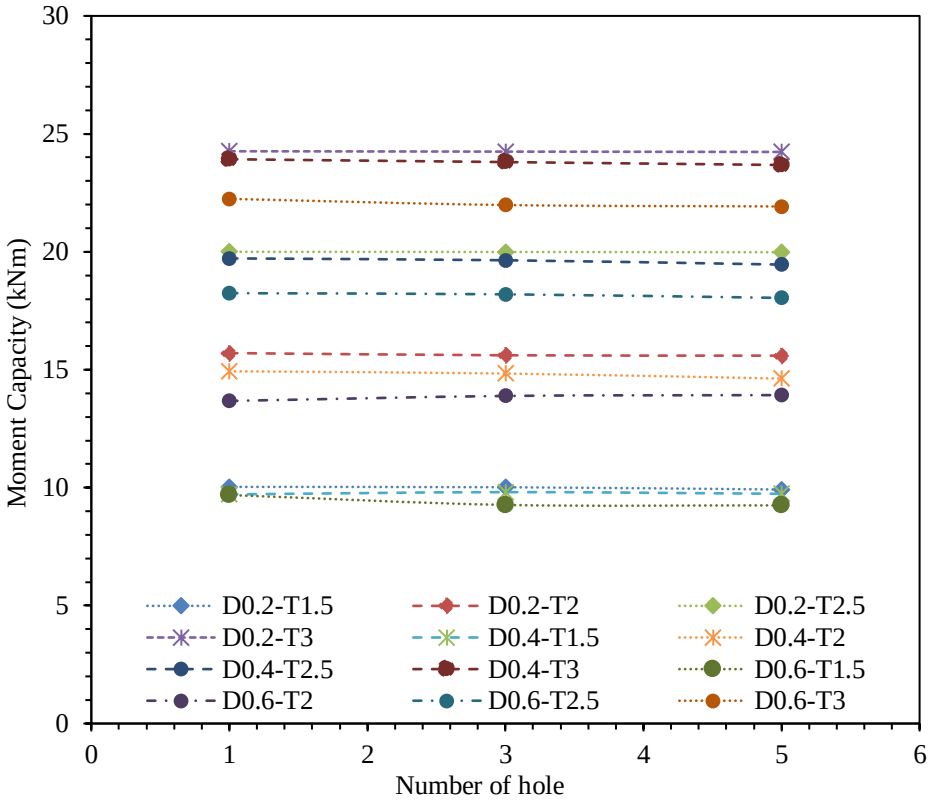

(a) Austenitic C300-L4000-UH-D-T

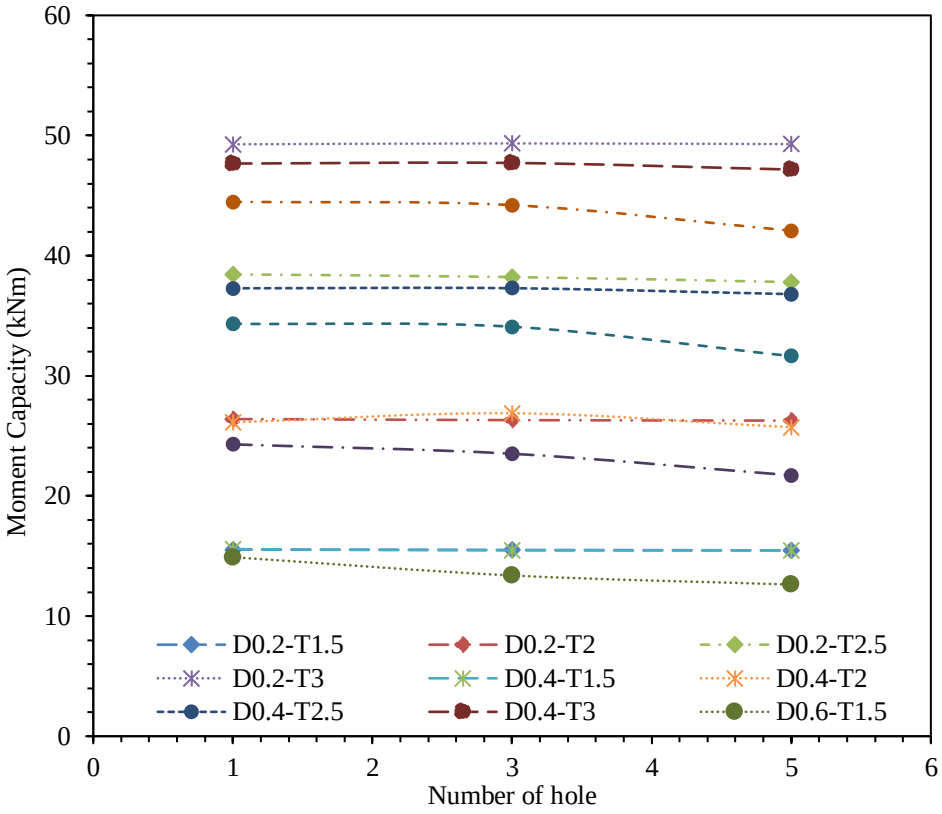

(b) Duplex C300-L4000-UH-D-T

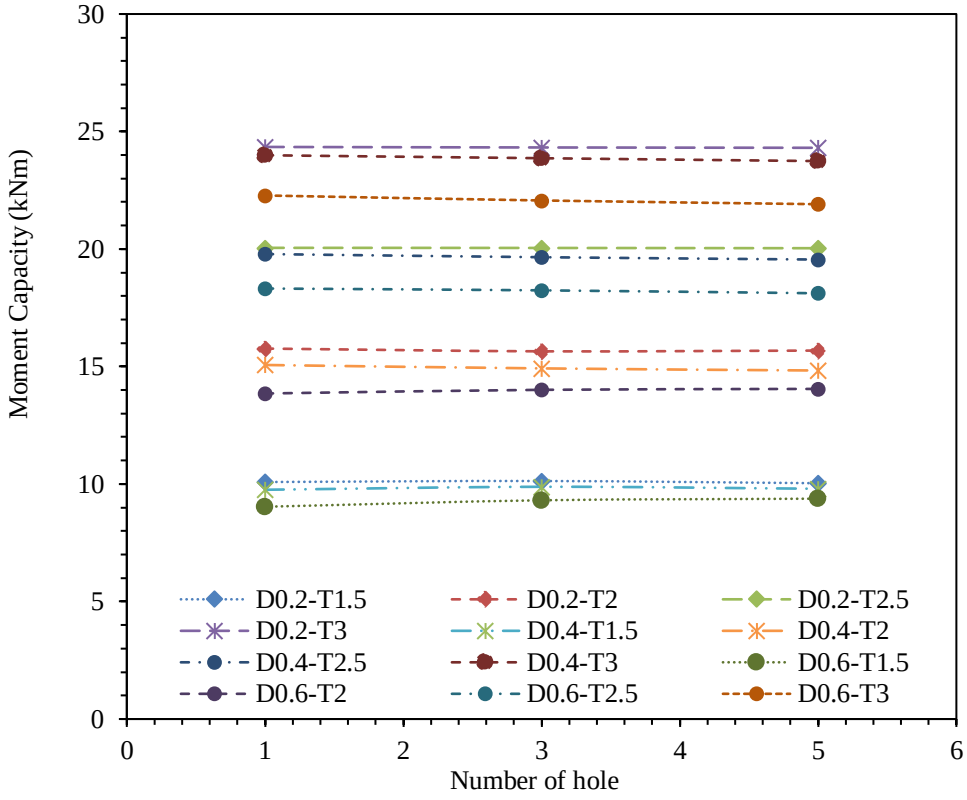

(C) Ferritic C300-L4000-UH-D-T

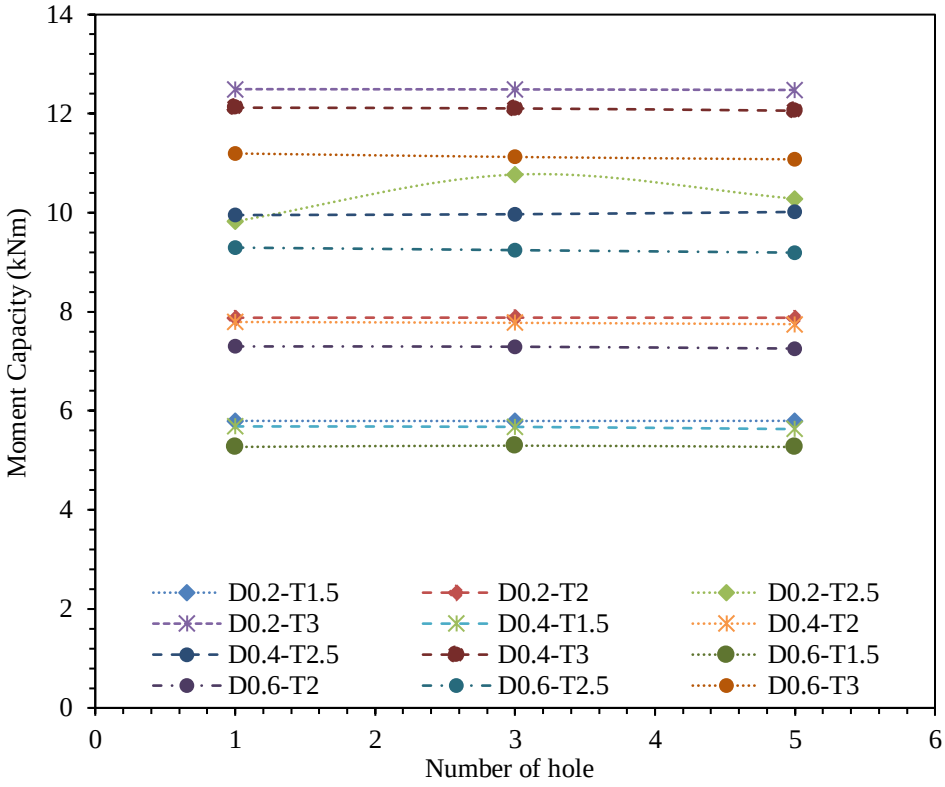

(d) Austenitic C200-L4000-UH-D-T

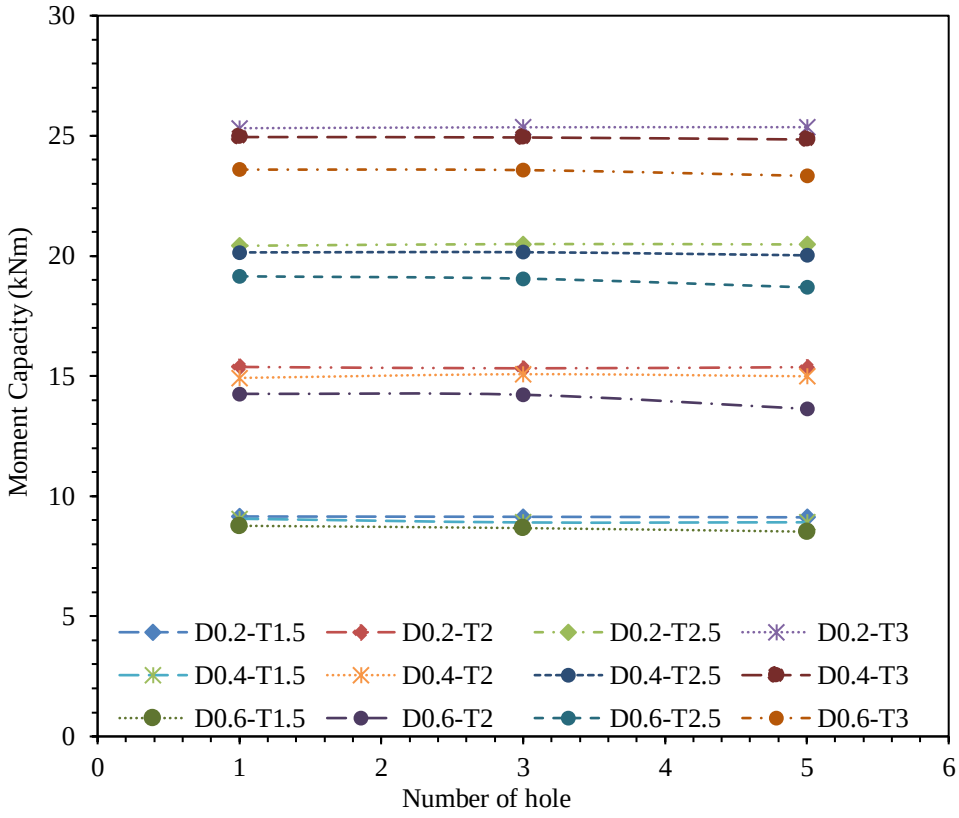

(e) Duplex C200-L4000-UH-D-T

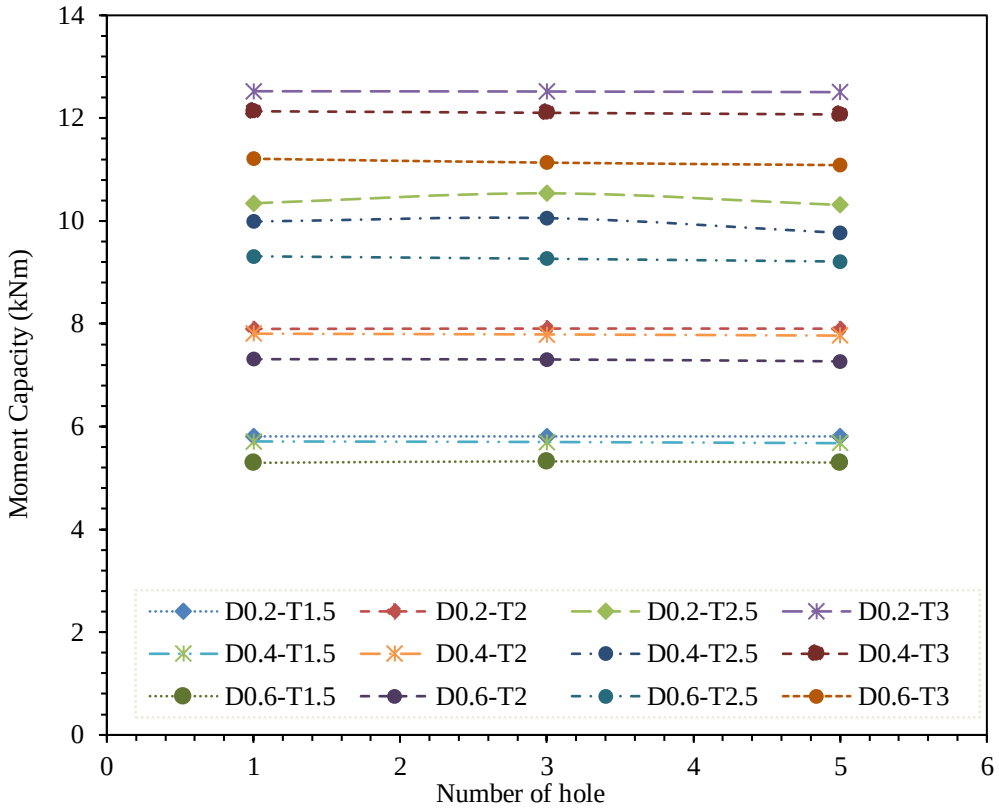

(f) Ferritic C200-L4000-UH-D-T

Figure 4-6: Effect of number of holes for CFSS unstiffened channel sections.

4.3.3 Effect of thickness on moment capacity for CFSS channel section

The effect of thickness on the moment capacity of CFSS channel sections is shown in Figure 4-7. There is an apparent increase in moment capacity as the thickness of the CFSS channel sections increases for all investigated stainless steel grades. From the parametric results, it was found that increasing the thickness from 1.5mm to 2mm has increased moment capacity to 51.4% on average for all three stainless steel grades. Similarly, when the thickness is increased from 2 mm to 2.5 mm, the moment capacity increases to 31.2% and when the thickness is increased from 2.5 mm to 3 mm, the moment capacity increases to 22.3%. It is important to note that the thickness of the CFSS channel section has a significant effect on moment capacity.

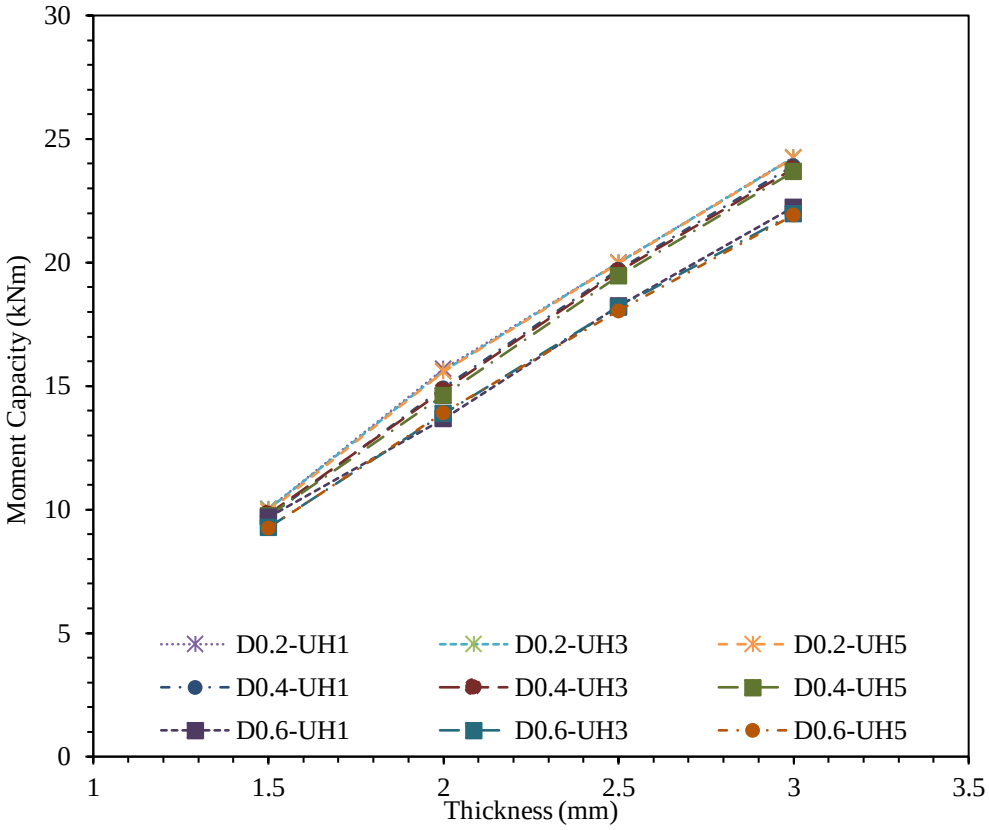

(a) Austenitic C300-L4000-T-UH-D

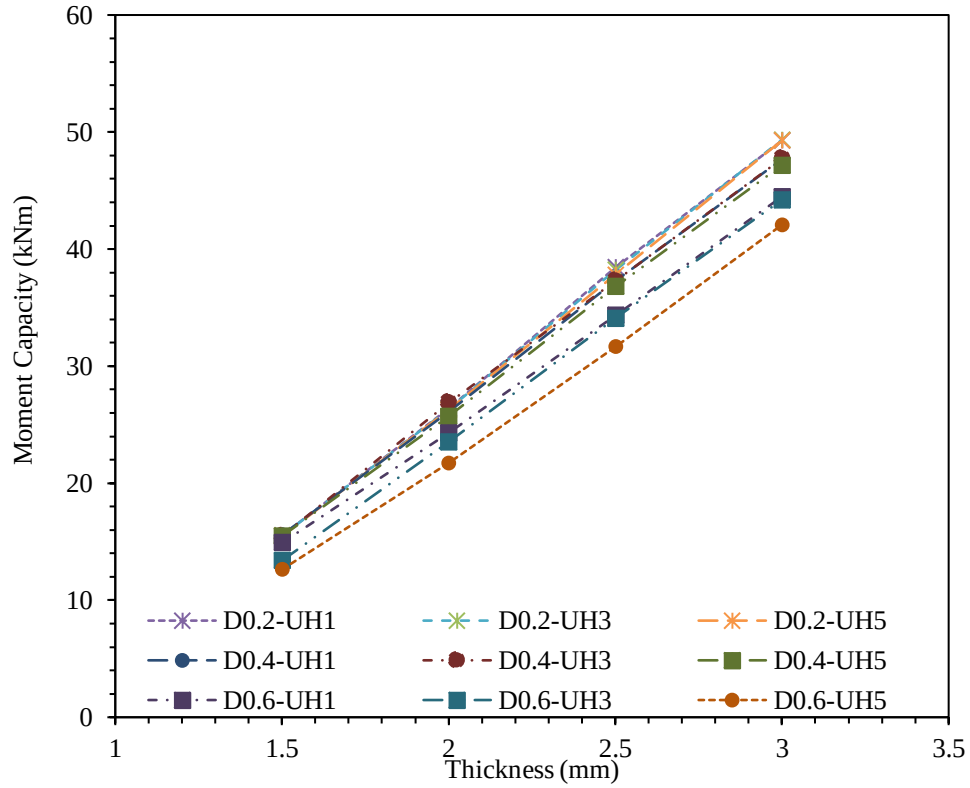

(b) Duplex C300-L4000-T-UH-D

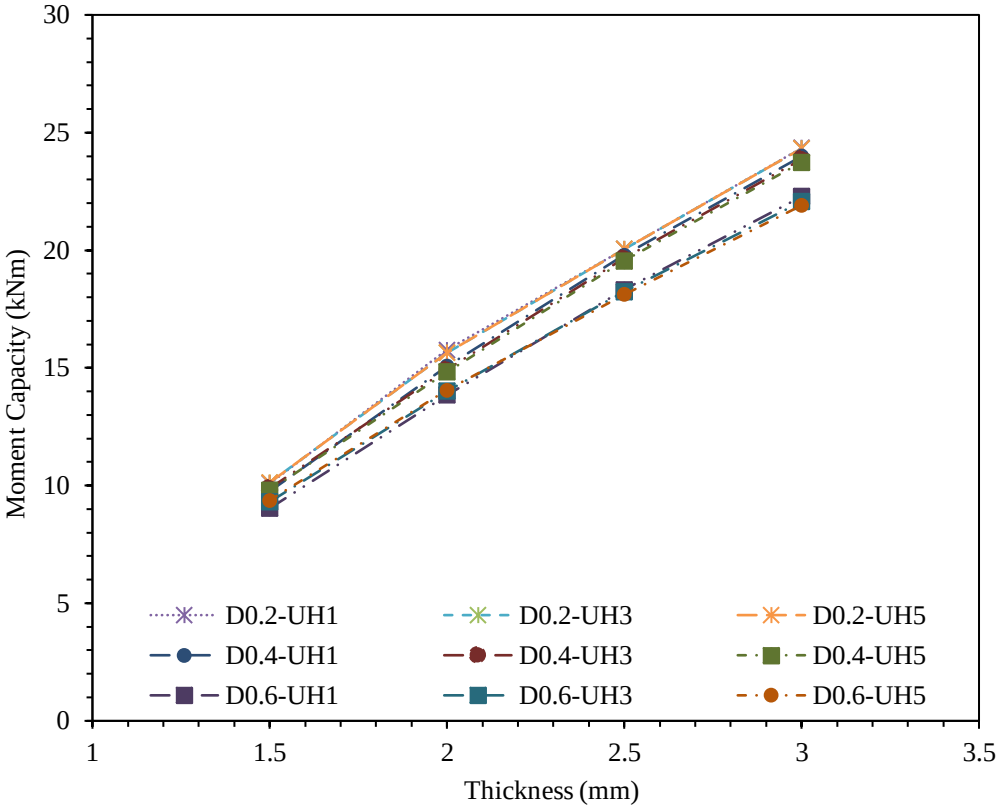

(C) Ferritic C300-L4000-T-UH-D

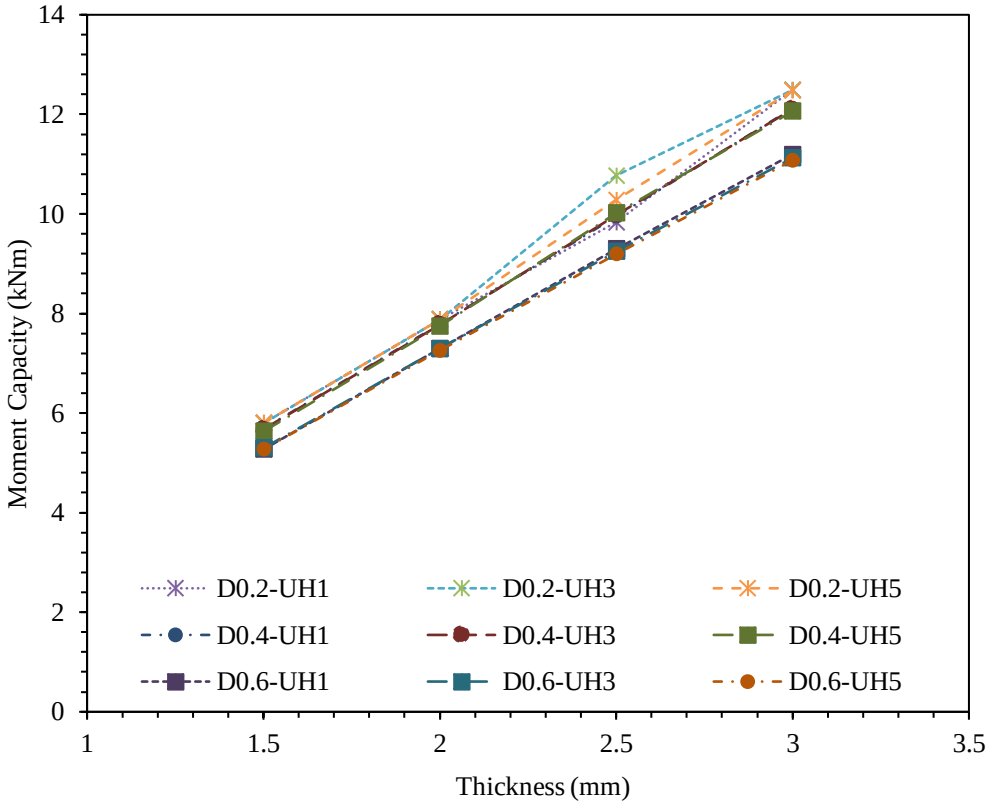

(d) Austenitic C200-L4000-T-UH-D

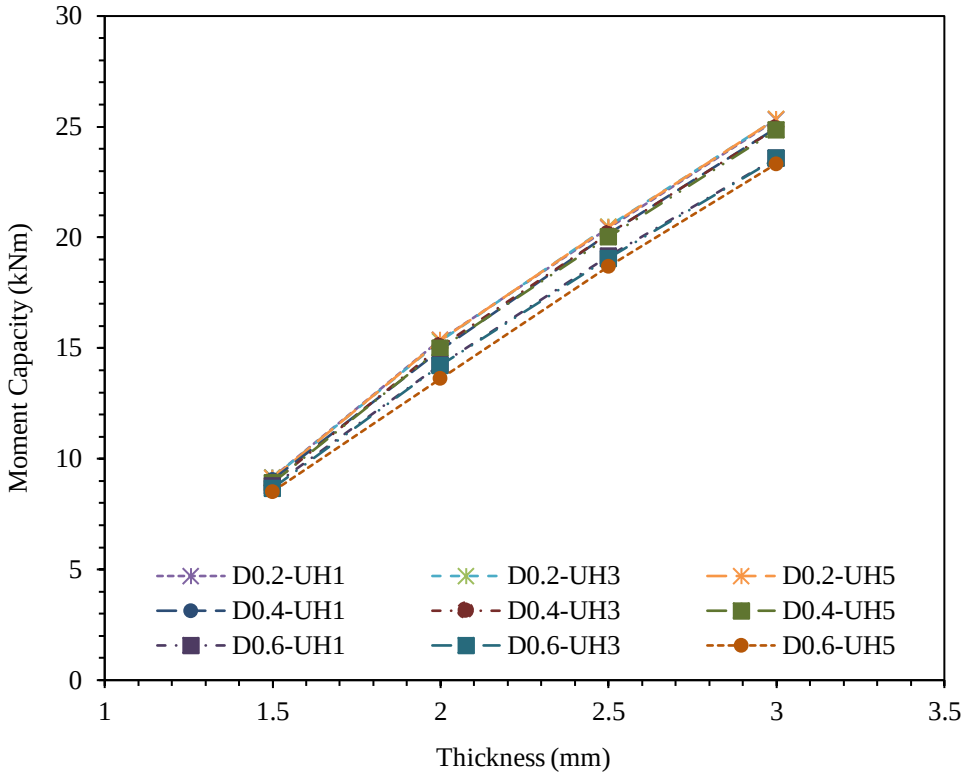

(e) Duplex C200-L4000-T-UH-D

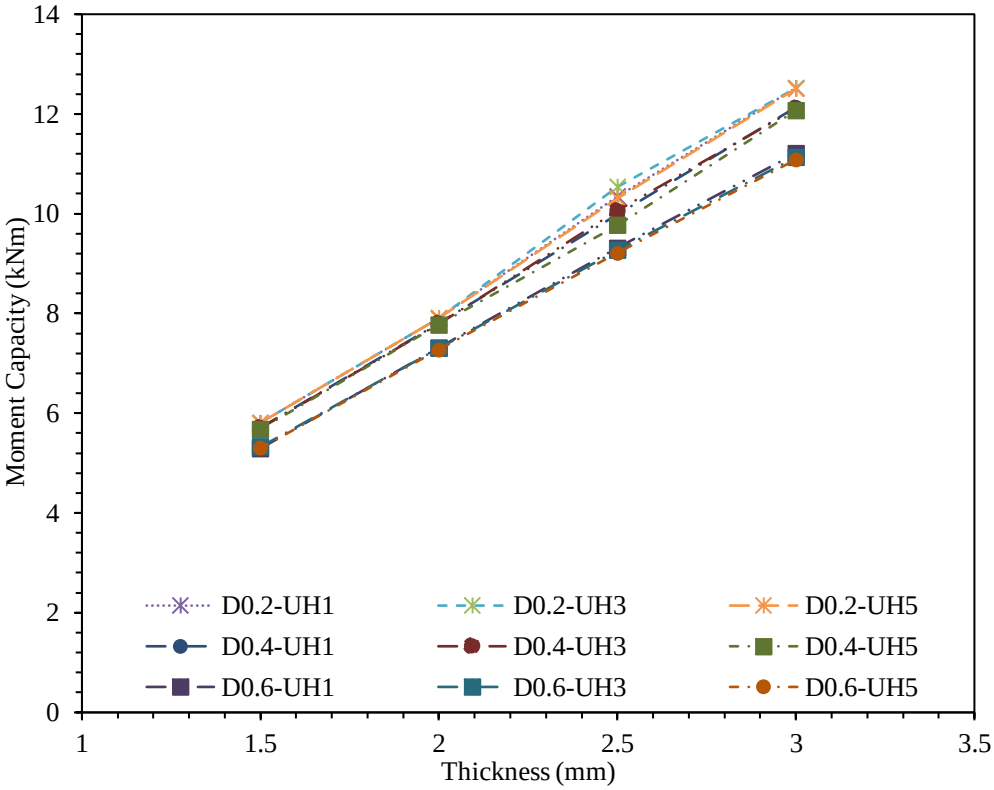

(f) Ferritic C200-L4000-T-UH-D

Figure 4-7: Effect of thickness for CFSS unstiffened channel sections.

4.3.4 Effect of channel dimensions on moment capacity for CFSS channel section

Tables 4, 5 and 6 show the moment capacity obtained for the two cross-sectional dimensions of the CFSS channel section considered in this paper for austenitic, duplex and ferritic grades of stainless steel, respectively. It is evident that, on average, the moment capacity increased to 91.8% from C200x65x15 to C300x80x20.

4.4 CFSS channel sections with Edge-stiffened web holes

4.4.1 Effect of stiffener length on moment capacity for CFSS channel section

The effect of stiffener length on the moment capacity for CFSS channel sections with edge-stiffened web holes was also investigated in this paper and the average increase in moment capacity was only 0.67% when stiffener varied from 5 mm to 7 mm. Likewise, for the ranges of 7 mm to 10 mm and 5 mm to 10 mm, there were slight increases in moment capacity to 0.12% and 0.78%, respectively, as shown in Figure 4-8.

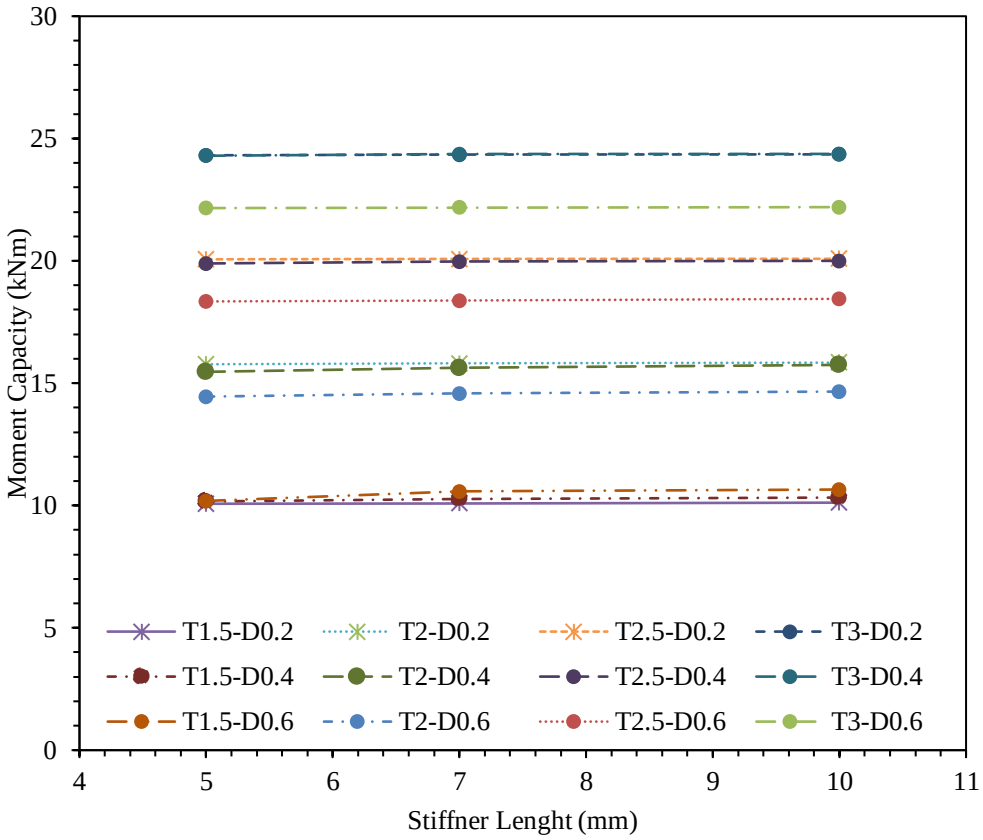

(a) Austenitic C300-L4000-T-EH3-D-Q

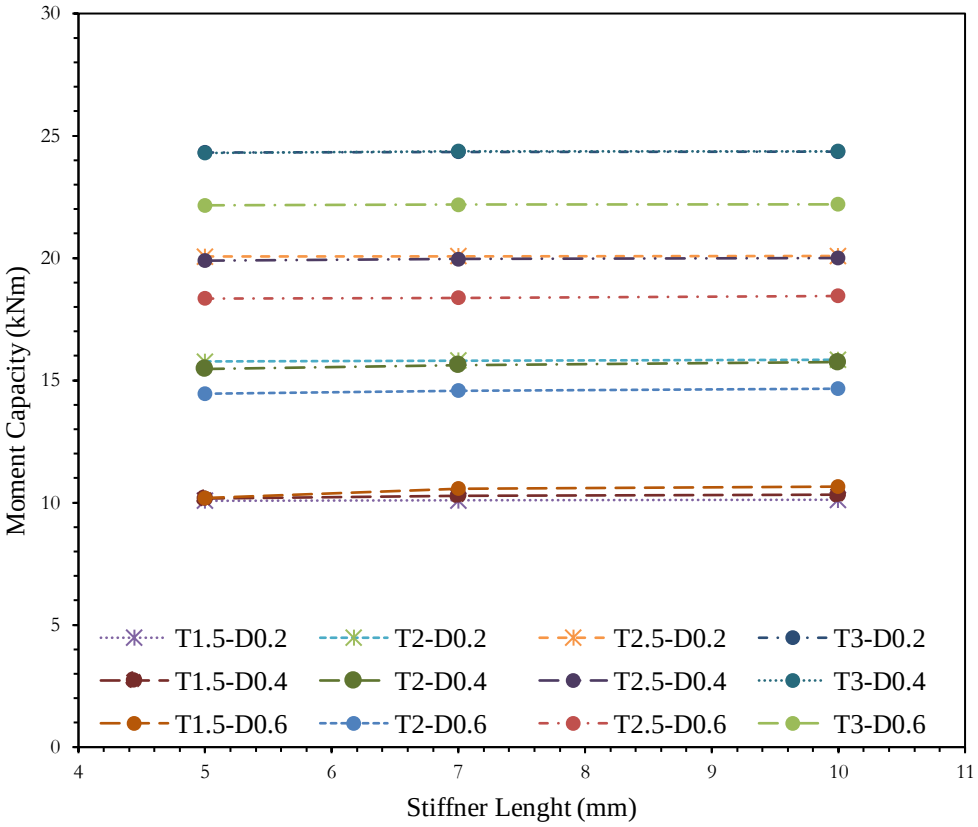

(b) Duplex C300-L4000-T-EH3-D-Q

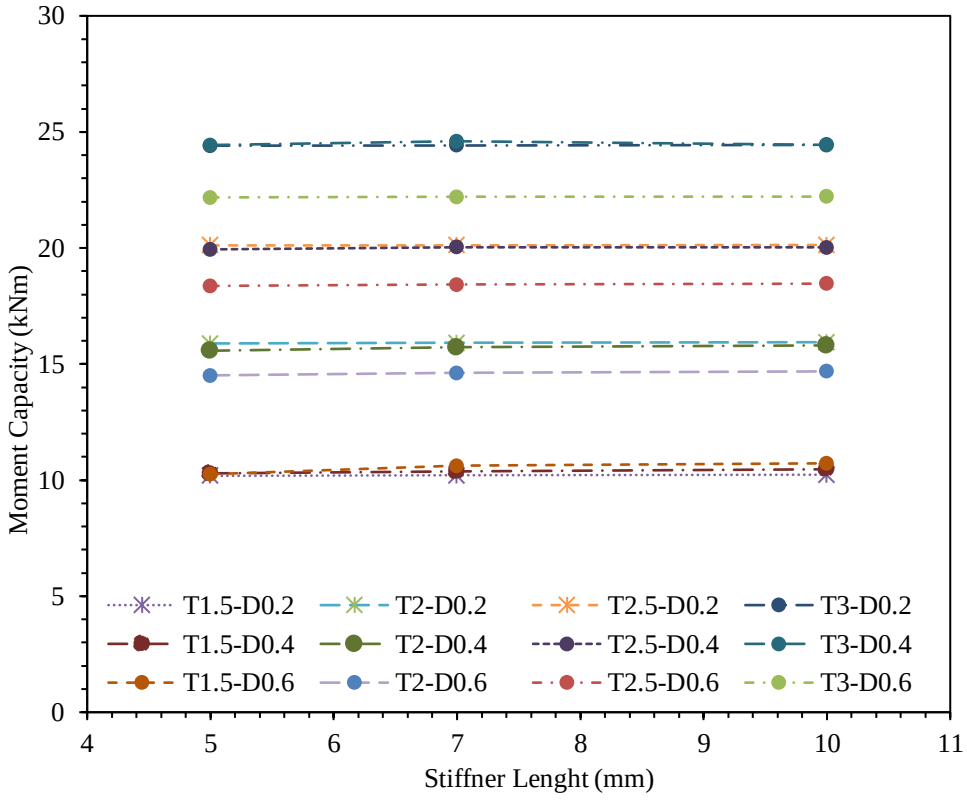

(C) Ferritic C300-L4000-T-EH3-D-Q

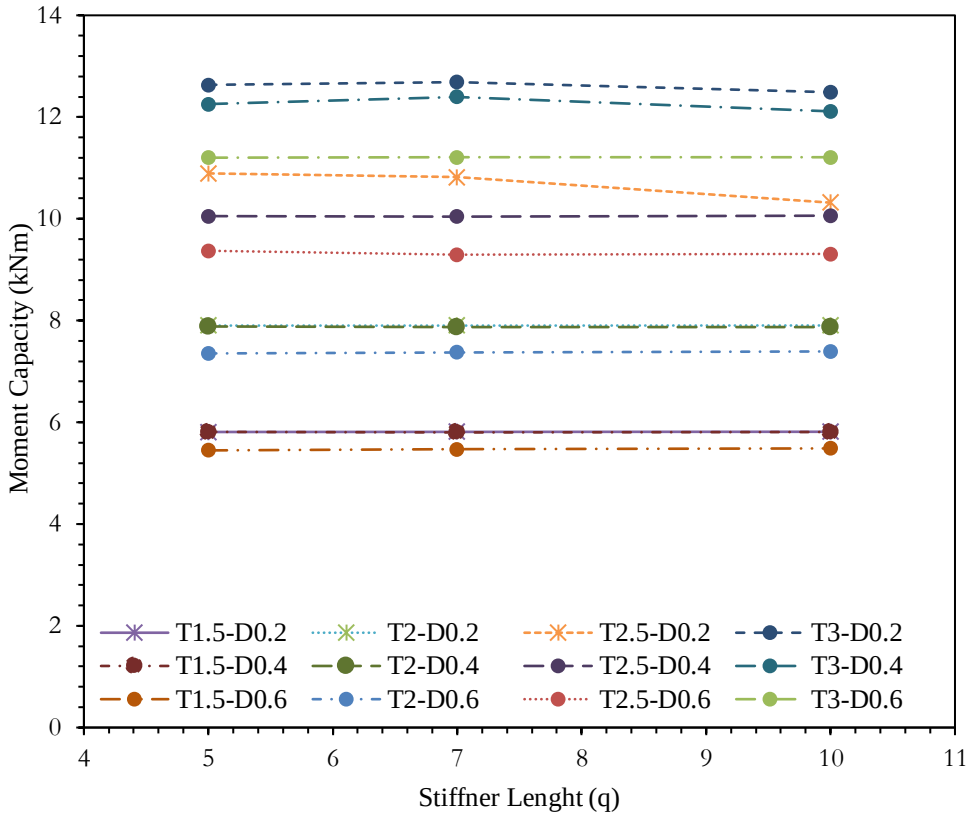

(d) Austenitic C200-L4000-T-EH3-D-Q

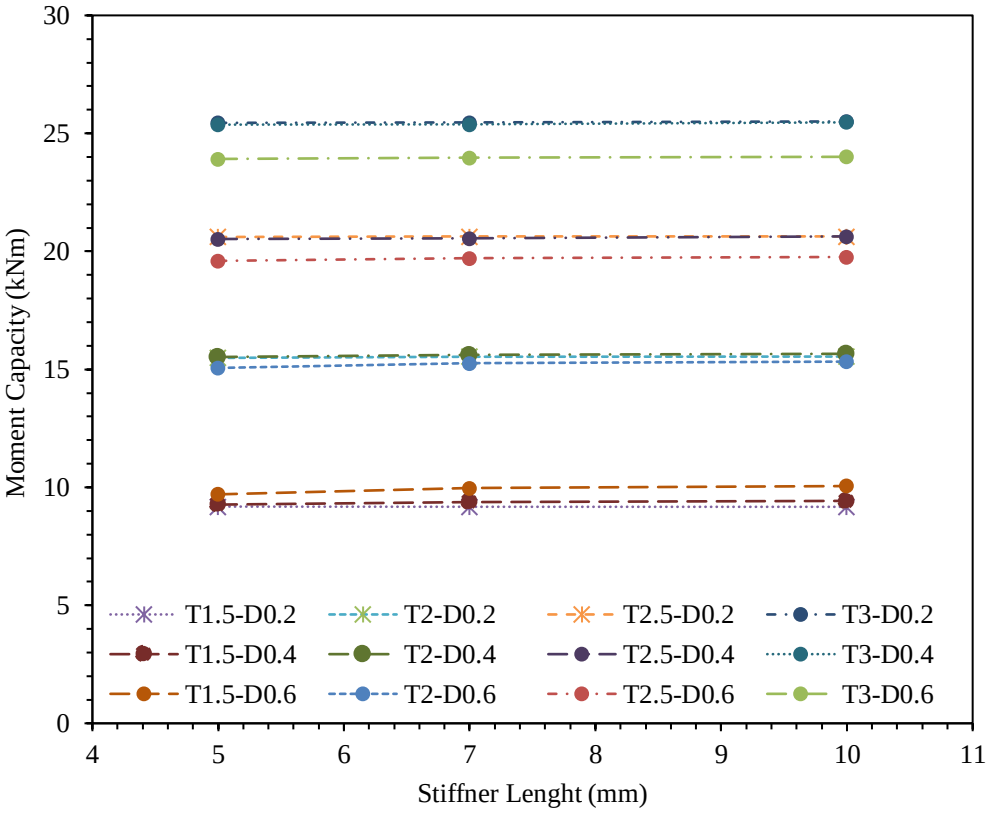

(e) Duplex C200-L4000-T-EH3-D-Q

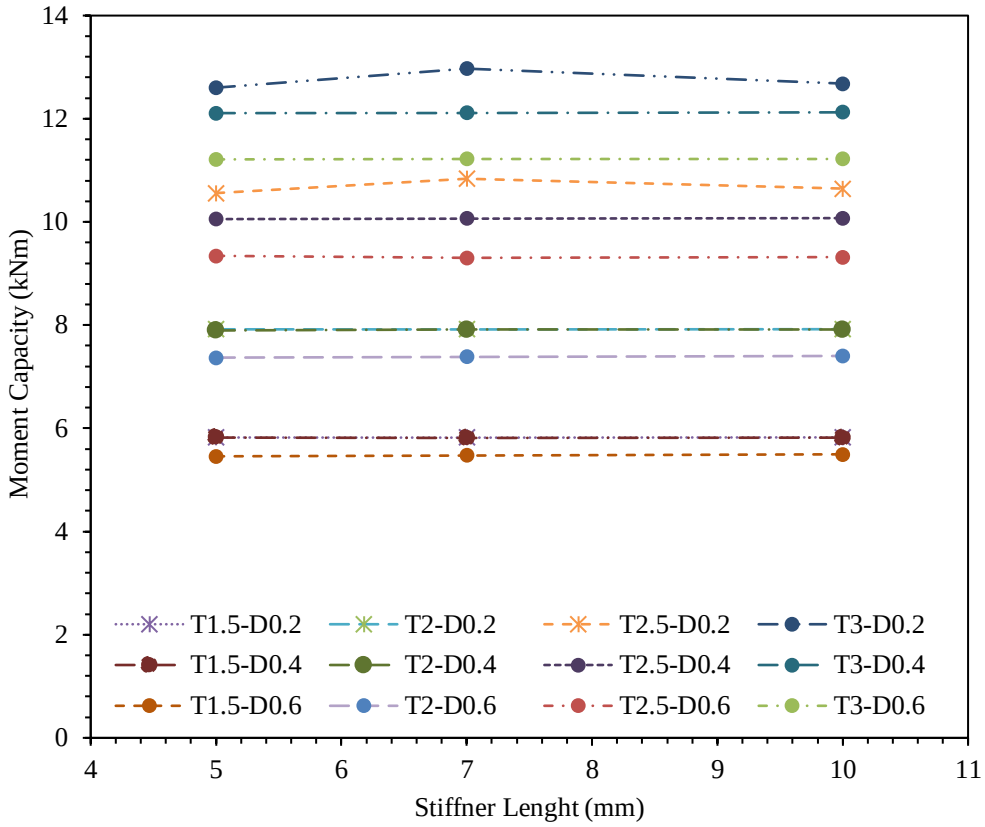

(f) Ferritic C200-L4000-T-EH3-D-Q

Figure 4-8: Effect of stiffener length for CFSS edge stiffened channel sections.

4.4.2 Comparison from un-stiffened to edge-stiffened web holes for austenitic, duplex, ferritic stainless-steel

Table 6 shows the moment capacity obtained from the FEA for unstiffened and edge-stiffened web holes for austenitic, duplex and ferritic stainless steel. For edge-stiffened one web hole where the a/h ratio varied from 0.2, 0.4 and 0.6, the average moment capacity increased by 1%; with three web holes, the moment capacity increased to 2.9%; and with five web holes, the moment capacity increased to 6%, irrespective of the grade of the stainless steel.

4.4.3 Effect of a/h ratio on moment capacity for CFSS channel section

The effect of the a/h ratio on the moment capacity of a CFSS channel section with edge-stiffened web holes is shown in Figure 4-9. From the results of the parametric study, it was found that for austenitic stainless steel, when the a/h ratio increased from 0.2 to 0.4, the moment capacity decreased by 1.02%. Similarly, for duplex CFSS channels, the moment capacity decreased by 0.5%, and for ferritic CFSS channels, it decreased by 1.2%. Likewise, when the a/h ratio was increased from

0.2 to 0.6, the moment capacity decreased for each stainless steel grade. For austenitic stainless steel, the moment capacity decreased by 7.2%, for duplex stainless steel, it decreased by 1.5%, and for ferritic stainless steel, it decreased by 7.3%. Similarly, when comparing the a/h ratio from 0.2 to 0.6, the moment capacity decreased by 6.3%, 2%, and 6.2% for austenitic, duplex, and ferritic stainless steel, respectively.

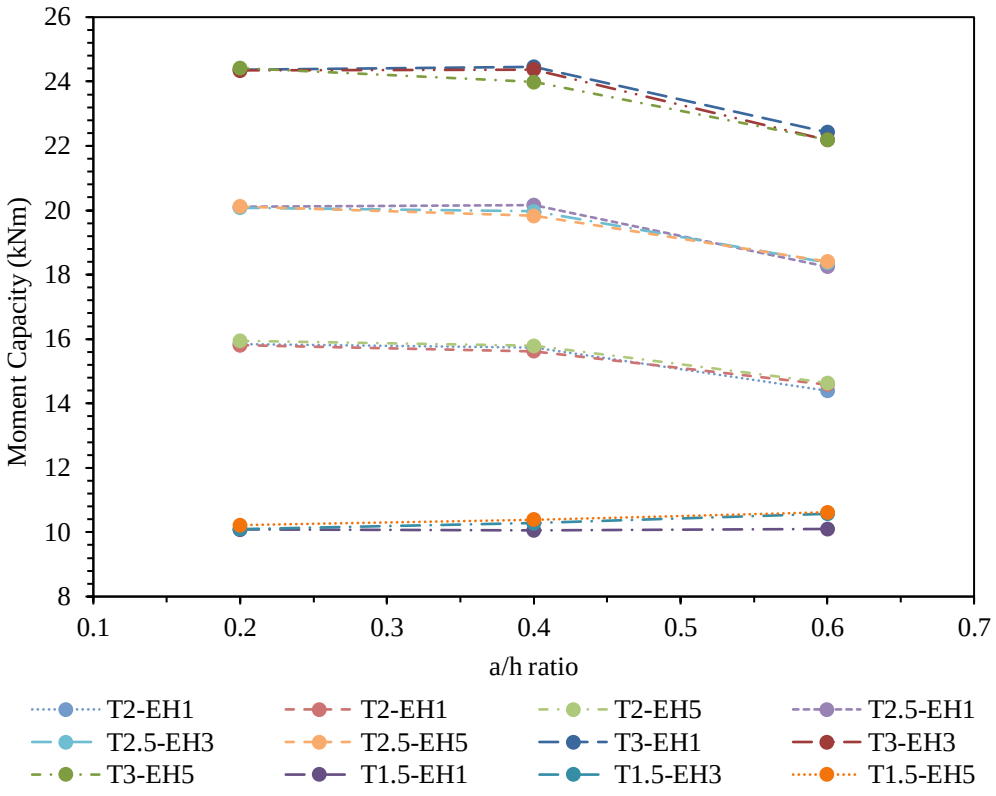

(a) Austenitic C300-T-UH-D

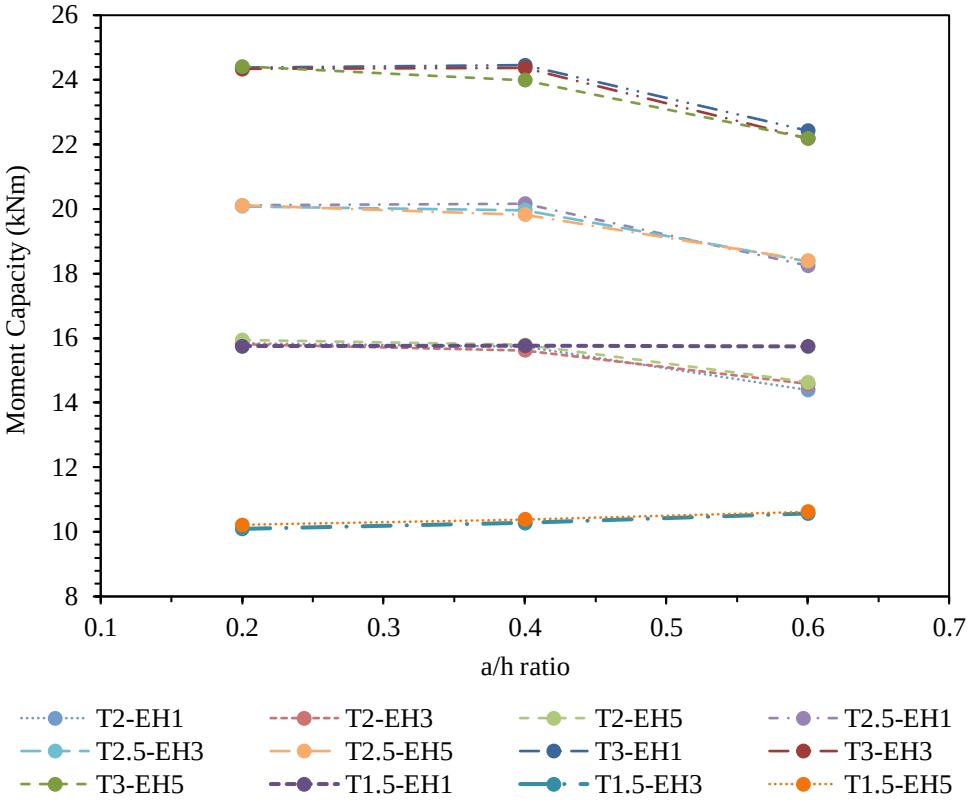

(b) Duplex C300-L4000-T-UH-D

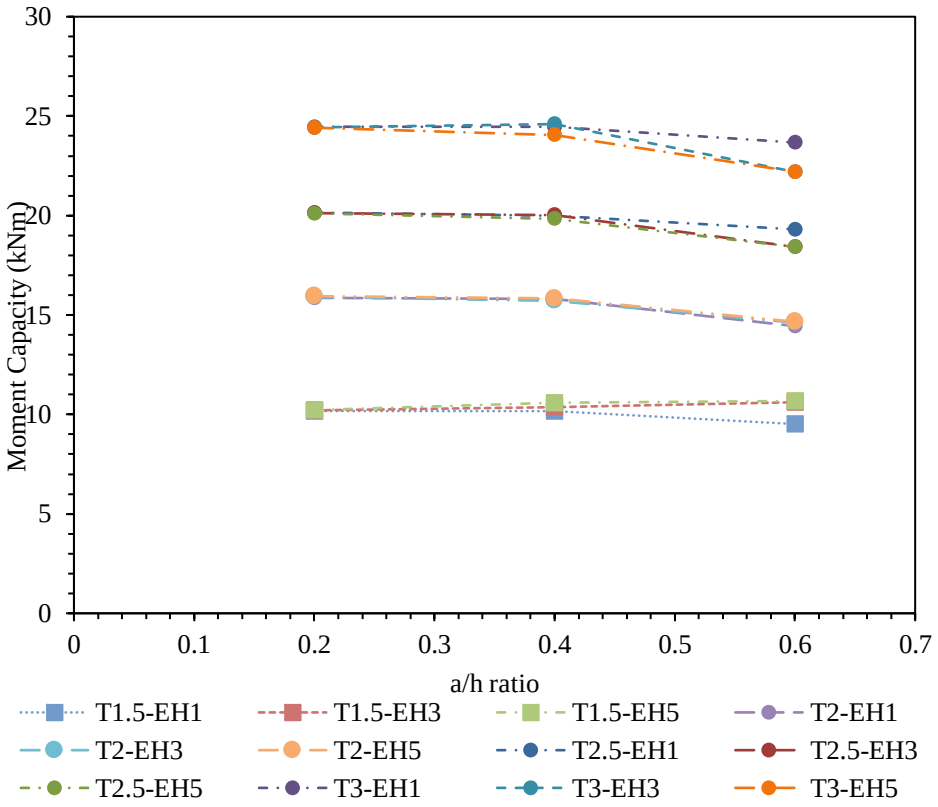

(C) Ferritic C300-L4000-T-UH-D

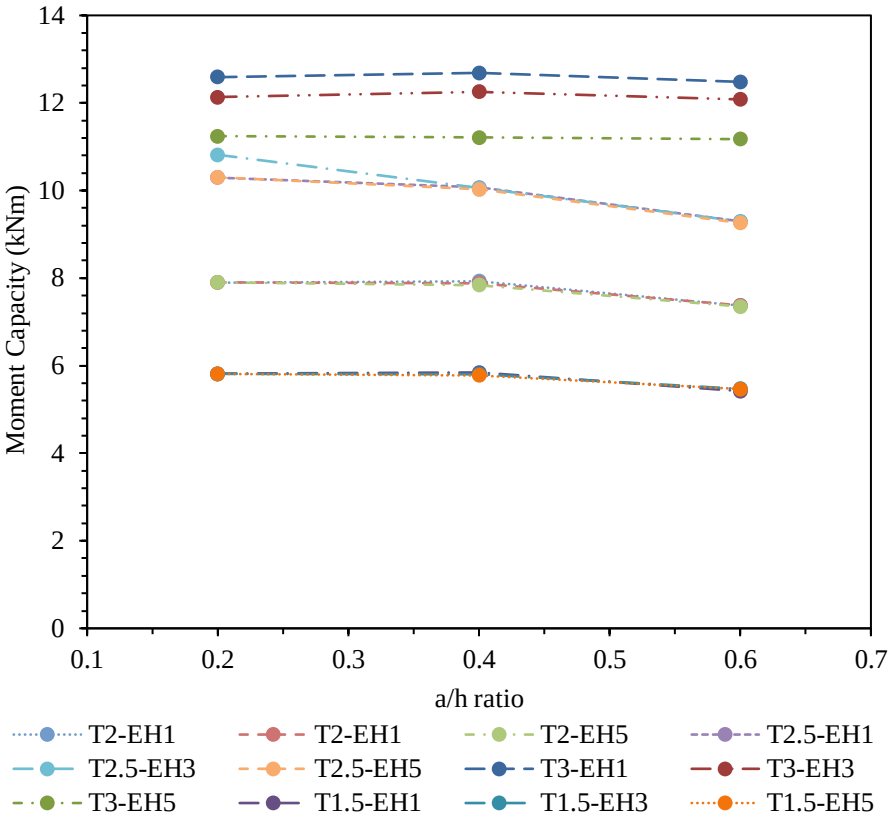

(d) Austenitic C200-T-UH-D

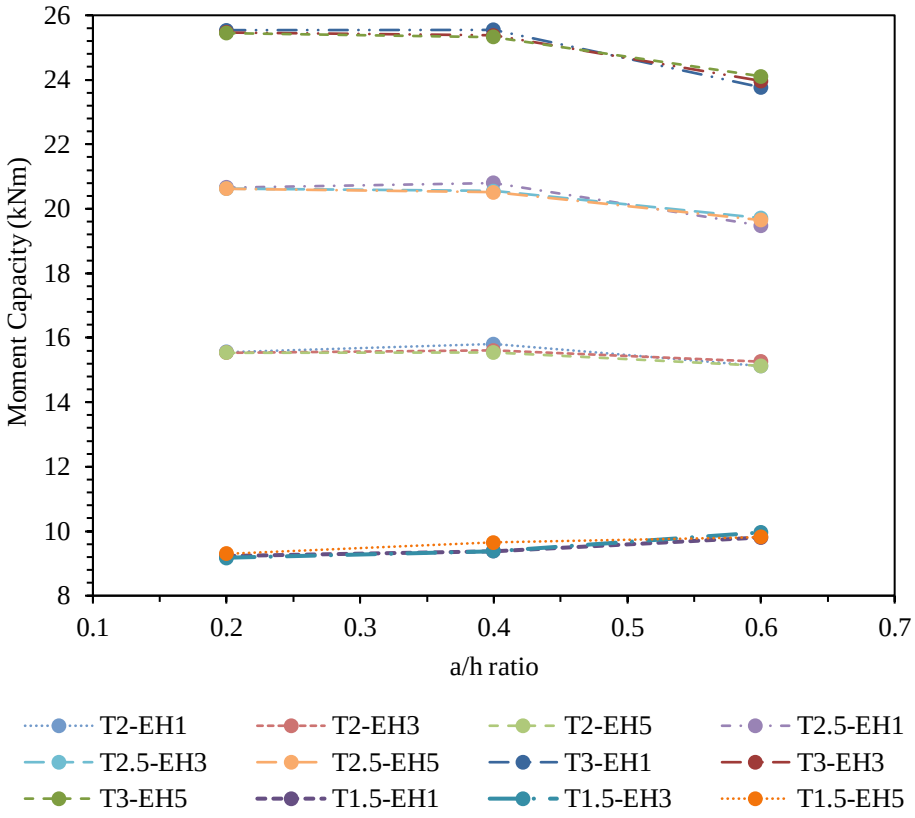

(e) Duplex C200-L4000-T-UH-D

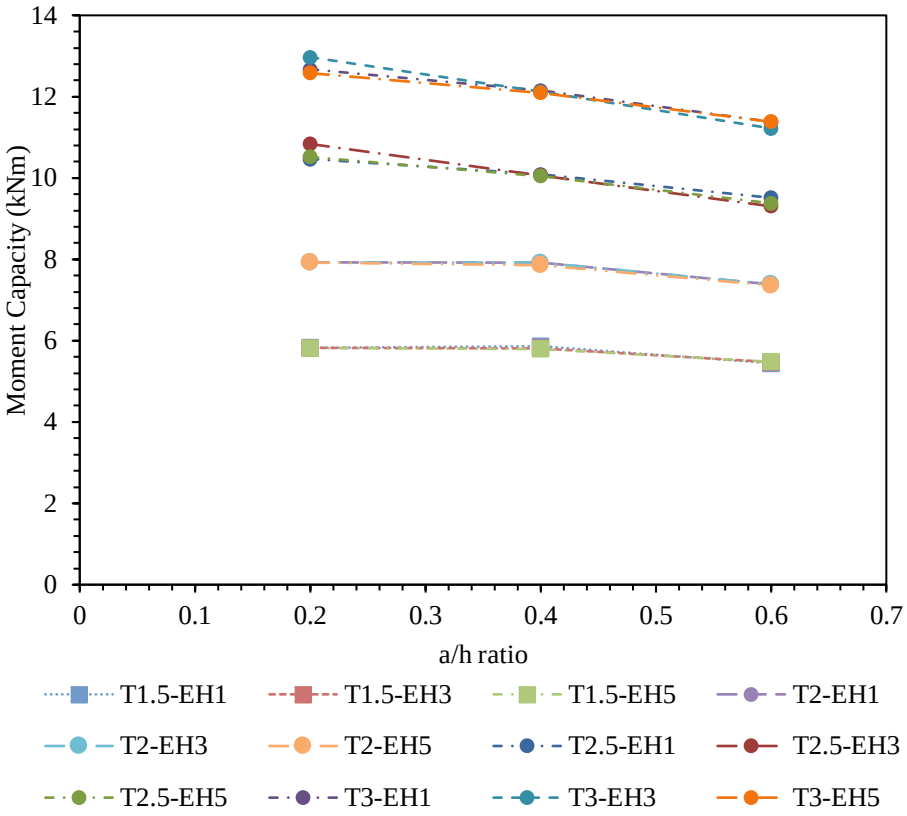

(f) Ferritic C200-L4000-T-UH-D

Figure 4-9: Effect of web hole diameter to web depth ratio for CFSS edge stiffened channel sections.

4.3.4 Effect of Number of holes on moment capacity for CFSS channel section

Figure 4-10 shows the effect of the number of holes on the moment capacity of the CFSS channel sections with unstiffened web holes. When the number of web holes increased from 1 to 3, the moment capacity decreased by 1.06%, 2.1%, and 1.8% for austenitic, duplex, and ferritic stainless steel, respectively. Similarly, when the number of holes increased from 1 to 5, the moment capacity decreased by 7.5%, 8.7%, and 8.4%. respectively.

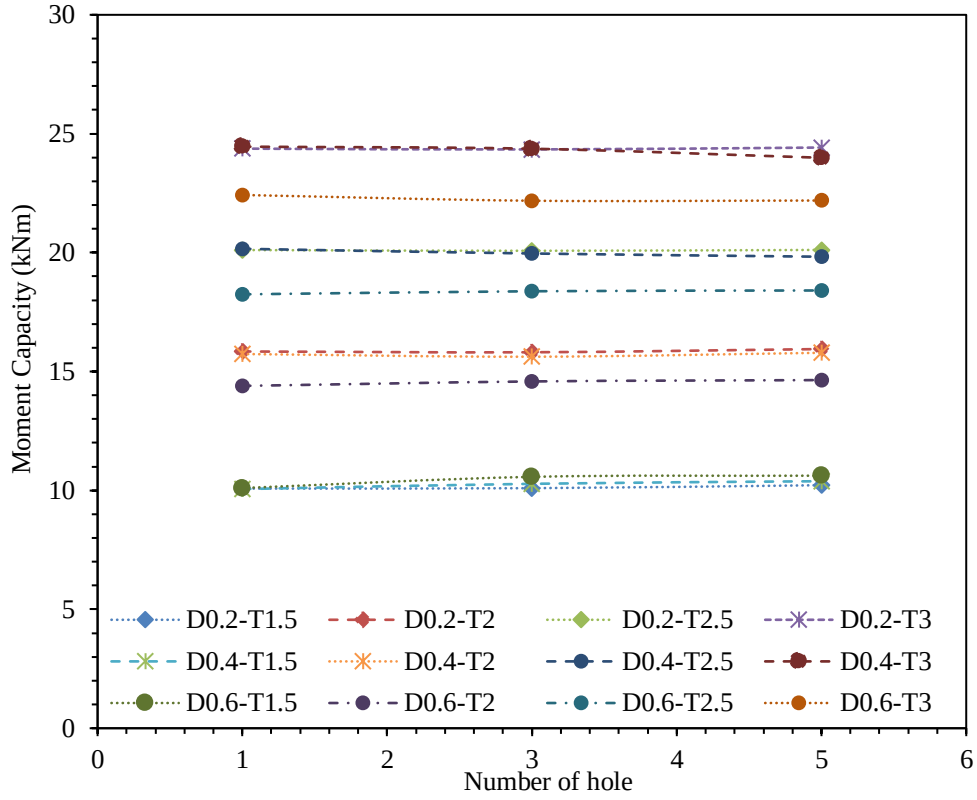

(a) Austenitic C300-L4000-EH-D-T-Q7

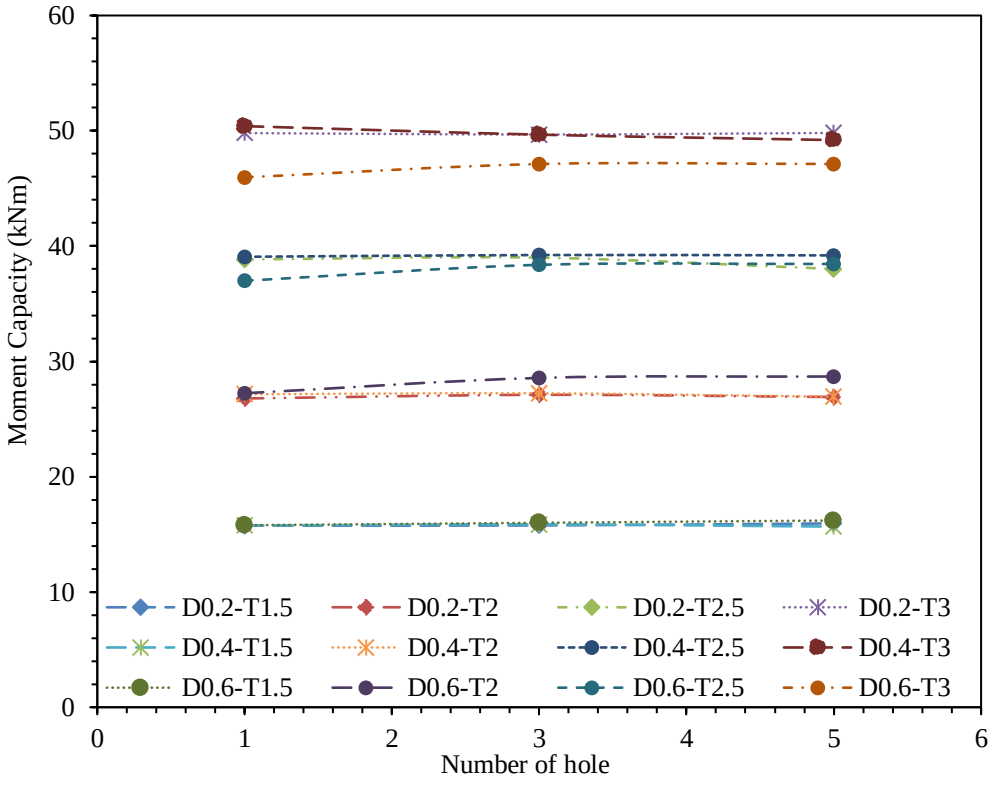

(b) Duplex C300-L4000-EH-D-T-Q7

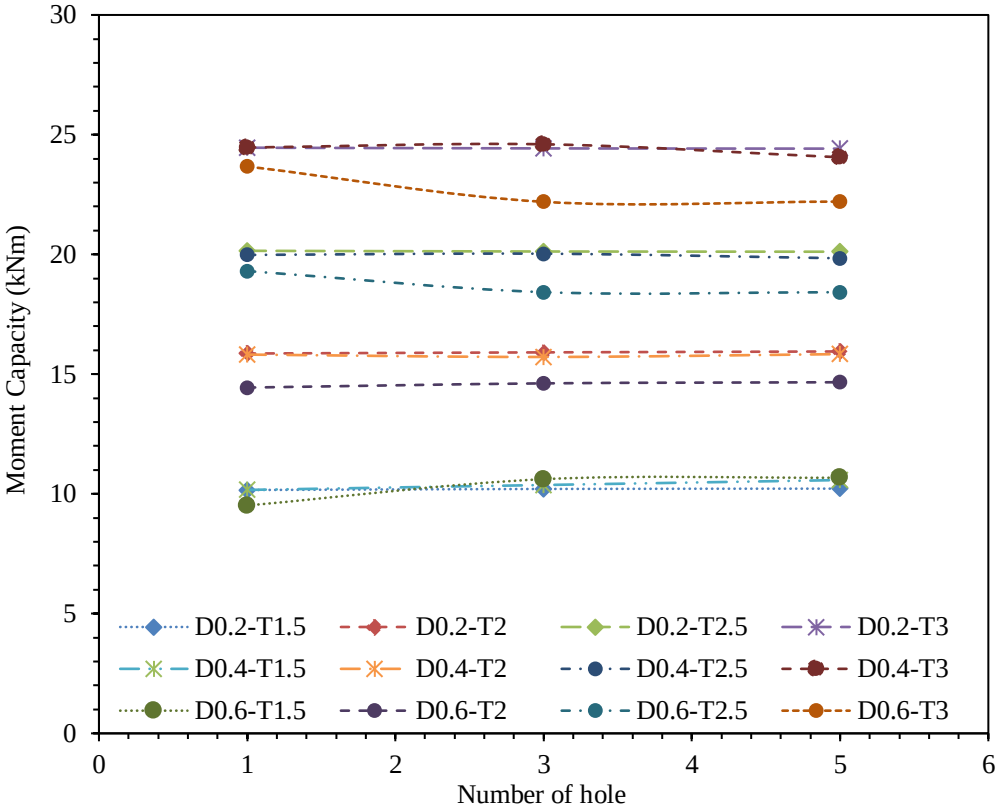

(C) Ferritic C300-L4000-EH-D-T-Q7

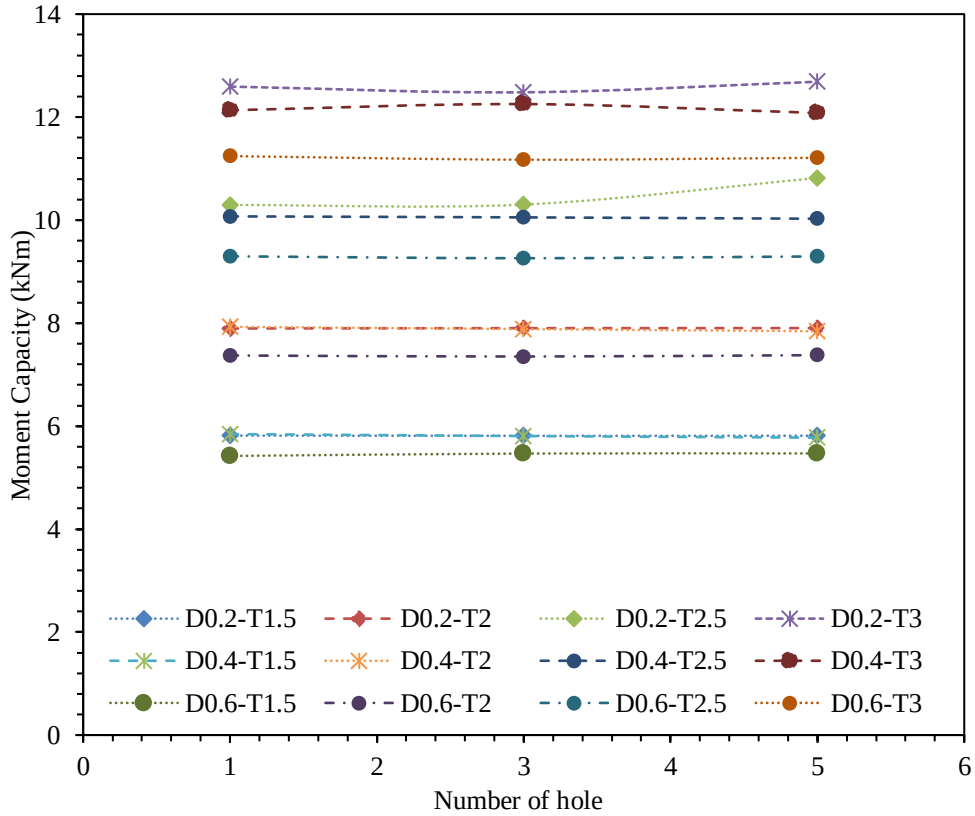

(d) Austenitic C200-L4000-EH-D-T-Q7

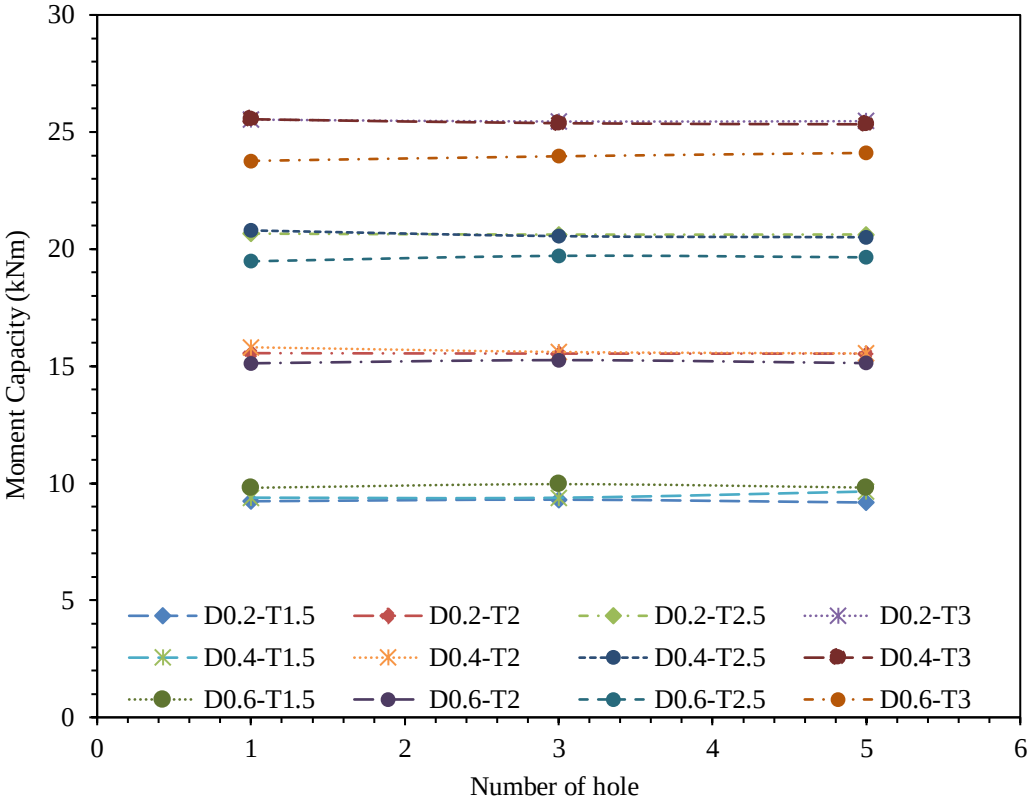

(e) Duplex C200-L4000-EH-D-T-Q7

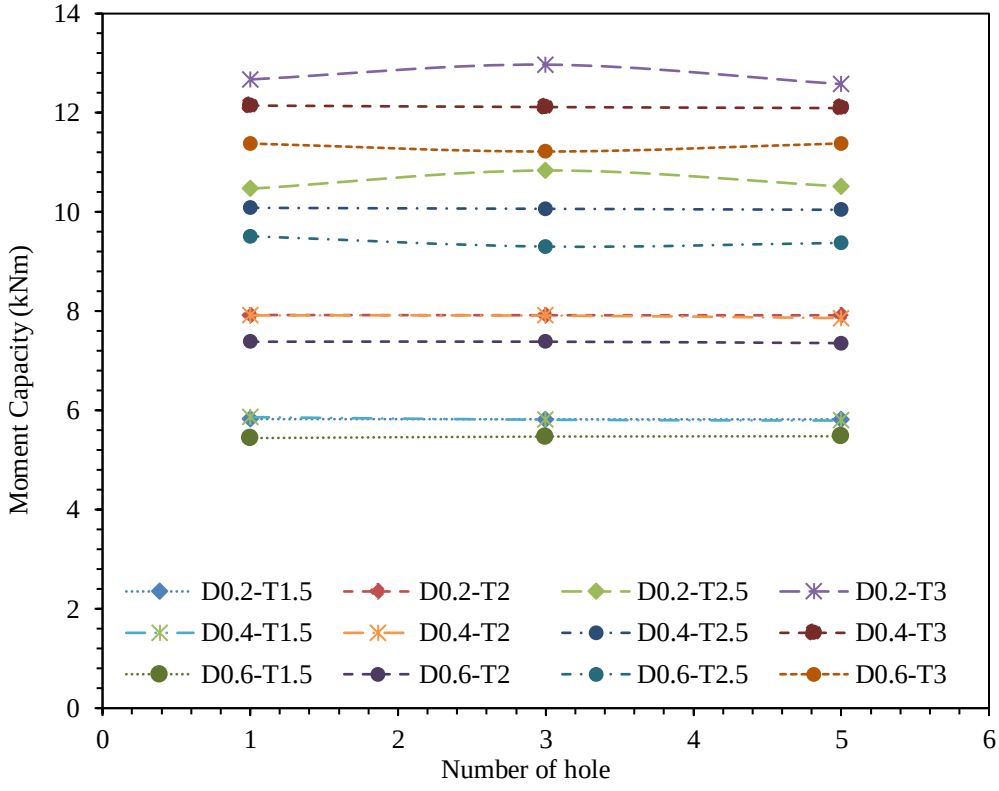

(f) Ferritic C200-L4000-EH-D-T-Q7

Figure 4-10: Effect of number of holes for CFSS edge stiffened channel section.

CHAPTER 5. Design recommendation in accordance with the AS/NZS [15]

5.1 Direct strength method (AISI 2016 and AS/NZ 2018) [14, 15]

AS/NZ [15] and AISI [14] both standards have given the recommendation for calculating the moment capacity for the CFS channel sections, and these formulae have the potential to be used for other thin-walled members (such as the CFSS section) for predicting the moment capacity.

5.1.1 DSM based formulae for CFSS without holes

The following equations can be used to calculate critical local and distortional buckling moment. The nominal design moment capacity of CFSS channel sections without web holes can be predicted from the following equations:

For local buckling

$$\lambda_1 \leq 0.776;\ \mathrm{M_l} = \mathrm{M_{be}} \tag{3}$$

$$\lambda_2 > 0.776;\ \mathrm{M_l} = \left(1 - 0.15\left(\frac{\mathrm{M_{crl}}}{\mathrm{M_{be}}}\right)^{0.4}\right)\left(\frac{\mathrm{M_{crl}}}{\mathrm{M_{be}}}\right)^{0.4}\mathrm{M_{be}} \tag{4}$$

For distortional buckling

$$\lambda_d \leq 0.673;\quad \mathrm{M_d} = \mathrm{M_y} \tag{5}$$

$$\lambda_d > 0.673;\quad \mathrm{M_d} = \left(1 - 0.22\frac{\mathrm{M_{crd}}}{\mathrm{M_y}}\right)^{0.5}\left(\frac{\mathrm{M_{crd}}}{\mathrm{M_y}}\right)^{0.5} \tag{6}$$

5.1.2 DSM based formulae for CFSS channel section with holes

5.1.2.1 Local buckling

For local buckling ($\mathrm{M_l}$), the nominal moment capacity of the channel sections with unstiffened web holes was calculated using Eq. (7) and (8), as given next.

$$\lambda_\mathrm{l} \leq 0.776;\ \mathrm{M_l} = \mathrm{M_{be}} \leq \mathrm{M_{ynet}} \tag{7}$$

$$\lambda_\mathrm{l} \leq 0.776;\quad \mathrm{M_l} = \left[1 - 0.15\left(\frac{\mathrm{M_{crl}}}{\mathrm{M_{be}}}\right)^{0.4}\right]\left(\frac{\mathrm{M_{crl}}}{\mathrm{M_{be}}}\right)^{0.4}\mathrm{M_{be}} \leq \mathrm{M_{ynet}} \tag{8}$$

$$\mathrm{M_{crl}} = \min\left(\mathrm{M_{crlg}}, \mathrm{M_{crln}}\right) \tag{9}$$

5.1.2.2. Distortional buckling

Moen and Schafer [19] proposed the details for obtaining the distortional buckling load for unstiffened web hole. The followings are the equations for calculating the distortional buckling load (M_d).

$$\text{For, } \lambda_d \leq \lambda_{1d};\ M_d = M_{ynet} \tag{10}$$

$$\text{For, } \lambda_{1d} < \lambda_d \leq \lambda_{2d};\ M_d = M_{ynet} - \left(\frac{M_{ynet} - M_{2d}}{\lambda_{2d} - \lambda_{1d}}\right)(\lambda_d - \lambda_{1d}) \tag{11}$$

$$\text{For, } \lambda_d > \lambda_{d2};\ M_d = [1 - 0.22\left(\frac{M_{crd}}{M_y}\right)^{0.5}]\left(\frac{M_{crd}}{M_y}\right)^{0.5} M_y \tag{12}$$

$$\lambda_d = \sqrt{\frac{M_y}{M_{crd}}} \tag{13}$$

$$\lambda_{1d} = 0.673\left(\frac{M_{ynet}}{M_y}\right)^3 \tag{14}$$

$$\lambda_{2d} = 0.673\left[1.7\left(\frac{M_y}{M_{ynet}}\right)^{2.7} - 0.7\right] \tag{15}$$

$$M_{2d} = \left[1 - 0.22\left(\frac{1}{\lambda_{2d}}\right)\right]\left(\frac{1}{\lambda_{2d}}\right) M_y \tag{16}$$

The elastic distortional buckling moment of CFS channel sections with un-stiffened web holes can be calculated using Equation (17), as given next.

$$M_{crd} = \min (M_{crdg}, M_{crdn}) \tag{17}$$

M_{crdg} and M_{crdn} can be obtained from the CUFSM hole module.

5.2 Comparison of design moment capacity with FEA results

The moment capacity obtained from the parametric study for CFSS plain webs channel sections were compared with the design strength predicted by the AISI [14] and AS/NZS [15] for the cold formed carbon steel channel sections. It was observed that the mean values for austenitic, duplex, and ferritic stainless steel are 0.96, and the coefficient of variation (COV) for the $M_{FEA}/M_{(AISI\ \&\ AS/NZS)}$ ratio is 0.04 (see Table 7 and Figure 5-1).

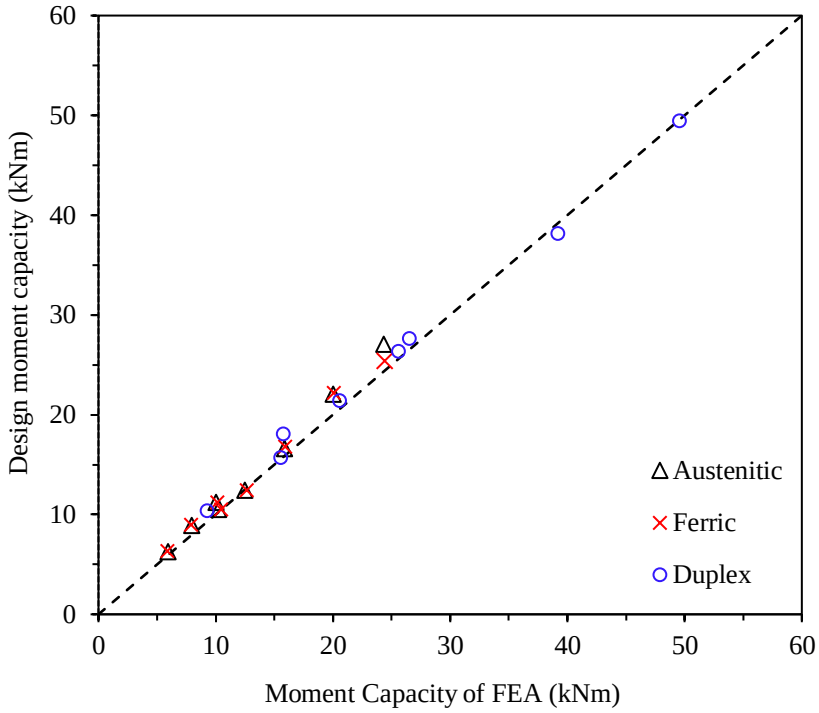

Figure 5-1: Comparison of design moment capacity from AISI [14] and AS/NZS [15] with FEA results for plain channel sections.

The moment capacity of the CFSS channel sections with unstiffened web holes obtained from the parametric results was compared with the strengths determined by the AISI [14] and AS/NZS [15]. From the comparison results (see Table 8 and Figure 5-2), it was found that the mean values for austenitic, duplex, and ferritic stainless steel are 0.99, 0.99 and 1.05, respectively and the COVs of $M_{FEA}/M_{(AISI\ \&\ AS/NZS)}$ ratio are 0.03, 0.03 and 0.07, respectively.

For the CFSS channel section with edge-stiffened web holes, the FEA results for the CFSS channel sections were compared with the design equation proposed by Dai et al. [29]. Dai et al.'s design equations were conservative on average by 1.5%, 1.8% and 10.3% for austenitic, duplex, and ferritic stainless steel, respectively (see Table 9 and Figure 5-3).

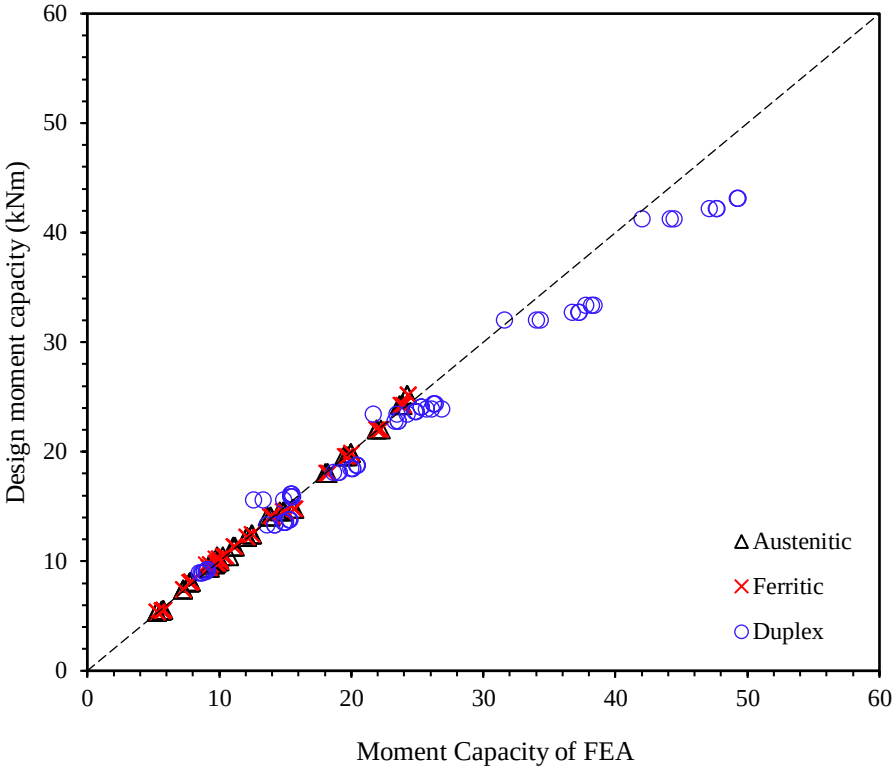

Figure 5-2: Comparison of design moment capacity from AISI [14] and AS/NZS [15] with FEA results for unstiffened channel sections.

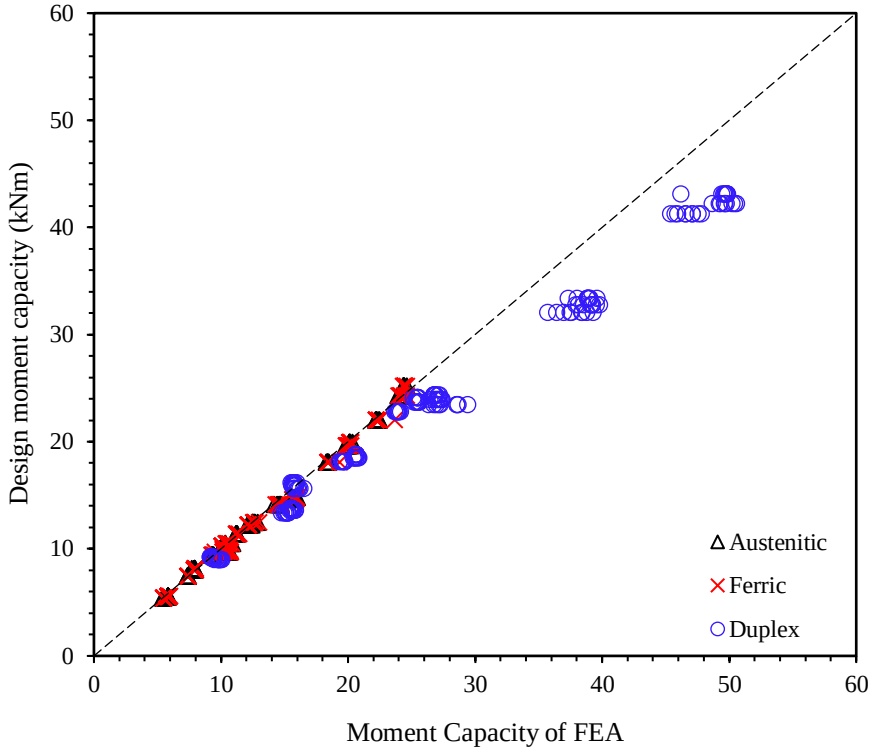

Figure 5-3 Comparison of design moment capacity from AISI [14] and AS/NZS [15] with FEA results for edge stiffened channel sections.

CHAPTER 6. Proposed design equation and Reliability analysis

6.1 Proposed design equation

Based on the comparison of the FE results with the current DSM equation, it can be concluded that the DSM equation effectively predicts the moment capacity of CFSS channels without any web openings when subjected to distortional buckling conditions. However, it is crucial to note that the introduction of web openings significantly reduces the section's moment capacity, which needs further investigation and predicted using design equations.

Reduction factor design equations (Eqs. 18, 19, and 20) were proposed herein, considering key parameters such as web hole ratio $^{a}/_{h}$, thickness ratio $^{t}/_{h}$ and stiffener length ratio $^{q}/_{h}$ Therefore, the ultimate moment capacity of CFSS sections with holes can be obtained by applying the proposed reduction factor equation to the moment capacity of the solid sections. The moment capacity of solid sections can be predicted using DSM equations. Besides, the comparison of the numerical results with the proposed reduction factor equations resulted in a well-matched mean value of 0.99 and a COV value of 0.02.

$$M_{opening} = M_{solid} \times q_{s.prop} \tag{18}$$

For unstiffened web holes,

$$q_{s,Prop} = 0.909 - 0.225\left(\frac{a}{h}\right) + 8.575\left(\frac{t}{h}\right) \qquad for \quad 0 < \frac{a}{h} \leq 0.6 \tag{19}$$

For edge-stiffened web holes,

$$q_{s,Prop} = 0.942 + 0.124\left(\frac{a}{h}\right) + 4.145\left(\frac{t}{h}\right) - 0.142\left(\frac{q}{h}\right) \qquad for \quad 0 < \frac{a}{h} \leq 0.6 \tag{20}$$

The proposed reduction factor equations are limited to CFSS channel sections with unstiffened and edge-stiffened web holes within these ranges: 200 mm ≤ web depth (h) ≤ 300 mm, 0.2 ≤ ratio of hole depth to web depth ($^{a}/_{h}$) ≤ 0.6, 1.5mm ≤ thickness (t) ≤ 3 mm, 5mm ≤ stiffener length (q) ≤ 10 mm.

6.2 Reliability analysis

A reliability analysis was also carried out to assess the reliability of the proposed reduction factor equations for CFSS channel sections with unstiffened and edge-stiffened web holes. The ASCE [7] provides an equation [Eq. 21] and suggests that the minimum target reliability index value for CFSS structural members should be 2.5. The reliability of the design equations is considered reliable when the value of the reliability index (β) is 2.5 or above. The modified reduction factor equations were found to be trustworthy while calculating the moment capacity of CFSS channel sections with unstiffened and edge-stiffened web holes (see Tables 10).

$$\varphi = 1.52 M_m F_m \, P_m e^{-\beta \sqrt{\{V_m{}^2 + V_f{}^2 + C_p V_p{}^2 + V_q{}^2\}}} \tag{21}$$

where β is the reliability index, φ for resistance factor (0.85), M_m and V_m for mean (1.1) and COV (0.1) of the material factor, F_m and V_f for mean (1.0) and COV (0.05) of the fabrication factor, P_m and V_P for mean and COV of the proposed equation, V_q for COV (0.21) of the load effect, C_p for correction factor $\left[1 + \frac{1}{n}\right]\left[\frac{m}{m-2}\right]$, *n* for number of tests, and *m* for degree of freedom (*m = n-1*).

CHAPTER 7. Conclusions, limitations of the current study and future study

7.1 Conclusions

This research investigates the flexural behavior of CFSS channel sections, considering both unstiffened and edge-stiffened web holes. The finite element (FE) model incorporates non-linear material properties and initial geometric imperfections. Validation of the FE model was conducted using experimental results reported by Chen et al. [9], demonstrating good agreement in terms of failure modes and ultimate moment capacity. A comprehensive parametric study involving 888 FE models, based on the validated FE model, examined the influence of web depth, number of holes, thickness, hole diameter, and stiffener lengths on the moment capacity of CFSS channel sections with unstiffened web holes, edge-stiffened web holes, and sections without web holes (refer to Table 4, 5 and 6).

The moment capacity obtained from the FE analysis was compared with the design moment capacity according to the AISI [14] and AS/NZS [15] for sections with unstiffened web holes. Results showed a slight unconservative of 0.6% and 0.3% for austenitic and ferritic stainless-steel materials, respectively, and an over conservative of 5% for duplex stainless-steel materials.

Additionally, the design equations proposed by Dai et al. [29] for sections with edge-stiffened web holes were compared with FEA results. The equations were found to be overconservative by 1.5%, 10%, and 2% for austenitic, duplex, and ferritic stainless-steel materials, respectively. To address distortional buckling failure, modified DSM-based design equations, accounting for reduction factors, were proposed for CFSS channel sections with edge-stiffened web holes to predict their moment capacity. Finally, a reliability analysis was performed to demonstrate the reliability of the proposed equations.

7.2 Limitations of the current study and future study

These are the limitations of the current study:

- The research is confined to specific grades of stainless steel (austenitic, duplex, and ferritic).
- Only two cross-sectional dimensions (C200x65x15 and C300x80x20) were investigated numerically.
- Only one channel length (L = 4000 mm) was considered.

Therefore, the proposed reduction factor equations were limited to the considered parameters using FEA analysis. However, it is known from previous research studies that the length of channel sections will also influence the structural behaviour and moment capacity of the CFSS channel sections. Therefore, here are some of the further research recommendations.

- Conduct experimental research on the CFSS channel sections.
- Investigate different loading conditions like shear behaviour and axial strength.
- Further exploration is needed to examine the parametric effects of the varied length of the CFSS channel sections, cross-section dimensions and other grades of stainless steel.

Table 1 Summary of the material properties used in this study [3-6].

Stainless Steel Material	Yield stress, f_y MPa	Ultimate stress, f_u MPa	Modulus of elasticity, E GPa
Austenitic	205.62	825	193
Duplex	451.91	860	200
Ferritic	205.62	597	200

Table 2 Comparison of moment capacity obtained from Chen et al. [9] test results with FEA.

Section dimensions									Moment capacity	
Web	Flange	Lip	Length	Thickness	Stiffener	Diameter	Hole spacing	Number of holes	Test	FEA
h	b_f	b_l	L	t	q	a	s	n	M_{EXP}	M_{FEA}
(mm)	(mm)	(mm)	(mm)	(mm)	(mm)	(mm)	(mm)	(mm)	(kN·m)	(kN·m)
Plain wens										
240.0	45	15	4000	1.81	-	-	-	-	11.9	13.13
240.0	45	15	4000	2.11	-	-	-	-	18.0	21.28
Edge stiffened web holes										
240.0	45	15	4000	1.81	13	140	-	1	12.9	13.7
240.0	45	15	4000	1.81	13	140	240	3	13.3	13.29
240.0	45	15	4000	1.81	13	140	190	5	13.7	12.85
290.0	45	15	4000	2.11	13	140	-	1	19.3	21.34
290.0	45	15	4000	2.11	13	140	-	3	19.8	21.29
290.0	45	15	4000	2.11	13	140	-	5	20.5	21.38

Unstiffened web holes										
240.0	45	15	4000	1.81	-	140	-	1	11.0	12.59
240.0	45	15	4000	1.81	-	140	240	3	10.6	12.16
240.0	45	15	4000	1.81	-	140	190	5	10.2	11.31
290.0	45	15	4000	2.11	-	140	-	1	16.7	20.40
290.0	45	15	4000	2.11	-	140	-	3	16.3	20.21
290.0	45	15	4000	2.11	-	140	-	5	15.7	19.87

Table 3 Selected variables for parametric study.

Channel sections	Web h	Flange b	lip l	Stiffner lenght q	Thickness t	Length of the channel section L	Ratio of hole depth to web depth a/h	Material Properties
					(mm)			
C 200 x 65 x 15	200	65	15	5	[1.5- 3.0]	4000	0.2	Ferritic stainless steel
C 300 x 80 x 20	300	80	20	7			0.4	Duplex stainless steel
				10			0.6	Austenitic stainless steel

Table 4 Moment capacity obtained from the parametric study results for austenitic CFSS channel sections.

Specimens	Plain webs	Edge stiffened web holes									Unstiffened web holes		
		EH1			EH3			EH5			UH1	UH3	UH5
		Q5	Q7	Q10	Q5	Q7	Q10	Q5	Q7	Q10			
C200T1.5D0.2	5.78	5.815	5.816	5.819	5.81	5.813	5.814	5.809	5.811	5.812	5.796	5.794	5.797
C200T1.5D0.4	5.78	5.825	5.845	5.846	5.801	5.807	5.81	5.764	5.776	5.78	5.684	5.675	5.63
C200T1.5D0.6	5.78	5.379	5.42	5.461	5.448	5.469	5.487	5.452	5.467	5.471	5.27	5.296	5.269
C200T2.0D0.2	7.9	7.907	7.896	7.688	7.902	7.903	7.904	7.9	7.902	7.904	7.879	7.881	7.878
C200T2.0D0.4	7.9	7.934	7.928	7.979	7.872	7.884	7.872	7.826	7.841	7.848	7.793	7.776	7.749
C200T2.0D0.6	7.9	7.338	7.372	7.4	7.354	7.378	7.393	7.338	7.351	7.366	7.299	7.294	7.256
C200T2.5D0.2	10.283	10.301	10.294	10.287	10.893	10.817	10.318	10.3	10.302	10.304	9.827	10.77	10.283
C200T2.5D0.4	10.283	10.062	10.073	10.081	10.043	10.053	10.062	10.116	10.027	10.036	9.952	9.969	10.015
C200T2.5D0.6	10.283	9.373	9.297	9.321	9.372	9.295	9.307	9.247	9.26	9.271	9.295	9.244	9.193
C200T3.0D0.2	12.498	12.892	12.593	12.493	12.631	12.687	12.489	12.499	12.482	12.486	12.494	12.489	12.478
C200T3.0D0.4	12.498	12.127	12.133	12.142	12.395	12.253	12.113	12.071	12.081	12.09	12.121	12.105	12.059
C200T3.0D0.6	12.498	11.219	11.243	11.259	11.202	11.21	11.211	11.165	11.173	11.176	11.196	11.125	11.077

C300T1.5D0.2	10.069	10.086	10.079	10.07	10.072	10.094	10.117	10.193	10.22	10.326	10.032	10.017	9.921
C300T1.5D0.4	10.069	10.065	10.056	10.046	10.166	10.279	10.325	10.254	10.387	10.525	9.715	9.811	9.74
C300T1.5D0.6	10.069	10.053	10.1	10.113	10.188	10.571	10.654	10.402	10.62	10.706	8.987	9.269	9.249
C300T2.0D0.2	15.869	15.837	15.843	15.746	15.774	15.81	15.841	15.903	15.944	15.989	15.705	15.613	15.597
C300T2.0D0.4	15.869	15.585	15.736	15.788	15.464	15.623	15.747	15.669	15.787	15.84	14.934	14.838	14.624
C300T2.0D0.6	15.869	14.2	14.395	14.502	14.453	14.583	14.658	14.568	14.64	14.679	13.676	13.888	13.924
C300T2.5D0.2	20.068	20.109	20.109	20.111	20.065	20.077	20.085	20.106	20.114	20.304	20	19.993	19.98
C300T2.5D0.4	20.068	20.08	20.161	20.24	19.894	19.963	20.001	19.795	19.827	19.86	19.719	19.641	19.457
C300T2.5D0.6	20.068	18.329	18.245	18.362	18.343	18.375	18.448	18.373	18.408	18.449	18.244	18.197	18.044
C300T3.0D0.2	24.359	24.354	24.372	24.378	24.315	24.339	24.353	24.389	24.418	24.621	24.262	24.247	24.233
C300T3.0D0.4	24.359	24.387	24.456	24.462	24.297	24.368	24.366	23.887	23.988	24.05	23.923	23.803	23.679
C300T3.0D0.6	24.359	22.317	22.424	22.43	22.158	22.182	22.196	22.166	22.191	22.217	22.244	21.982	21.922

Table 5 Moment capacity obtained from the parametric study results for duplex CFSS channel sections.

Specimens	Plain webs	Edge stiffened web holes									Unstiffened web holes		
		EH1			EH3			EH5			UH1	UH3	UH5
		Q5	Q7	Q10	Q5	Q7	Q10	Q5	Q7	Q10			
C200T1.5D0.2	9.315	9.251	9.23	9.355	9.176	9.177	9.174	9.29	9.298	9.311	9.155	9.141	9.12
C200T1.5D0.4	9.315	9.43	9.383	9.445	9.269	9.381	9.426	9.475	9.646	9.679	9.061	8.907	8.914
C200T1.5D0.6	9.315	9.763	9.805	9.856	9.703	9.961	10.055	9.49	9.814	9.958	8.767	8.672	8.522
C200T2.0D0.2	15.547	15.54	15.556	15.422	15.486	15.536	15.543	15.512	15.537	15.555	15.379	15.322	15.37
C200T2.0D0.4	15.547	15.694	15.806	15.843	15.524	15.608	15.66	15.391	15.542	15.631	14.922	15.076	14.989
C200T2.0D0.6	15.547	14.962	15.122	15.241	15.061	15.258	15.329	14.772	15.13	15.281	14.258	14.221	13.633
C200T2.5D0.2	20.591	20.633	20.661	20.635	20.61	20.624	20.635	20.601	20.619	20.629	20.421	20.494	20.476
C200T2.5D0.4	20.591	20.746	20.797	20.834	20.525	20.554	20.635	20.387	20.507	20.525	20.146	20.154	20.024
C200T2.5D0.6	20.591	19.34	19.478	19.598	19.598	19.712	19.763	19.326	19.648	19.725	19.15	19.054	18.689
C200T3.0D0.2	25.618	25.479	25.53	25.12	25.447	25.465	25.507	25.435	25.447	25.46	25.316	25.354	25.358
C200T3.0D0.4	25.618	25.62	25.547	25.541	25.371	25.376	25.467	25.204	25.33	25.388	24.947	24.93	24.845
C200T3.0D0.6	25.618	23.67	23.767	23.855	23.917	23.964	24.008	23.846	24.108	23.992	23.592	23.572	23.33

C300T1.5D0.2	15.765	15.759	15.752	15.739	15.76	15.769	15.759	15.619	15.948	15.973	15.527	15.506	15.468
C300T1.5D0.4	15.765	15.77	15.766	15.745	15.877	15.866	15.545	15.843	15.671	15.747	15.573	15.473	15.47
C300T1.5D0.6	15.765	15.71	15.786	15.814	15.764	16.001	16.109	15.701	16.2	16.534	14.901	13.381	12.625
C300T2.0D0.2	26.53	26.794	26.783	26.841	26.768	27.101	26.838	26.764	26.911	26.971	26.401	26.311	26.27
C300T2.0D0.4	26.53	26.812	27.147	27.073	27.331	27.236	27.365	26.445	26.936	27.397	26.122	26.881	25.713
C300T2.0D0.6	26.53	26.322	27.234	27.136	26.965	28.566	28.563	26.758	28.686	29.395	24.292	23.512	21.719
C300T2.5D0.2	39.225	38.842	38.843	38.877	38.89	38.997	39.03	37.614	38.016	38.871	38.443	38.223	37.801
C300T2.5D0.4	39.225	38.121	39.073	39.224	38.548	39.225	39.552	37.932	39.193	39.82	37.284	37.291	36.799
C300T2.5D0.6	39.225	35.708	36.991	37.593	37.457	38.375	38.792	36.426	38.451	39.292	34.331	34.082	31.639
C300T3.0D0.2	49.597	49.659	49.802	49.867	49.55	49.678	49.75	48.212	49.816	49.995	49.271	49.34	49.286
C300T3.0D0.4	49.597	50.241	50.404	50.564	49.321	49.665	49.774	48.668	49.195	49.625	47.668	47.718	47.167
C300T3.0D0.6	49.597	45.373	45.962	46.53	46.58	47.119	47.555	45.728	47.122	47.787	44.48	44.207	42.075

Table 6 Moment capacity obtained from the parametric study results for ferritic CFSS channel sections.

Specimens	Plain webs	Edge stiffened web holes									Unstiffened web holes		
		EH1			EH3			EH5			UH1	UH3	UH5
		Q5	Q7	Q10	Q5	Q7	Q10	Q5	Q7	Q10			
C200T1.5D0.2	5.896	5.826	5.827	5.971	5.822	5.823	5.824	5.835	5.822	5.823	5.808	5.808	5.808
C200T1.5D0.4	5.896	5.861	5.866	5.85	5.82	5.813	5.817	5.789	5.798	5.798	5.71	5.699	5.676
C200T1.5D0.6	5.896	5.39	5.444	5.478	5.457	5.474	5.496	5.45	5.48	5.476	5.293	5.323	5.298
C200T2.0D0.2	7.917	7.924	7.925	7.926	7.919	7.92	7.921	7.917	7.919	7.993	7.899	7.906	7.904
C200T2.0D0.4	7.917	7.912	7.916	7.965	7.896	7.914	7.915	7.846	7.862	7.869	7.806	7.792	7.769
C200T2.0D0.6	7.917	7.353	7.386	7.412	7.37	7.387	7.402	7.342	7.358	7.374	7.31	7.305	7.268
C200T2.5D0.2	10.48	10.407	10.469	10.521	10.559	10.837	10.641	10.326	10.517	10.43	10.344	10.537	10.31
C200T2.5D0.4	10.48	10.074	10.085	10.095	10.055	10.065	10.074	10.035	10.045	10.054	9.988	10.054	9.767
C200T2.5D0.6	10.48	9.386	9.513	9.336	9.343	9.304	9.316	9.256	9.378	9.278	9.312	9.264	9.21
C200T3.0D0.2	12.689	12.583	12.673	12.624	12.602	12.971	12.681	12.519	12.579	12.615	12.523	12.518	12.506
C200T3.0D0.4	12.689	12.141	12.146	12.154	12.109	12.116	12.124	12.086	12.095	12.104	12.134	12.104	12.071
C200T3.0D0.6	12.689	11.236	11.381	11.275	11.212	11.22	11.22	11.175	11.383	11.185	11.21	11.134	11.086

C300T1.5D0.2	10.178	10.187	10.162	10.129	10.183	10.207	10.232	10.167	10.22	10.289	10.086	10.129	10.035
C300T1.5D0.4	10.178	10.112	10.167	10.151	10.29	10.372	10.466	10.375	10.578	10.678	9.756	9.883	9.798
C300T1.5D0.6	10.178	10.197	9.516	10.19	10.254	10.614	10.723	10.445	10.676	10.755	9.033	9.308	9.377
C300T2.0D0.2	15.958	15.654	15.863	15.869	15.887	15.91	15.941	15.76	15.948	15.688	15.764	15.647	15.679
C300T2.0D0.4	15.958	14.268	15.818	15.874	15.573	15.719	15.803	15.739	15.837	15.89	15.066	14.92	14.831
C300T2.0D0.6	15.958	15.933	14.44	14.551	14.512	14.616	14.684	14.576	14.663	14.702	13.852	14.009	14.047
C300T2.5D0.2	20.116	20.075	20.152	20.154	20.112	20.123	20.13	20.084	20.114	20.211	20.05	20.046	20.034
C300T2.5D0.4	20.116	18.431	19.98	20.231	19.939	20.03	20.026	19.825	19.839	19.879	19.786	19.652	19.552
C300T2.5D0.6	20.116	20.143	19.307	18.384	18.366	18.425	18.462	18.39	18.424	18.462	18.319	18.242	18.117
C300T3.0D0.2	24.425	24.387	24.457	24.463	24.408	24.428	24.44	24.315	24.418	24.621	24.343	24.322	24.307
C300T3.0D0.4	24.425	22.414	24.464	24.108	24.435	24.6	24.448	23.945	24.056	24.134	23.991	23.864	23.742
C300T3.0D0.6	24.425	24.443	23.673	22.416	22.178	22.197	22.212	22.184	22.207	22.236	22.279	22.066	21.908

Table 7 Comparison of FEA results with the design strength obtained from the DSM proposed equations for CFSS plain channel sections.

Specimens	Austenitic CFSS			Duplex CFSS			Ferritic CFSS		
		Mean			Mean			Mean	
	M_{FEA}	M_{FEA}/M_{DSM}	$M_{FEA}/M_{Proposed}$	M_{FEA}	M_{FEA}/M_{DSM}	$M_{FEA}/M_{Proposed}$	M_{FEA}	M_{FEA}/M_{DSM}	$M_{FEA}/M_{Proposed}$
C200-T1.5-NH	5.97	0.955	-	9.315	0.934	-	5.896	0.896	-
C200-T2-NH	7.986	0.896	-	15.547	0.883	-	7.917	0.990	-
C200-T2.5-NH	10.283	0.978	-	20.591	0.997	-	10.48	0.962	-
C200-T3-NH	12.498	1.003	-	25.618	1.018	-	12.689	0.972	-
C300-T1.5-NH	10.069	0.896061	-	15.765	0.909652	-	10.178	0.872101	-
C300-T2-NH	15.869	0.95448	-	26.53	0.949815	-	15.958	0.960518	-
C300-T2.5-NH	20.068	0.910126	-	39.225	0.906048	-	20.116	1.027866	-
C300-T3-NH	24.359	0.900392	-	49.597	0.960551	-	24.425	1.003131	-

Table 8 Comparison of FEA results with the design strength obtained from the DSM proposed equations for CFSS unstiffened channel sections.

Specimens	Austenitic CFSS			Duplex CFSS			Ferritic CFSS		
		Mean			Mean			Mean	
	M_{FEA}	M_{FEA}/M_{DSM}	$M_{FEA}/M_{Proposed}$	M_{FEA}	M_{FEA}/M_{DSM}	$M_{FEA}/M_{Proposed}$	M_{FEA}	M_{FEA}/M_{DSM}	$M_{FEA}/M_{Proposed}$
C200-T1.5-UH1-D0.2	5.796	1.040	0.957	9.155	0.997	0.945	5.808	1.042	0.943
C200-T2-UH1-D0.2	7.879	0.968	0.963	15.379	1.118	0.961	7.899	0.971	0.953
C200-T2.5-UH1-D0.2	9.827	0.937	1.017	20.421	1.090	0.980	10.344	0.987	0.985
C200-T3-UH1-D0.2	12.494	1.005	0.994	25.316	1.053	1.005	12.523	1.008	1.007
C200-T1.5-UH3-D0.2	5.794	1.039	0.957	9.141	0.995	0.947	5.808	1.042	0.943
C200-T2-UH3-D0.2	7.881	0.968	0.963	15.322	1.114	0.964	7.906	0.972	0.952
C200-T2.5-UH3-D0.2	10.77	1.027	0.928	20.494	1.094	0.977	10.537	1.005	0.967
C200-T3-UH3-D0.2	12.489	1.005	0.994	25.354	1.055	1.004	12.518	1.007	1.007
C200-T1.5-UH5-D0.2	5.797	1.040	0.957	9.12	0.993	0.949	5.808	1.042	0.943
C200-T2-UH5-D0.2	7.878	0.968	0.964	15.37	1.118	0.961	7.904	0.971	0.952
C200-T2.5-UH5-D0.2	10.283	0.981	0.972	20.476	1.093	0.977	10.31	0.983	0.988

C200-T3-UH5-D0.2	12.478	1.004	0.995	25.358	1.055	1.004	12.506	1.006	1.008
C200-T1.5-UH1-D0.4	5.684	1.032	0.929	9.061	1.001	0.909	5.71	1.036	0.913
C200-T2-UH1-D0.4	7.793	0.969	0.928	14.922	1.102	0.943	7.806	0.971	0.918
C200-T2.5-UH1-D0.4	9.952	0.973	0.958	20.146	1.093	0.947	9.988	0.977	0.973
C200-T3-UH1-D0.4	12.121	0.994	0.978	24.947	1.056	0.974	12.134	0.995	0.992
C200-T1.5-UH3-D0.4	5.675	1.030	0.930	8.907	0.984	0.925	5.699	1.034	0.915
C200-T2-UH3-D0.4	7.776	0.967	0.930	15.076	1.114	0.934	7.792	0.969	0.920
C200-T2.5-UH3-D0.4	9.969	0.975	0.956	20.154	1.094	0.947	10.054	0.983	0.966
C200-T3-UH3-D0.4	12.105	0.993	0.979	24.93	1.055	0.975	12.104	0.993	0.994
C200-T1.5-UH5-D0.4	5.63	1.022	0.937	8.914	0.985	0.924	5.676	1.030	0.918
C200-T2-UH5-D0.4	7.749	0.964	0.933	14.989	1.107	0.939	7.769	0.966	0.923
C200-T2.5-UH5-D0.4	10.015	0.979	0.952	20.024	1.087	0.953	9.767	0.955	0.995
C200-T3-UH5-D0.4	12.059	0.989	0.983	24.845	1.052	0.978	12.071	0.990	0.997
C200-T1.5-UH1-D0.6	5.27	0.978	0.950	8.767	0.983	0.891	5.293	0.982	0.935
C200-T2-UH1-D0.6	7.299	0.987	0.941	14.258	1.072	0.938	7.31	0.988	0.932
C200-T2.5-UH1-D0.6	9.295	0.990	0.976	19.15	1.059	0.948	9.312	0.992	0.993

C200-T3-UH1-D0.6	11.196	0.987	1.008	23.592	1.036	0.981	11.21	0.988	1.023
C200-T1.5-UH3-D0.6	5.296	0.982	0.946	8.672	0.973	0.901	5.323	0.987	0.929
C200-T2-UH3-D0.6	7.294	0.986	0.942	14.221	1.069	0.941	7.305	0.988	0.933
C200-T2.5-UH3-D0.6	9.244	0.985	0.981	19.054	1.054	0.953	9.264	0.987	0.998
C200-T3-UH3-D0.6	11.125	0.981	1.015	23.572	1.035	0.982	11.134	0.981	1.030
C200-T1.5-UH5-D0.6	5.269	0.977	0.951	8.522	0.956	0.917	5.298	0.983	0.934
C200-T2-UH5-D0.6	7.256	0.981	0.947	13.633	1.025	0.981	7.268	0.983	0.937
C200-T2.5-UH5-D0.6	9.193	0.980	0.986	18.689	1.034	0.972	9.21	0.981	1.004
C200-T3-UH5-D0.6	11.077	0.976	1.019	23.33	1.024	0.992	11.086	0.977	1.034
C300-T1.5-UH1-D0.2	10.032	1.005	0.911	15.527	0.964	0.922	10.086	1.011	0.916
C300-T2-UH1-D0.2	15.705	1.062	0.932	26.401	1.086	0.926	15.764	1.066	0.933
C300-T2.5-UH1-D0.2	20	1.005	0.939	38.443	1.153	0.955	20.05	1.008	0.939
C300-T3-UH1-D0.2	24.262	0.963	0.954	49.271	1.144	0.957	24.343	0.967	0.954
C300-T1.5-UH3-D0.2	10.017	1.004	0.912	15.506	0.963	0.923	10.129	1.015	0.912
C300-T2-UH3-D0.2	15.613	1.056	0.937	26.311	1.082	0.930	15.647	1.058	0.940
C300-T2.5-UH3-D0.2	19.993	1.005	0.940	38.223	1.146	0.961	20.046	1.008	0.939

C300-T3-UH3-D0.2	24.247	0.963	0.955	49.34	1.145	0.955	24.322	0.966	0.955
C300-T1.5-UH5-D0.2	9.921	0.994	0.921	15.468	0.960	0.925	10.035	1.006	0.921
C300-T2-UH5-D0.2	15.597	1.055	0.938	26.27	1.080	0.931	15.679	1.061	0.938
C300-T2.5-UH5-D0.2	19.98	1.004	0.940	37.801	1.133	0.971	20.034	1.007	0.940
C300-T3-UH5-D0.2	24.233	0.962	0.955	49.286	1.144	0.957	24.307	0.965	0.955
C300-T1.5-UH1-D0.4	9.715	0.987	0.894	15.573	0.982	0.873	9.756	0.991	0.900
C300-T2-UH1-D0.4	14.934	1.025	0.932	26.122	1.094	0.891	15.066	1.035	0.929
C300-T2.5-UH1-D0.4	19.719	1.007	0.907	37.284	1.140	0.938	19.786	1.010	0.906
C300-T3-UH1-D0.4	23.923	0.985	0.922	47.668	1.130	0.942	23.991	0.988	0.922
C300-T1.5-UH3-D0.4	9.811	0.997	0.885	15.473	0.976	0.879	9.883	1.004	0.888
C300-T2-UH3-D0.4	14.838	1.019	0.938	26.881	1.125	0.865	14.92	1.025	0.938
C300-T2.5-UH3-D0.4	19.641	1.003	0.911	37.291	1.140	0.937	19.652	1.003	0.912
C300-T3-UH3-D0.4	23.803	0.980	0.927	47.718	1.131	0.941	23.864	0.983	0.927
C300-T1.5-UH5-D0.4	9.74	0.990	0.892	15.47	0.976	0.879	9.798	0.996	0.896
C300-T2-UH5-D0.4	14.624	1.004	0.952	25.713	1.076	0.905	14.831	1.018	0.944
C300-T2.5-UH5-D0.4	19.457	0.993	0.919	36.799	1.125	0.950	19.552	0.998	0.917

C300-T3-UH5-D0.4	23.679	0.975	0.931	47.167	1.118	0.952	23.742	0.978	0.932
C300-T1.5-UH1-D0.6	9.687	0.999	0.850	14.901	0.956	0.865	9.033	0.932	0.921
C300-T2-UH1-D0.6	13.676	0.969	0.965	24.292	1.037	0.909	13.852	0.982	0.958
C300-T2.5-UH1-D0.6	18.244	1.010	0.931	34.331	1.073	0.967	18.319	1.014	0.929
C300-T3-UH1-D0.6	22.244	1.010	0.942	44.48	1.079	0.959	22.279	1.012	0.943
C300-T1.5-UH3-D0.6	9.269	0.956	0.888	13.381	0.859	0.963	9.308	0.960	0.894
C300-T2-UH3-D0.6	13.888	0.984	0.951	23.512	1.004	0.939	14.009	0.993	0.948
C300-T2.5-UH3-D0.6	18.197	1.007	0.933	34.082	1.065	0.974	18.242	1.009	0.933
C300-T3-UH3-D0.6	21.982	0.999	0.954	44.207	1.073	0.965	22.066	1.002	0.952
C300-T1.5-UH5-D0.6	9.249	0.954	0.890	12.625	0.810	1.021	9.377	0.967	0.887
C300-T2-UH5-D0.6	13.924	0.987	0.948	21.719	0.927	1.016	14.047	0.996	0.945
C300-T2.5-UH5-D0.6	18.044	0.999	0.941	31.639	0.988	1.049	18.117	1.003	0.940
C300-T3-UH5-D0.6	21.922	0.996	0.956	42.075	1.021	1.014	21.908	0.995	0.959

Table 9 Comparison of FEA results with the design strength obtained from the DSM proposed equations for CFSS edge stiffened channel sections.

Specimens	Austenitic CFSS			Duplex CFSS			Ferritic CFSS		
		Mean			Mean			Mean	
	M_{FEA}	M_{FEA}/M_{DSM}	$M_{FEA}/M_{Proposed}$	M_{FEA}	M_{FEA}/M_{DSM}	$M_{FEA}/M_{Proposed}$	M_{FEA}	M_{FEA}/M_{DSM}	$M_{FEA}/M_{Proposed}$
C200-T1.5-EH1-D0.2-Q5	5.815	1.043	1.031	9.251	1.007	1.051	5.826	1.045	1.046
C200-T2-EH1-D0.2-Q5	7.907	0.972	1.037	15.54	1.130	1.046	7.924	0.974	1.048
C200-T2.5-EH1-D0.2-Q5	10.301	0.982	1.038	20.633	1.101	1.038	10.407	0.993	1.028
C200-T3-EH1-D0.2-Q5	12.892	1.037	1.057	25.479	1.060	1.019	12.583	1.012	1.016
C200-T1.5-EH3-D0.2-Q5	5.81	1.042	1.030	9.176	0.999	1.043	5.822	1.044	1.045
C200-T2-EH3-D0.2-Q5	7.902	0.971	1.036	15.486	1.126	1.043	7.919	0.973	1.047
C200-T2.5-EH3-D0.2-Q5	10.893	1.039	1.097	20.61	1.100	1.037	10.559	1.007	1.044
C200-T3-EH3-D0.2-Q5	12.631	1.016	1.036	25.447	1.059	1.018	12.602	1.014	1.018
C200-T1.5-EH5-D0.2-Q5	5.809	1.042	1.030	9.29	1.012	1.056	5.835	1.047	1.047
C200-T2-EH5-D0.2-Q5	7.9	0.971	1.036	15.512	1.128	1.045	7.917	0.973	1.047
C200-T2.5-EH5-D0.2-Q5	10.3	0.982	1.037	20.601	1.099	1.036	10.326	0.985	1.020

C200-T3-EH5-D0.2-Q5	12.499	1.006	1.025	25.435	1.058	1.017	12.519	1.007	1.011
C200-T1.5-EH1-D0.4-Q5	5.825	1.057	1.061	9.43	1.042	1.100	5.861	1.064	1.081
C200-T2-EH1-D0.4-Q5	7.934	0.987	1.068	15.694	1.159	1.085	7.912	0.984	1.074
C200-T2.5-EH1-D0.4-Q5	10.062	0.984	1.040	20.746	1.126	1.071	10.074	0.985	1.022
C200-T3-EH1-D0.4-Q5	12.127	0.994	1.020	25.62	1.085	1.052	12.141	0.996	1.006
C200-T1.5-EH3-D0.4-Q5	5.801	1.053	1.056	9.269	1.024	1.082	5.82	1.056	1.073
C200-T2-EH3-D0.4-Q5	7.872	0.979	1.060	15.524	1.147	1.073	7.896	0.982	1.072
C200-T2.5-EH3-D0.4-Q5	10.043	0.982	1.038	20.525	1.114	1.060	10.055	0.983	1.020
C200-T3-EH3-D0.4-Q5	12.395	1.016	1.043	25.371	1.074	1.041	12.109	0.993	1.003
C200-T1.5-EH5-D0.4-Q5	5.764	1.046	1.049	9.475	1.046	1.106	5.789	1.051	1.067
C200-T2-EH5-D0.4-Q5	7.826	0.973	1.053	15.391	1.137	1.064	7.846	0.976	1.065
C200-T2.5-EH5-D0.4-Q5	10.116	0.989	1.046	20.387	1.106	1.053	10.035	0.981	1.018
C200-T3-EH5-D0.4-Q5	12.071	0.990	1.016	25.204	1.067	1.034	12.086	0.991	1.002
C200-T1.5-EH1-D0.6-Q5	5.379	0.998	1.007	9.763	1.095	1.171	5.39	1.000	1.021
C200-T2-EH1-D0.6-Q5	7.338	0.992	1.015	14.962	1.125	1.063	7.353	0.994	1.026
C200-T2.5-EH1-D0.6-Q5	9.373	0.999	0.995	19.34	1.070	1.026	9.386	1.000	0.978

C200-T3-EH1-D0.6-Q5	11.219	0.989	0.969	23.67	1.039	0.998	11.236	0.990	0.956
C200-T1.5-EH3-D0.6-Q5	5.448	1.011	1.019	9.703	1.088	1.164	5.457	1.012	1.034
C200-T2-EH3-D0.6-Q5	7.354	0.994	1.017	15.061	1.132	1.070	7.37	0.996	1.028
C200-T2.5-EH3-D0.6-Q5	9.372	0.999	0.995	19.598	1.084	1.039	9.343	0.996	0.973
C200-T3-EH3-D0.6-Q5	11.202	0.987	0.968	23.917	1.050	1.008	11.212	0.988	0.954
C200-T1.5-EH5-D0.6-Q5	5.452	1.011	1.020	9.49	1.064	1.138	5.45	1.011	1.033
C200-T2-EH5-D0.6-Q5	7.338	0.992	1.015	14.772	1.110	1.049	7.342	0.993	1.024
C200-T2.5-EH5-D0.6-Q5	9.247	0.985	0.982	19.326	1.069	1.025	9.256	0.986	0.964
C200-T3-EH5-D0.6-Q5	11.165	0.984	0.965	23.846	1.047	1.005	11.175	0.985	0.951
C300-T1.5-EH1-D0.2-Q5	10.086	1.011	1.071	15.759	0.979	1.068	10.197	1.022	1.071
C300-T2-EH1-D0.2-Q5	15.837	1.071	1.059	26.794	1.102	1.072	15.933	1.078	1.059
C300-T2.5-EH1-D0.2-Q5	20.109	1.011	1.055	38.842	1.165	1.043	20.143	1.013	1.055
C300-T3-EH1-D0.2-Q5	24.354	0.967	1.045	49.659	1.153	1.047	24.443	0.971	1.046
C300-T1.5-EH3-D0.2-Q5	10.072	1.009	1.069	15.76	0.979	1.068	10.183	1.020	1.069
C300-T2-EH3-D0.2-Q5	15.774	1.067	1.055	26.768	1.101	1.070	15.887	1.075	1.056
C300-T2.5-EH3-D0.2-Q5	20.065	1.009	1.053	38.89	1.166	1.044	20.112	1.011	1.053

C300-T3-EH3-D0.2-Q5	24.315	0.965	1.044	49.55	1.150	1.045	24.408	0.969	1.045
C300-T1.5-EH5-D0.2-Q5	10.193	1.021	1.082	15.71	0.000	1.062	10.167	1.019	1.068
C300-T2-EH5-D0.2-Q5	15.903	1.076	1.063	26.76	0.000	1.069	15.76	1.066	1.048
C300-T2.5-EH5-D0.2-Q5	20.106	1.011	1.055	38.05	0.000	1.040	20.084	1.010	1.052
C300-T3-EH5-D0.2-Q5	24.389	0.968	1.047	50.11	0.000	1.040	24.315	0.965	1.041
C300-T1.5-EH1-D0.4-Q5	10.065	1.023	1.098	15.77	0.995	1.098	10.187	1.035	1.099
C300-T2-EH1-D0.4-Q5	15.585	1.070	1.070	26.812	1.122	1.101	15.654	1.075	1.069
C300-T2.5-EH1-D0.4-Q5	20.08	1.025	1.082	38.121	1.166	1.051	20.075	1.025	1.079
C300-T3-EH1-D0.4-Q5	24.387	1.004	1.075	50.241	1.191	1.087	24.387	1.004	1.072
C300-T1.5-EH3-D0.4-Q5	10.166	1.033	1.109	15.877	1.002	1.106	10.29	1.046	1.110
C300-T2-EH3-D0.4-Q5	15.464	1.062	1.062	27.331	1.144	1.123	15.573	1.069	1.063
C300-T2.5-EH3-D0.4-Q5	19.894	1.016	1.072	38.548	1.179	1.063	19.939	1.018	1.072
C300-T3-EH3-D0.4-Q5	24.297	1.001	1.071	49.321	1.169	1.068	24.435	1.006	1.074
C300-T1.5-EH5-D0.4-Q5	10.254	1.042	1.118	15.843	0.999	1.103	10.375	1.054	1.119
C300-T2-EH5-D0.4-Q5	15.669	1.076	1.076	26.445	1.107	1.086	15.739	1.081	1.075
C300-T2.5-EH5-D0.4-Q5	19.795	1.011	1.067	37.932	1.160	1.046	19.825	1.012	1.066

C300-T3-EH5-D0.4-Q5	23.887	0.984	1.053	48.668	1.154	1.053	23.945	0.986	1.052
C300-T1.5-EH1-D0.6-Q5	10.053	1.037	1.127	15.71	1.008	1.125	10.112	1.043	1.121
C300-T2-EH1-D0.6-Q5	14.2	1.007	1.002	26.322	1.124	1.111	14.268	1.011	1.001
C300-T2.5-EH1-D0.6-Q5	18.329	1.014	1.015	35.708	1.116	1.012	18.431	1.020	1.018
C300-T3-EH1-D0.6-Q5	22.317	1.014	1.010	45.373	1.101	1.009	22.414	1.018	1.012
C300-T1.5-EH3-D0.6-Q5	10.188	1.051	1.142	15.764	1.011	1.129	10.254	1.058	1.137
C300-T2-EH3-D0.6-Q5	14.453	1.024	1.020	26.965	1.151	1.138	14.512	1.029	1.019
C300-T2.5-EH3-D0.6-Q5	18.343	1.015	1.016	37.457	1.170	1.061	18.366	1.016	1.015
C300-T3-EH3-D0.6-Q5	22.158	1.007	1.003	46.58	1.130	1.036	22.178	1.007	1.001
C300-T1.5-EH5-D0.6-Q5	10.402	1.073	1.166	15.701	1.007	1.124	10.445	1.077	1.158
C300-T2-EH5-D0.6-Q5	14.568	1.033	1.028	26.758	1.142	1.130	14.576	1.033	1.023
C300-T2.5-EH5-D0.6-Q5	18.373	1.017	1.018	36.426	1.138	1.032	18.39	1.018	1.016
C300-T3-EH5-D0.6-Q5	22.166	1.007	1.004	45.728	1.110	1.017	22.184	1.008	1.002
C200-T1.5-EH1-D0.2-Q7	5.816	1.043	1.033	9.23	1.005	1.050	5.827	1.045	1.048
C200-T2-EH1-D0.2-Q7	7.896	0.970	1.037	15.556	1.131	1.049	7.925	0.974	1.050
C200-T2.5-EH1-D0.2-Q7	10.294	0.982	1.038	20.661	1.103	1.041	10.469	0.998	1.036

C200-T3-EH1-D0.2-Q7	12.593	1.013	1.034	25.53	1.062	1.023	12.673	1.020	1.025
C200-T1.5-EH3-D0.2-Q7	5.813	1.043	1.032	9.177	0.999	1.044	5.823	1.044	1.047
C200-T2-EH3-D0.2-Q7	7.903	0.971	1.038	15.536	1.130	1.048	7.92	0.973	1.049
C200-T2.5-EH3-D0.2-Q7	10.817	1.032	1.091	20.624	1.101	1.039	10.837	1.034	1.073
C200-T3-EH3-D0.2-Q7	12.687	1.021	1.042	25.465	1.060	1.020	12.971	1.044	1.049
C200-T1.5-EH5-D0.2-Q7	5.811	1.042	1.032	9.298	1.012	1.058	5.822	1.044	1.047
C200-T2-EH5-D0.2-Q7	7.902	0.971	1.037	15.537	1.130	1.048	7.919	0.973	1.049
C200-T2.5-EH5-D0.2-Q7	10.302	0.983	1.039	20.619	1.100	1.039	10.517	1.003	1.041
C200-T3-EH5-D0.2-Q7	12.482	1.004	1.025	25.447	1.059	1.019	12.579	1.012	1.017
C200-T1.5-EH1-D0.4-Q7	5.845	1.061	1.066	9.383	1.036	1.097	5.866	1.065	1.083
C200-T2-EH1-D0.4-Q7	7.928	0.986	1.069	15.806	1.168	1.094	7.916	0.985	1.076
C200-T2.5-EH1-D0.4-Q7	10.073	0.985	1.043	20.797	1.129	1.075	10.085	0.986	1.025
C200-T3-EH1-D0.4-Q7	12.133	0.995	1.022	25.547	1.082	1.050	12.146	0.996	1.008
C200-T1.5-EH3-D0.4-Q7	5.807	1.054	1.059	9.381	1.036	1.096	5.813	1.055	1.073
C200-T2-EH3-D0.4-Q7	7.884	0.981	1.063	15.608	1.153	1.081	7.914	0.984	1.076
C200-T2.5-EH3-D0.4-Q7	10.053	0.983	1.041	20.554	1.115	1.063	10.065	0.984	1.022

C200-T3-EH3-D0.4-Q7	12.253	1.005	1.032	25.376	1.074	1.043	12.116	0.994	1.005
C200-T1.5-EH5-D0.4-Q7	5.776	1.048	1.053	9.646	1.065	1.127	5.798	1.052	1.071
C200-T2-EH5-D0.4-Q7	7.841	0.975	1.057	15.542	1.148	1.076	7.862	0.978	1.069
C200-T2.5-EH5-D0.4-Q7	10.027	0.981	1.038	20.507	1.113	1.060	10.045	0.982	1.020
C200-T3-EH5-D0.4-Q7	12.081	0.991	1.018	25.33	1.072	1.041	12.095	0.992	1.004
C200-T1.5-EH1-D0.6-Q7	5.42	1.005	1.016	9.805	1.100	1.178	5.444	1.010	1.033
C200-T2-EH1-D0.6-Q7	7.372	0.997	1.021	15.122	1.137	1.076	7.386	0.999	1.032
C200-T2.5-EH1-D0.6-Q7	9.297	0.991	0.989	19.478	1.077	1.034	9.513	1.014	0.993
C200-T3-EH1-D0.6-Q7	11.243	0.991	0.973	23.767	1.044	1.003	11.381	1.003	0.970
C200-T1.5-EH3-D0.6-Q7	5.469	1.015	1.025	9.961	1.117	1.197	5.474	1.015	1.039
C200-T2-EH3-D0.6-Q7	7.378	0.998	1.022	15.258	1.147	1.086	7.387	0.999	1.032
C200-T2.5-EH3-D0.6-Q7	9.295	0.990	0.988	19.712	1.090	1.047	9.304	0.991	0.971
C200-T3-EH3-D0.6-Q7	11.21	0.988	0.970	23.964	1.052	1.012	11.22	0.989	0.956
C200-T1.5-EH5-D0.6-Q7	5.467	1.014	1.025	9.814	1.101	1.179	5.48	1.017	1.040
C200-T2-EH5-D0.6-Q7	7.351	0.994	1.018	15.13	1.137	1.076	7.358	0.995	1.028
C200-T2.5-EH5-D0.6-Q7	9.26	0.987	0.985	19.648	1.087	1.043	9.378	0.999	0.979

C200-T3-EH5-D0.6-Q7	11.173	0.985	0.967	24.108	1.058	1.018	11.383	1.003	0.970
C300-T1.5-EH1-D0.2-Q7	10.079	1.010	1.071	15.752	0.978	1.069	10.162	1.018	1.068
C300-T2-EH1-D0.2-Q7	15.843	1.072	1.060	26.783	1.101	1.072	15.863	1.073	1.056
C300-T2.5-EH1-D0.2-Q7	20.109	1.011	1.056	38.843	1.165	1.044	20.152	1.013	1.056
C300-T3-EH1-D0.2-Q7	24.372	0.968	1.047	49.802	1.156	1.051	24.457	0.971	1.048
C300-T1.5-EH3-D0.2-Q7	10.094	1.011	1.073	15.769	0.979	1.070	10.207	1.023	1.073
C300-T2-EH3-D0.2-Q7	15.81	1.069	1.058	27.101	1.114	1.085	15.91	1.076	1.059
C300-T2.5-EH3-D0.2-Q7	20.077	1.009	1.055	38.997	1.169	1.048	20.123	1.012	1.055
C300-T3-EH3-D0.2-Q7	24.339	0.966	1.046	49.678	1.153	1.048	24.428	0.970	1.047
C300-T1.5-EH5-D0.2-Q7	10.22	1.024	1.086	15.948	0.990	1.082	10.22	1.024	1.074
C300-T2-EH5-D0.2-Q7	15.944	1.079	1.067	26.911	1.107	1.077	15.948	1.079	1.061
C300-T2.5-EH5-D0.2-Q7	20.114	1.011	1.057	38.016	1.140	1.022	20.114	1.011	1.054
C300-T3-EH5-D0.2-Q7	24.418	0.970	1.049	49.816	1.156	1.051	24.418	0.970	1.046
C300-T1.5-EH1-D0.4-Q7	10.056	1.022	1.098	15.766	0.995	1.099	10.167	1.033	1.098
C300-T2-EH1-D0.4-Q7	15.736	1.081	1.082	27.147	1.136	1.116	15.818	1.086	1.081
C300-T2.5-EH1-D0.4-Q7	20.161	1.029	1.088	39.073	1.195	1.078	19.98	1.020	1.075

C300-T3-EH1-D0.4-Q7	24.456	1.007	1.079	50.404	1.195	1.092	24.464	1.008	1.076
C300-T1.5-EH3-D0.4-Q7	10.279	1.044	1.122	15.866	1.001	1.106	10.372	1.054	1.120
C300-T2-EH3-D0.4-Q7	15.623	1.073	1.074	27.236	1.140	1.120	15.719	1.079	1.074
C300-T2.5-EH3-D0.4-Q7	19.963	1.019	1.077	39.225	1.199	1.083	20.03	1.023	1.078
C300-T3-EH3-D0.4-Q7	24.368	1.004	1.075	49.665	1.177	1.076	24.6	1.013	1.082
C300-T1.5-EH5-D0.4-Q7	10.387	1.055	1.134	15.671	0.989	1.093	10.578	1.075	1.142
C300-T2-EH5-D0.4-Q7	15.787	1.084	1.085	26.936	1.128	1.108	15.837	1.087	1.083
C300-T2.5-EH5-D0.4-Q7	19.827	1.012	1.070	39.193	1.198	1.082	19.839	1.013	1.068
C300-T3-EH5-D0.4-Q7	23.988	0.988	1.058	49.195	1.166	1.066	24.056	0.991	1.058
C300-T1.5-EH1-D0.6-Q7	10.1	1.042	1.133	15.786	1.013	1.131	9.516	0.981	1.056
C300-T2-EH1-D0.6-Q5	14.395	1.020	1.017	27.234	1.163	1.151	14.44	1.024	1.015
C300-T2.5-EH1-D0.6-Q7	18.245	1.010	1.012	36.991	1.156	1.049	19.307	1.068	1.068
C300-T3-EH1-D0.6-Q57	22.424	1.019	1.016	45.962	1.115	1.023	23.673	1.075	1.070
C300-T1.5-EH3-D0.6-Q7	10.571	1.090	1.186	16.001	1.027	1.147	10.614	1.095	1.178
C300-T2-EH3-D0.6-Q7	14.583	1.034	1.030	28.566	1.219	1.207	14.616	1.036	1.027
C300-T2.5-EH3-D0.6-Q7	18.375	1.017	1.019	38.375	1.199	1.088	18.425	1.020	1.019

C300-T3-EH3-D0.6-Q7	22.182	1.008	1.005	47.119	1.143	1.049	22.197	1.008	1.003
C300-T1.5-EH5-D0.6-Q7	10.62	1.095	1.192	16.2	1.039	1.161	10.676	1.101	1.185
C300-T2-EH5-D0.6-Q7	14.64	1.038	1.034	28.686	1.224	1.212	14.663	1.039	1.030
C300-T2.5-EH5-D0.6-Q7	18.408	1.019	1.021	38.451	1.201	1.091	18.424	1.020	1.019
C300-T3-EH5-D0.6-Q7	22.191	1.008	1.006	47.122	1.143	1.049	22.207	1.009	1.004
C200-T1.5-EH1-D0.2-Q10	5.819	1.044	1.036	9.355	1.019	1.067	5.971	1.071	1.076
C200-T2-EH1-D0.2-Q10	7.688	0.945	1.012	15.422	1.121	1.042	7.926	0.974	1.052
C200-T2.5-EH1-D0.2-Q5	10.287	0.981	1.040	20.635	1.101	1.042	10.521	1.003	1.044
C200-T3-EH1-D0.2-Q10	12.493	1.005	1.028	25.12	1.045	1.008	12.624	1.016	1.023
C200-T1.5-EH3-D0.2-Q10	5.814	1.043	1.035	9.174	0.999	1.046	5.85	1.062	1.049
C200-T2-EH3-D0.2-Q10	7.904	0.971	1.040	15.543	1.130	1.051	7.965	0.991	1.051
C200-T2.5-EH3-D0.2-Q10	10.318	0.984	1.043	20.635	1.101	1.042	10.095	0.987	1.055
C200-T3-EH3-D0.2-Q10	12.489	1.005	1.028	25.507	1.061	1.024	12.154	0.997	1.028
C200-T1.5-EH5-D0.2-Q10	5.812	1.042	1.034	9.311	1.014	1.062	5.478	1.016	1.049
C200-T2-EH5-D0.2-Q10	7.904	0.971	1.040	15.555	1.131	1.051	7.412	1.002	1.061
C200-T2.5-EH5-D0.2-Q10	10.304	0.983	1.042	20.629	1.101	1.041	9.336	0.995	1.035

C200-T3-EH5-D0.2-Q10	12.486	1.005	1.027	25.46	1.059	1.022	11.275	0.994	1.022
C200-T1.5-EH1-D0.4-Q10	5.846	1.061	1.069	9.445	1.043	1.106	5.824	1.045	1.083
C200-T2-EH1-D0.4-Q10	7.979	0.993	1.078	15.843	1.170	1.100	7.921	0.973	1.086
C200-T2.5-EH1-D0.4-Q10	7.872	0.979	1.046	20.834	1.131	1.080	10.641	1.015	1.028
C200-T3-EH1-D0.4-Q10	12.142	0.996	1.025	25.541	1.081	1.052	12.681	1.020	1.011
C200-T1.5-EH3-D0.4-Q10	5.81	1.055	1.062	9.426	1.041	1.104	5.817	1.056	1.077
C200-T2-EH3-D0.4-Q10	7.848	0.976	1.064	15.66	1.157	1.087	7.915	0.985	1.079
C200-T2.5-EH3-D0.4-Q10	10.081	0.986	1.044	20.635	1.120	1.069	10.074	0.985	1.026
C200-T3-EH3-D0.4-Q10	12.113	0.993	1.023	25.467	1.078	1.049	12.124	0.994	1.008
C200-T1.5-EH5-D0.4-Q10	5.78	1.049	1.056	9.679	1.069	1.134	5.496	1.020	1.073
C200-T2-EH5-D0.4-Q10	10.062	0.984	1.060	15.631	1.155	1.085	7.402	1.001	1.072
C200-T2.5-EH5-D0.4-Q10	10.036	0.981	1.041	20.525	1.114	1.064	9.316	0.993	1.024
C200-T3-EH5-D0.4-Q10	12.09	0.991	1.021	25.388	1.075	1.046	11.22	0.989	1.007
C200-T1.5-EH1-D0.6-Q10	5.461	1.013	1.026	9.856	1.105	1.187	5.823	1.044	1.042
C200-T2-EH1-D0.6-Q10	7.4	1.000	1.027	15.241	1.145	1.087	7.993	0.982	1.038
C200-T2.5-EH1-D0.6-Q10	9.321	0.993	0.994	19.598	1.084	1.043	10.43	0.995	0.976

C200-T3-EH1-D0.6-Q10	11.259	0.992	0.976	23.855	1.047	1.009	12.615	1.015	0.963
C200-T1.5-EH3-D0.6-Q10	5.487	1.018	1.031	10.055	1.128	1.211	5.798	1.052	1.046
C200-T2-EH3-D0.6-Q10	7.393	1.000	1.026	15.329	1.152	1.093	7.869	0.979	1.037
C200-T2.5-EH3-D0.6-Q10	9.307	0.992	0.992	19.763	1.093	1.052	10.054	0.983	0.974
C200-T3-EH3-D0.6-Q10	11.211	0.988	0.972	24.008	1.054	1.016	12.104	0.993	0.958
C200-T1.5-EH5-D0.6-Q10	5.471	1.015	1.028	9.958	1.117	1.199	5.476	1.016	1.042
C200-T2-EH5-D0.6-Q10	7.366	0.996	1.023	15.281	1.148	1.090	7.374	0.997	1.033
C200-T2.5-EH5-D0.6-Q10	9.271	0.988	0.988	19.725	1.091	1.050	9.278	0.989	0.970
C200-T3-EH5-D0.6-Q10	11.176	0.985	0.969	23.992	1.053	1.015	11.185	0.986	0.955
C300-T1.5-EH1-D0.2-Q10	10.07	1.009	1.072	15.739	0.977	1.070	10.129	1.015	1.066
C300-T2-EH1-D0.2-Q10	15.746	1.065	1.055	26.841	1.104	1.076	15.869	1.073	1.058
C300-T2.5-EH1-D0.2-Q10	20.111	1.011	1.058	38.877	1.166	1.047	20.154	1.013	1.058
C300-T3-EH1-D0.2-Q10	24.378	0.968	1.049	49.867	1.158	1.054	24.463	0.971	1.050
C300-T1.5-EH3-D0.2-Q10	10.117	1.014	1.077	15.759	0.979	1.071	10.232	1.025	1.077
C300-T2-EH3-D0.2-Q5	15.841	1.072	1.062	26.838	1.104	1.076	15.941	1.078	1.063
C300-T2.5-EH3-D0.2-Q10	20.085	1.010	1.057	39.03	1.170	1.051	20.13	1.012	1.057

C300-T3-EH3-D0.2-Q510	24.353	0.967	1.048	49.75	1.155	1.051	24.44	0.970	1.049
C300-T1.5-EH5-D0.2-Q10	10.326	1.035	1.099	0	0.000	1.069	10.289	1.031	1.083
C300-T2-EH5-D0.2-Q10	15.989	1.082	1.072	0	0.000	1.072	15.688	1.061	1.046
C300-T2.5-EH5-D0.2-Q10	20.304	1.021	1.068	0	0.000	1.039	20.211	1.016	1.061
C300-T3-EH5-D0.2-Q10	24.621	0.978	1.060	0	0.000	1.047	24.621	0.978	1.057
C300-T1.5-EH1-D0.4-Q10	10.046	1.021	1.098	15.745	0.993	1.099	10.151	1.031	1.098
C300-T2-EH1-D0.4-Q10	15.788	1.084	1.087	27.073	1.133	1.115	15.874	1.090	1.087
C300-T2.5-EH1-D0.4-Q10	20.24	1.033	1.094	39.224	1.199	1.084	20.231	1.033	1.091
C300-T3-EH1-D0.4-Q10	24.462	1.007	1.081	50.564	1.199	1.097	24.108	0.993	1.062
C300-T1.5-EH3-D0.4-Q10	10.325	1.049	1.129	15.545	0.981	1.085	10.466	1.063	1.132
C300-T2-EH3-D0.4-Q10	15.747	1.081	1.084	27.365	1.146	1.127	15.803	1.085	1.082
C300-T2.5-EH3-D0.4-Q10	20.001	1.021	1.081	39.552	1.209	1.093	20.026	1.023	1.079
C300-T3-EH3-D0.4-Q10	24.366	1.004	1.077	49.774	1.180	1.080	24.448	1.007	1.077
C300-T1.5-EH5-D0.4-Q10	10.525	1.069	1.151	15.747	0.993	1.100	10.678	1.085	1.155
C300-T2-EH5-D0.4-Q10	15.84	1.088	1.091	27.397	1.147	1.128	15.89	1.091	1.088
C300-T2.5-EH5-D0.4-Q10	19.86	1.014	1.073	39.82	1.218	1.101	19.879	1.015	1.072

C300-T3-EH5-D0.4-Q10	24.05	0.991	1.063	49.625	1.176	1.077	24.134	0.994	1.063
C300-T1.5-EH1-D0.6-Q10	10.113	1.043	1.137	15.814	1.015	1.135	10.19	1.051	1.133
C300-T2-EH1-D0.6-Q10	14.502	1.028	1.026	27.136	1.158	1.149	14.551	1.031	1.024
C300-T2.5-EH1-D0.6-Q10	18.362	1.016	1.020	37.593	1.174	1.068	18.384	1.017	1.018
C300-T3-EH1-D0.6-Q10	22.43	1.019	1.018	46.53	1.129	1.037	22.416	1.018	1.015
C300-T1.5-EH3-D0.6-Q10	10.654	1.099	1.198	16.109	1.034	1.156	10.723	1.106	1.192
C300-T2-EH3-D0.6-Q10	14.658	1.039	1.037	28.563	1.219	1.209	14.684	1.041	1.033
C300-T2.5-EH3-D0.6-Q10	18.448	1.021	1.024	38.792	1.212	1.102	18.462	1.022	1.023
C300-T3-EH3-D0.6-Q10	22.196	1.008	1.008	47.555	1.154	1.060	22.212	1.009	1.006
C300-T1.5-EH5-D0.6-Q10	10.706	1.104	1.203	16.534	1.061	1.187	10.755	1.109	1.196
C300-T2-EH5-D0.6-Q10	14.679	1.040	1.039	29.395	1.255	1.244	14.702	1.042	1.035
C300-T2.5-EH5-D0.6-Q10	18.449	1.021	1.024	39.292	1.228	1.116	18.462	1.022	1.023
C300-T3-EH5-D0.6-Q10	22.217	1.009	1.009	47.787	1.159	1.065	22.236	1.010	1.007

Table 10 Reliability analysis results of proposed moment capacity reduction factor equations for CFSS channel sections.

	Unstiffened web holes	Edge-stiffened web holes
	Eq. 19	Eq. 20
Total number of data	216	648
Mean, P_m	1.06	1.00
Coefficient of variation, V_p	0.29	0.05
Reliability index, β	2.91	2.69
Resistance factor, φ	0.85	0.85

REFERENCES

[1] Yousefi, A. M., Samali, B., Hajirasouliha, I., Yu, Y., & Clifton, G. C. (2022). Unified design equations for web crippling failure of cold-formed ferritic stainless steel unlipped channel-sections with web holes. Journal of Building Engineering, 45, 103685.

[2] Yu, C. (2012). Cold-formed steel flexural member with edge stiffened holes: Behaviour, optimization, and design. Journal of Constructional Steel Research, 71, 210-218.

[3] Yousefi, A. M., Lim, J. B., Uzzaman, A., Lian, Y., Clifton, G. C., & Young, B. (2016). Web crippling strength of cold-formed stainless steel lipped channel-sections with web openings subjected to interior-one-flange loading condition. Steel and Composite Structures, 21(3), 629-659.

[4] Fang, Z., Roy, K., Padiyara, S., Chen, B., Raftery, G. M., & Lim, J. B. (2023, January). Web crippling design of cold-formed stainless-steel channels under interior-two-flange loading condition using deep belief network. In Structures (Vol. 47, pp. 1967-1990). Elsevier.

[5] Fang Zhiyuan, Roy Krishanu, Ma Quincy, Uzzaman Asraf, Lim James BP. Application of deep learning method in web crippling strength prediction of cold-formed stainless steel channel beams under end-two-flange loading. Struct 2021; 33:2903–42.

[6] Yousefi, A. M., Samali, B., & Yu, Y. (2021, October). Shear behaviour and design of cold-formed ferritic stainless-steel channels with circular web openings. In Structures (Vol. 33, pp. 4162-4175). Elsevier.

[7] American Society of Civil Engineers (ASCE). Specification for the Design of Cold-formed Stainless Steel Structural Members. Reston, Va: SEI/ASCE 8-02; 2002.

[8] BADDOO, N. (2009). Designing structural stainless steel members to Eurocode 3. New steel construction, 17(4).

[9] Chen, B., Roy, K., Uzzaman, A., & Lim, J. B. (2020). Moment capacity of cold-formed channel sections with edge-stiffened web holes, un-stiffened web holes and plain webs. Thin-Walled Structures, 157, 107070.

[10] Howick Floor, Joist System, 2013.

[11] Amouzegar, H., Schafer, B., and Tootkaboni, M. (2016). "An incremental numerical method for calculation of residual stresses and strains in cold-formed steel members." Thin-Walled Struct., 106, 61-74.

[12] SCI Steel knowledge. (2010). The pavilion, regent's place: structural stainless steel case study 07. Report. https://www.teamstainless.org/resources/information-center-for-stainless-steel-in-construction/case-studies/structure/

[13] SCI Steel knowledge. (2010). The Helix pedestrian bridge: structural stainless steel case study 07. Report. https://www.teamstainless.org/resources/information-center-for-stainless-steel-in-construction/case-studies/structure/

[14] AISI (American Iron and Steel Institute). 2016. North American specification for the design of cold-formed steel structural members, 2016 edition. AISI S100-16w. Washington, DC: AISI

[15] AS/NZS (Australia/New Zealand Standard). 2018. Cold-formed steel structures. AS/NZS 4600:2018. Sydney, Australia: AS/NZS.

[16] Yousefi, A. M., Lim, J. B., & Clifton, G. C. (2019). Web crippling design of cold-formed ferritic stainless steel unlipped channels with fastened flanges under end-two-flange loading condition. Journal of constructional steel research, 152, 12-28.

[17] Eurocode 3: Design of steel structures—part 1.4 (EN 1993-1-4). General Rules—Supplementary Rules for Stainless Steels, European Committee for Standardization (CEN), Brussel (2006)

[18] Ishqy, M. F. M., Wanniarachchi, S., Poologanathan, K., Gunalan, S., Gatheeshgar, P., Suntharalingam, T., & Navaratnam, S. (2021, June). Shear behaviour of cold-formed stainless-steel beams with web openings: Numerical studies. In Structures (Vol. 31, pp. 127-144). Elsevier.

[19] Moen, C. D., & Schafer, B. W. (2009). Elastic buckling of cold-formed steel columns and beams with holes. Engineering Structures, 31(12), 2812-2824.

[20] Moen, C. D., Schudlich, A., & von der Heyden, A. (2013). Experiments on cold-formed steel C-section joists with unstiffened web holes. Journal of Structural Engineering, 139(5), 695-704

[21] Zhao, J., Sun, K., Yu, C., & Wang, J. (2019). Tests and direct strength design on cold-formed steel channel beams with web holes. Engineering Structures, 184, 434-446.

[22] Yu, N. T., Kim, B., Yuan, W. B., Li, L. Y., & Yu, F. (2019). An analytical solution of distortional buckling resistance of cold-formed steel channel-section beams with web openings. Thin-Walled Structures, 135, 446-452.

[23] Yu, N. T., Kim, B., Li, L. Y., Hong, W. J., & Yuan, W. B. (2020). Distortional buckling of perforated cold-formed steel beams subject to uniformly distributed transverse loads. Thin-Walled Structures, 148, 106569.

[24] Thirunavukkarasu, K., Kanthasamy, E., Poologanathan, K., Gunalan, S., Gatheeshgar, P., Tsavdaridis, K. D., & Corradi, M. (2023). Flexural behaviour and design rules for SupaCee sections with web openings. Journal of Building Engineering, 63, 105539.

[25] Degtyareva, N., Gatheeshgar, P., Poologanathan, K., Gunalan, S., Shyha, I., & McIntosh, A. (2020). Local buckling strength and design of cold-formed steel beams with slotted perforations. Thin-Walled Structures, 156, 106951.

[26] Degtyareva, N., Gatheeshgar, P., Poologanathan, K., Gunalan, S., Tsavdaridis, K. D., & Napper, S. (2020). New distortional buckling design rules for slotted perforated cold-formed steel beams. Journal of Constructional Steel Research, 168, 106006.

[27] Chen, B., Roy, K., Fang, Z., Uzzaman, A., Raftery, G., & Lim, J. B. (2021). Moment capacity of back-to-back cold-formed steel channels with edge-stiffened holes, un-stiffened holes, and plain webs. Engineering Structures, 235, 112042.

[28] Yu, C. (2012). Cold-formed steel flexural member with edge stiffened holes: Behaviour, optimization, and design. Journal of Constructional Steel Research, 71, 210-218.

[29] Dai, Y., Roy, K., Fang, Z., Chen, B., Raftery, G. M., & Lim, J. B. (2022). A novel machine learning model to predict the moment capacity of cold-formed steel channel beams with edge-stiffened and un-stiffened web holes. Journal of Building Engineering, 53, 104592.

[30] Chen, B., Roy, K., Fang, Z., Uzzaman, A., Pham, C. H., Raftery, G. M., & Lim, J. B. (2022). Shear capacity of cold-formed steel channels with edge-stiffened web holes, unstiffened web holes, and plain webs. Journal of Structural Engineering, 148(2), 04021268.

[31] Kanthasamy, E., Thirunavukkarasu, K., Poologanathan, K., Gatheeshgar, P., Todhunter, S., Suntharalingam, T., & Ishqy, M. F. M. (2022). Shear behaviour of doubly symmetric rectangular hollow flange beam with circular edge-stiffened openings. Engineering Structures, 250, 113366.

[32] Pham, D. K., Pham, C. H., Pham, S. H., & Hancock, G. J. (2020b). Experimental investigation of high strength cold-formed channel sections in shear with rectangular and slotted web openings. Journal of Constructional Steel Research, 165, 105889.

[33] Pham, D. K., Pham, C. H., & Hancock, G. J. (2020). Parametric study for shear design of cold-formed channels with elongated web openings. Journal of Constructional Steel Research, 172, 106222.

[34] Chen, B., Roy, K., Uzzaman, A., Raftery, G. M., Nash, D., Clifton, G. C., ... & Lim, J. B. (2019). Effects of edge-stiffened web openings on the behaviour of cold-formed steel channel sections under compression. Thin-Walled Structures, 144, 106307.

[35] Chen, B., Roy, K., Uzzaman, A., Raftery, G. M., & Lim, J. B. (2020). Parametric study and simplified design equations for cold-formed steel channels with edge-stiffened holes under axial compression. Journal of Constructional Steel Research, 172, 106161.

[36] Fang, Z., Roy, K., Chen, B., Sham, C. W., Hajirasouliha, I., & Lim, J. B. (2021). Deep learning-based procedure for structural design of cold-formed steel channel sections with edge-stiffened and un-stiffened holes under axial compression. Thin-Walled Structures, 166, 108076.

[37] Sivakumaran, K. S., & Abdel-Rahman, N. (1998). A finite element analysis model for the behaviour of cold-formed steel members. Thin-walled structures, 31(4), 305-324.

[38] Zhao, J., Liu, S., & Chen, B. (2023). Axial strength of slotted perforated cold-formed steel channels under pinned-pinned boundary conditions. Journal of Constructional Steel Research, 200, 107673

[39] Uzzaman, A., Lim, J. B., Nash, D., & Roy, K. (2020). Cold-formed steel channel sections under end-two-flange loading condition: Design for edge-stiffened holes, unstiffened holes and plain webs. Thin-Walled Structures, 147, 106532.

[40] Chen, B., Roy, K., Fang, Z., Uzzaman, A., Chi, Y., & Lim, J. B. (2021). Web crippling capacity of fastened cold-formed steel channels with edge-stiffened web holes, un-stiffened web holes and plain webs under two-flange loading. Thin-Walled Structures, 163, 107666.

[41] ABAQUS Analysis User's Manual-Version 6.14-2, ABAQUS Inc., USA, 2018.

Notation	
a	Diameter of circular web holes;
h	Depth of the flat portion of web;
L	Total length of the CFSS channel section;
n	Number of web holes;
q	Length of edge-stiffener;
s	Web hole spacing;
E	Young's modulus of elasticity;
σ	Engineering stress
σ_u	Ultimate tensile strength
σ_{true}	True stress
ε	Engineering strain
b_f	Overall flange width of section;
b_l	Overall lip width of section;
t	Thickness of the channel section;
CFS	Cold formed steel;
$CFSS$	Cold formed stainless-steel;
M_{EXP}	Moment capacity obtained from experiment;
M_{FEA}	Moment capacity obtained from FEA;
$M_{AS/NZS}$	Moment capacity predicted from the AS/NZS (2018)
$M_{AISI\ \&\ AS/NZS}$	Moment capacity predicted from the AISI & AS/NZ
M_{DSM}	Moment capacity predicted from direct strength method
$M_{Proposed}$	Moment capacity obtained from proposed reduction factor equation
M_l	Moment capacity for local buckling

M_{be}	Moment capacity for lateral-torsional buckling
M_y	Member yield moment
M_{ynet}	Member yield moment for net section
M_{crl}	Critical local buckling capacity
M_{crd}	Critical distortional buckling capacity
M_{crlg}	Critical local buckling moment for gross section
M_{crdg}	Critical distortional buckling moment for the gross section
a/h	Ration of hole depth to web depth
COV	Coefficient of variation;
d	Overall web depth of section;
DSM	Direct strength method;
FEA	Finite element analysis;
f_{ol}	Elastic local buckling stress;
f_{od}	Elastic distortional stress;
f_y	Yield stress
f_u	Ultimate stress

Appendix A

Phyton scripting to develop FEA models:

```
from abaqus import *
from abaqusConstants import *
from part import *
from material import *
from section import *
from assembly import *
from step import *
from interaction import *
from load import *
from mesh import *
from optimization import *
from job import *
from sketch import *
from visualization import *
from connectorBehavior import *
session.journalOptions.setValues(replayGeometry=COORDINATE, recoverGeometry=COORDINATE)
#Geometric Detals of the Channel Section
L=4000              # Length of the Channel
O=150           # First Offset of the lenght of partion
SL=100              # Weidth of the support Block
d=240               # Depth of the Channel Section
b=45                # Weidth of the Channel Section
l=15                # Lip of the Channel Section
r= 3                # Corner radius of the Channel
Fy= 205.62          # Yeild stress of the channel
ey= 0
Fu= 597             # Ulitimate stress of the channel
eu= 0.2796
E= 200000           # Young's Modulus of the channel
v= 0.3              # Void ratio
Den= 7.86E-06     # Density of the channel
Ec= 200000          # Young's Modulus of the channel corner
Er= 200000          # Young's Modulus of the rigid portion
Ehrs= 200000        # Young's Modulus of the solid block
Fyhrs= 500          # Yeild stress of the HRS
M=10                # Mesh of the Channel
Mp=10
dq=d-l
dq2=d-2*l
le=((L-2*O-4*SL)/3)
S=50                # Horizontal spacing
D=0.5*d          # Diameter of the hole
N=5                 # Number of hole
Z=5                 # Edge stiffen if needed
se=7                # Shell Excrude for edgestiffen
sr=3                #           corner radius of edge siffener
# Create a new model
```

```
myModel = mdb.Model(name='CFSSC240EH5')
# Create a new part
myPart = myModel.Part(name='Channel', dimensionality=THREE_D, type=DEFORMABLE_BODY)
# Create a 2D sketch for the base
mySketch = myModel.ConstrainedSketch(name='__profile__', sheetSize=500.0)
# Draw lines in the sketch
mySketch.Line(point1=(0.0, 0.0), point2=(0.0, -l))
mySketch.Line(point1=(0.0, -l), point2=(-b, -l))
mySketch.Line(point1=(-b, -l), point2=(-b, dq))
mySketch.Line(point1=(-b, dq), point2=(0.0, dq))
mySketch.Line(point1=(0.0, dq), point2=(0.0, dq2))
# Apply fillets to the corners ****/////// Correction required on order
mySketch.FilletByRadius(curve1=mySketch.geometry[4], curve2=mySketch.geometry[5], nearPoint1=(0, -(l-r)),
nearPoint2=(-r, -l), radius=r)
mySketch.FilletByRadius(curve1=mySketch.geometry[5], curve2=mySketch.geometry[6], nearPoint1=(-(b-r), -r),
nearPoint2=(-b, -(l-r)), radius=r)
mySketch.FilletByRadius(curve1=mySketch.geometry[4], curve2=mySketch.geometry[3], nearPoint1=(-b, (d-r-l)),
nearPoint2=(-(b-r), (d-l)), radius=r)
mySketch.FilletByRadius(curve1=mySketch.geometry[2], curve2=mySketch.geometry[3], nearPoint1=(-r, (d-l)),
nearPoint2=(0, (d-l-r)), radius=r)
# Create a part based on the sketch and extrude
myPart.BaseShellExtrude(sketch=mySketch, depth=L)
# Delete the sketch after creating the 3D part
mdb.models['CFSSC240EH5'].parts['Channel'].DatumPlaneByPrincipalPlane(offset=O,
   principalPlane=XYPLANE)
mdb.models['CFSSC240EH5'].parts['Channel'].DatumPlaneByPrincipalPlane(offset=SL+O,
   principalPlane=XYPLANE)
mdb.models['CFSSC240EH5'].parts['Channel'].DatumPlaneByPrincipalPlane(offset=le+SL+O,
  principalPlane=XYPLANE)
mdb.models['CFSSC240EH5'].parts['Channel'].DatumPlaneByPrincipalPlane(offset=le+2*SL+O,
   principalPlane=XYPLANE)
mdb.models['CFSSC240EH5'].parts['Channel'].DatumPlaneByPrincipalPlane(offset=2*le+2*SL+O,
   principalPlane=XYPLANE)
mdb.models['CFSSC240EH5'].parts['Channel'].DatumPlaneByPrincipalPlane(offset=2*le+3*SL+O,
   principalPlane=XYPLANE)
mdb.models['CFSSC240EH5'].parts['Channel'].DatumPlaneByPrincipalPlane(offset=3*le+3*SL+O,
   principalPlane=XYPLANE)
mdb.models['CFSSC240EH5'].parts['Channel'].DatumPlaneByPrincipalPlane(offset=3*le+4*SL+O,
   principalPlane=XYPLANE)
mdb.models['CFSSC240EH5'].parts['Channel'].PartitionFaceByDatumPlane(datumPlane=
   mdb.models['CFSSC240EH5'].parts['Channel'].datums[2], faces=
   mdb.models['CFSSC240EH5'].parts['Channel'].faces.findAt(((-b,(d/2),O), )))
mdb.models['CFSSC240EH5'].parts['Channel'].PartitionFaceByDatumPlane(datumPlane=
   mdb.models['CFSSC240EH5'].parts['Channel'].datums[3], faces=
   mdb.models['CFSSC240EH5'].parts['Channel'].faces.findAt(((-b, (d/2), SL+O), )))
mdb.models['CFSSC240EH5'].parts['Channel'].PartitionFaceByDatumPlane(datumPlane=
   mdb.models['CFSSC240EH5'].parts['Channel'].datums[4], faces=
   mdb.models['CFSSC240EH5'].parts['Channel'].faces.findAt(((-b, (d/2), le+SL+O), )))
mdb.models['CFSSC240EH5'].parts['Channel'].PartitionFaceByDatumPlane(datumPlane=
   mdb.models['CFSSC240EH5'].parts['Channel'].datums[5], faces=
   mdb.models['CFSSC240EH5'].parts['Channel'].faces.findAt(((-b, (d/2), le+2*SL+O), )))
mdb.models['CFSSC240EH5'].parts['Channel'].PartitionFaceByDatumPlane(datumPlane=
```

```
    mdb.models['CFSSC240EH5'].parts['Channel'].datums[6], faces=
    mdb.models['CFSSC240EH5'].parts['Channel'].faces.findAt(((-b, (d/2), 2*le+2*SL+O), )))
mdb.models['CFSSC240EH5'].parts['Channel'].PartitionFaceByDatumPlane(datumPlane=
    mdb.models['CFSSC240EH5'].parts['Channel'].datums[7], faces=
    mdb.models['CFSSC240EH5'].parts['Channel'].faces.findAt(((-b, (d/2), 2*le+3*SL+O), )))
mdb.models['CFSSC240EH5'].parts['Channel'].PartitionFaceByDatumPlane(datumPlane=
    mdb.models['CFSSC240EH5'].parts['Channel'].datums[8], faces=
    mdb.models['CFSSC240EH5'].parts['Channel'].faces.findAt(((-b, (d/2), 3*le+3*SL+O), )))
mdb.models['CFSSC240EH5'].parts['Channel'].PartitionFaceByDatumPlane(datumPlane=
    mdb.models['CFSSC240EH5'].parts['Channel'].datums[9], faces=
    mdb.models['CFSSC240EH5'].parts['Channel'].faces.findAt(((-b, (d/2), 3*le+4*SL+O), )))
#Make the cicular hole
if N == 5:
    mdb.models['CFSSC240EH5'].ConstrainedSketch(gridSpacing=128.4, name='__profile__',
        sheetSize=5136.27, transform=
        mdb.models['CFSSC240EH5'].parts['Channel'].MakeSketchTransform(
        sketchPlane=mdb.models['CFSSC240EH5'].parts['Channel'].faces.findAt((-b, 1, L/2), (1.0, 0.0, 0.0)),
sketchPlaneSide=SIDE1,
        sketchUpEdge=mdb.models['CFSSC240EH5'].parts['Channel'].edges.findAt((-b, (d/2-l), (O+2*SL+le)), ),
sketchOrientation=RIGHT, origin=(-b, (d/2-l), L/2)))
mdb.models['CFSSC240EH5'].parts['Channel'].projectReferencesOntoSketch(filter=
        COPLANAR_EDGES, sketch=mdb.models['CFSSC240EH5'].sketches['__profile__'])
mdb.models['CFSSC240EH5'].sketches['__profile__'].CircleByCenterPerimeter(center=(0.0, 0.0), point1=(D/2, 0.0))
mdb.models['CFSSC240EH5'].sketches['__profile__'].CircleByCenterPerimeter(center=((S+D), 0.0),
point1=((S+1.5*D), 0.0))
mdb.models['CFSSC240EH5'].sketches['__profile__'].CircleByCenterPerimeter(center=((2*S+2*D), 0.0),
point1=((2*S+2.5*D), 0.0))
mdb.models['CFSSC240EH5'].sketches['__profile__'].CircleByCenterPerimeter(center=(-(S+D), 0.0), point1=(-
(S+1.5*D), 0.0))    mdb.models['CFSSC240EH5'].sketches['__profile__'].CircleByCenterPerimeter(center=(-
(2*S+2*D), 0.0), point1=(-(2*S+2.5*D), 0.0))
mdb.models['CFSSC240EH5'].parts['Channel'].CutExtrude(flipExtrudeDirection=ON, sketch=
        mdb.models['CFSSC240EH5'].sketches['__profile__'], sketchOrientation=RIGHT,
        sketchPlane=mdb.models['CFSSC240EH5'].parts['Channel'].faces.findAt((-b, 1, L/2), (1.0, 0.0, 0.0)),
sketchPlaneSide=SIDE1, sketchUpEdge=
        mdb.models['CFSSC240EH5'].parts['Channel'].edges.findAt((-b, (d/2-l), (O+2*SL+le)), ))
    del mdb.models['CFSSC240EH5'].sketches['__profile__']
elif N == 3:
    mdb.models['CFSSC240EH5'].ConstrainedSketch(gridSpacing=128.4, name='__profile__',
        sheetSize=5136.27, transform=
        mdb.models['CFSSC240EH5'].parts['Channel'].MakeSketchTransform(
        sketchPlane=mdb.models['CFSSC240EH5'].parts['Channel'].faces.findAt((-b, 1, L/2), (1.0, 0.0, 0.0)),
sketchPlaneSide=SIDE1,
        sketchUpEdge=mdb.models['CFSSC240EH5'].parts['Channel'].edges.findAt((-b, (d/2-l), (O+2*SL+le)), ),
sketchOrientation=RIGHT, origin=(-b, (d/2-l), L/2)))
mdb.models['CFSSC240EH5'].parts['Channel'].projectReferencesOntoSketch(filter=
        COPLANAR_EDGES, sketch=mdb.models['CFSSC240EH5'].sketches['__profile__'])
mdb.models['CFSSC240EH5'].sketches['__profile__'].CircleByCenterPerimeter(center=(0.0, 0.0), point1=(D/2, 0.0))
mdb.models['CFSSC240EH5'].sketches['__profile__'].CircleByCenterPerimeter(center=((S+D), 0.0),
point1=((S+1.5*D), 0.0))    mdb.models['CFSSC240EH5'].sketches['__profile__'].CircleByCenterPerimeter(center=(-
(S+D), 0.0), point1=(-(S+1.5*D), 0.0))
mdb.models['CFSSC240EH5'].parts['Channel'].CutExtrude(flipExtrudeDirection=ON, sketch=
        mdb.models['CFSSC240EH5'].sketches['__profile__'], sketchOrientation=RIGHT,
```

```
        sketchPlane=mdb.models['CFSSC240EH5'].parts['Channel'].faces.findAt((-b, 1, L/2), (1.0, 0.0, 0.0)),
sketchPlaneSide=SIDE1, sketchUpEdge=
        mdb.models['CFSSC240EH5'].parts['Channel'].edges.findAt((-b, (d/2-l), (O+2*SL+le)), ))
    del mdb.models['CFSSC240EH5'].sketches['__profile__']
elif N == 1:
    mdb.models['CFSSC240EH5'].ConstrainedSketch(gridSpacing=128.4, name='__profile__',
        sheetSize=5136.27, transform=
        mdb.models['CFSSC240EH5'].parts['Channel'].MakeSketchTransform(
        sketchPlane=mdb.models['CFSSC240EH5'].parts['Channel'].faces.findAt((-b, 1, L/2), (1.0, 0.0, 0.0)),
sketchPlaneSide=SIDE1,
        sketchUpEdge=mdb.models['CFSSC240EH5'].parts['Channel'].edges.findAt((-b, (d/2-l), (O+2*SL+le)), ),
sketchOrientation=RIGHT, origin=(-b, (d/2-l), L/2)))
mdb.models['CFSSC240EH5'].parts['Channel'].projectReferencesOntoSketch(filter=
        COPLANAR_EDGES, sketch=mdb.models['CFSSC240EH5'].sketches['__profile__'])
    mdb.models['CFSSC240EH5'].sketches['__profile__'].CircleByCenterPerimeter(center=(0.0, 0.0), point1=(D/2, 0.0))
mdb.models['CFSSC240EH5'].parts['Channel'].CutExtrude(flipExtrudeDirection=ON, sketch=
        mdb.models['CFSSC240EH5'].sketches['__profile__'], sketchOrientation=RIGHT,
        sketchPlane=mdb.models['CFSSC240EH5'].parts['Channel'].faces.findAt((-b, 1, L/2), (1.0, 0.0, 0.0)),
sketchPlaneSide=SIDE1, sketchUpEdge=
        mdb.models['CFSSC240EH5'].parts['Channel'].edges.findAt((-b, (d/2-l), (O+2*SL+le)), ))
    del mdb.models['CFSSC240EH5'].sketches['__profile__']
elif N == 2:
    mdb.models['CFSSC240EH5'].ConstrainedSketch(gridSpacing=128.4, name='__profile__',
        sheetSize=5136.27, transform=
        mdb.models['CFSSC240EH5'].parts['Channel'].MakeSketchTransform(
        sketchPlane=mdb.models['CFSSC240EH5'].parts['Channel'].faces.findAt((-b, 2, L/2), (1.0, 0.0, 0.0)),
sketchPlaneSide=SIDE1,
        sketchUpEdge=mdb.models['CFSSC240EH5'].parts['Channel'].edges.findAt((-b, 2, (O+2*SL+le)), ),
sketchOrientation=RIGHT, origin=(-b, (d/2-l), L/2)))
mdb.models['CFSSC240EH5'].parts['Channel'].projectReferencesOntoSketch(filter=
        COPLANAR_EDGES, sketch=mdb.models['CFSSC240EH5'].sketches['__profile__'])
mdb.models['CFSSC240EH5'].sketches['__profile__'].CircleByCenterPerimeter(center=((S+D)/2, 0.0), point1=(S/2,
0.0))    mdb.models['CFSSC240EH5'].sketches['__profile__'].CircleByCenterPerimeter(center=(-(S+D)/2, 0.0),
point1=(-S/2, 0.0))    mdb.models['CFSSC240EH5'].parts['Channel'].CutExtrude(flipExtrudeDirection=OFF, sketch=
        mdb.models['CFSSC240EH5'].sketches['__profile__'], sketchOrientation=RIGHT,
        sketchPlane=mdb.models['CFSSC240EH5'].parts['Channel'].faces.findAt((-b, 2,
        L/2), (1.0, 0.0, 0.0)), sketchPlaneSide=SIDE1, sketchUpEdge=
        mdb.models['CFSSC240EH5'].parts['Channel'].edges.findAt((-b, 2, (O+2*SL+le)), ))
    del mdb.models['CFSSC240EH5'].sketches['__profile__']
elif N == 4:
    mdb.models['CFSSC240EH5'].ConstrainedSketch(gridSpacing=128.4, name='__profile__',
        sheetSize=5136.27, transform=
        mdb.models['CFSSC240EH5'].parts['Channel'].MakeSketchTransform(
        sketchPlane=mdb.models['CFSSC240EH5'].parts['Channel'].faces.findAt((-b, 2, L/2), (1.0, 0.0, 0.0)),
sketchPlaneSide=SIDE1,
        sketchUpEdge=mdb.models['CFSSC240EH5'].parts['Channel'].edges.findAt((-b, 2, (O+2*SL+le)), ),
sketchOrientation=RIGHT, origin=(-b, (d/2-l), L/2)))
mdb.models['CFSSC240EH5'].parts['Channel'].projectReferencesOntoSketch(filter=
        COPLANAR_EDGES, sketch=mdb.models['CFSSC240EH5'].sketches['__profile__'])
    mdb.models['CFSSC240EH5'].sketches['__profile__'].CircleByCenterPerimeter(center=((S+D)/2, 0.0), point1=(S/2,
0.0))    mdb.models['CFSSC240EH5'].sketches['__profile__'].CircleByCenterPerimeter(center=(1.5*(S+D), 0.0),
point1=((1.5*S+2*D), 0.0))
```

```
mdb.models['CFSSC240EH5'].sketches['__profile__'].CircleByCenterPerimeter(center=(-(S+D)/2, 0.0), point1=(-S/2,
0.0))    mdb.models['CFSSC240EH5'].sketches['__profile__'].CircleByCenterPerimeter(center=(-1.5*(S+D), 0.0),
point1=(-(1.5*S+2*D), 0.0))    mdb.models['CFSSC240EH5'].parts['Channel'].CutExtrude(flipExtrudeDirection=OFF,
sketch=
        mdb.models['CFSSC240EH5'].sketches['__profile__'], sketchOrientation=RIGHT,
        sketchPlane=mdb.models['CFSSC240EH5'].parts['Channel'].faces.findAt((-b, 2,
        L/2), (1.0, 0.0, 0.0)), sketchPlaneSide=SIDE1, sketchUpEdge=
        mdb.models['CFSSC240EH5'].parts['Channel'].edges.findAt((-b, 2, (O+2*SL+le)), ))
    del mdb.models['CFSSC240EH5'].sketches['__profile__']
else:
    print("Invalid value of N")
# Edge stiffen holes
if Z == 5:
    mdb.models['CFSSC240EH5'].ConstrainedSketch(gridSpacing=56.93, name='__profile__',
        sheetSize=2277.22, transform=
        mdb.models['CFSSC240EH5'].parts['Channel'].MakeSketchTransform(
        sketchPlane=mdb.models['CFSSC240EH5'].parts['Channel'].faces.findAt((-b, 0, L/2), (1.0, 0.0, 0.0)),
sketchPlaneSide=SIDE1,
        sketchUpEdge=mdb.models['CFSSC240EH5'].parts['Channel'].edges.findAt((-b, 0, (O+2*SL+le)), ),
sketchOrientation=RIGHT, origin=(-b, (d/2-l), L/2)))
mdb.models['CFSSC240EH5'].parts['Channel'].projectReferencesOntoSketch(filter=
        COPLANAR_EDGES, sketch=mdb.models['CFSSC240EH5'].sketches['__profile__'])
mdb.models['CFSSC240EH5'].sketches['__profile__'].CircleByCenterPerimeter(center=(0.0, 0.0), point1=(D/2, 0.0))
mdb.models['CFSSC240EH5'].sketches['__profile__'].CircleByCenterPerimeter(center=((S+D), 0.0),
point1=((S+1.5*D), 0.0))
mdb.models['CFSSC240EH5'].sketches['__profile__'].CircleByCenterPerimeter(center=((2*S+2*D), 0.0),
point1=((2*S+2.5*D), 0.0))
mdb.models['CFSSC240EH5'].sketches['__profile__'].CircleByCenterPerimeter(center=(-(S+D), 0.0), point1=(-
(S+1.5*D), 0.0))    mdb.models['CFSSC240EH5'].sketches['__profile__'].CircleByCenterPerimeter(center=(-
(2*S+2*D), 0.0), point1=(-(2*S+2.5*D), 0.0))
    mdb.models['CFSSC240EH5'].parts['Channel'].ShellExtrude(depth=se, flipExtrudeDirection=
        OFF, sketch=mdb.models['CFSSC240EH5'].sketches['__profile__'], sketchOrientation=
        RIGHT, sketchPlane=mdb.models['CFSSC240EH5'].parts['Channel'].faces.findAt((-b, 2, L/2), (1.0, 0.0, 0.0)),
sketchPlaneSide=SIDE1,
        sketchUpEdge=mdb.models['CFSSC240EH5'].parts['Channel'].edges.findAt((-b, 0, (O+2*SL+le)), ))
    del mdb.models['CFSSC240EH5'].sketches['__profile__']
    mdb.models['CFSSC240EH5'].parts['Channel'].Round(
        edgeList=(
            mdb.models['CFSSC240EH5'].parts['Channel'].edges.findAt((-b, (d-2*l-D)/2, L/2), ),
            mdb.models['CFSSC240EH5'].parts['Channel'].edges.findAt((-b, (d-2*l-D)/2, (L/2-S-D)), ),
            mdb.models['CFSSC240EH5'].parts['Channel'].edges.findAt((-b, (d-2*l-D)/2, (L/2-2*S-2*D)), ),
            mdb.models['CFSSC240EH5'].parts['Channel'].edges.findAt((-b, (d-2*l-D)/2, (L/2+S+D)), ),
            mdb.models['CFSSC240EH5'].parts['Channel'].edges.findAt((-b, (d-2*l-D)/2, (L/2+2*S+2*D)), )
        ),
        radius=sr
    )
elif Z == 3:
    mdb.models['CFSSC240EH5'].ConstrainedSketch(gridSpacing=56.93, name='__profile__',
        sheetSize=2277.22, transform=
        mdb.models['CFSSC240EH5'].parts['Channel'].MakeSketchTransform(
        sketchPlane=mdb.models['CFSSC240EH5'].parts['Channel'].faces.findAt((-b, 0, L/2), (1.0, 0.0, 0.0)),
sketchPlaneSide=SIDE1,
```

```
        sketchUpEdge=mdb.models['CFSSC240EH5'].parts['Channel'].edges.findAt((-b, 0, (O+2*SL+le)), ),
sketchOrientation=RIGHT, origin=(-b, (d/2-l), L/2)))
mdb.models['CFSSC240EH5'].parts['Channel'].projectReferencesOntoSketch(filter=
        COPLANAR_EDGES, sketch=mdb.models['CFSSC240EH5'].sketches['__profile__'])
mdb.models['CFSSC240EH5'].sketches['__profile__'].CircleByCenterPerimeter(center=(0.0, 0.0), point1=(D/2, 0.0))
mdb.models['CFSSC240EH5'].sketches['__profile__'].CircleByCenterPerimeter(center=((S+D), 0.0),
point1=((S+1.5*D), 0.0))    mdb.models['CFSSC240EH5'].sketches['__profile__'].CircleByCenterPerimeter(center=(-
(S+D), 0.0), point1=(-(S+1.5*D), 0.0))
    mdb.models['CFSSC240EH5'].parts['Channel'].ShellExtrude(depth=se, flipExtrudeDirection=
        OFF, sketch=mdb.models['CFSSC240EH5'].sketches['__profile__'], sketchOrientation=
        RIGHT, sketchPlane=mdb.models['CFSSC240EH5'].parts['Channel'].faces.findAt((-b, 2, L/2), (1.0, 0.0, 0.0)),
sketchPlaneSide=SIDE1,
        sketchUpEdge=mdb.models['CFSSC240EH5'].parts['Channel'].edges.findAt((-b, 0, (O+2*SL+le)), ))
    del mdb.models['CFSSC240EH5'].sketches['__profile__']
    mdb.models['CFSSC240EH5'].parts['Channel'].Round(
        edgeList=(
            mdb.models['CFSSC240EH5'].parts['Channel'].edges.findAt((-b, (d-2*l-D)/2, L/2), ),
            mdb.models['CFSSC240EH5'].parts['Channel'].edges.findAt((-b, (d-2*l-D)/2, (L/2-S-D)), ),
            mdb.models['CFSSC240EH5'].parts['Channel'].edges.findAt((-b, (d-2*l-D)/2, (L/2+S+D)), ),
        ),
        radius=sr
    )
elif Z == 1:
    mdb.models['CFSSC240EH5'].ConstrainedSketch(gridSpacing=56.93, name='__profile__',
        sheetSize=2277.22, transform=
        mdb.models['CFSSC240EH5'].parts['Channel'].MakeSketchTransform(
        sketchPlane=mdb.models['CFSSC240EH5'].parts['Channel'].faces.findAt((-b, 0, L/2), (1.0, 0.0, 0.0)),
sketchPlaneSide=SIDE1,
        sketchUpEdge=mdb.models['CFSSC240EH5'].parts['Channel'].edges.findAt((-b, 0, (O+2*SL+le)), ),
sketchOrientation=RIGHT, origin=(-b, (d/2-l), L/2)))
    mdb.models['CFSSC240EH5'].parts['Channel'].projectReferencesOntoSketch(filter=
        COPLANAR_EDGES, sketch=mdb.models['CFSSC240EH5'].sketches['__profile__'])
    mdb.models['CFSSC240EH5'].sketches['__profile__'].CircleByCenterPerimeter(center=(0.0, 0.0), point1=(D/2, 0.0))
    mdb.models['CFSSC240EH5'].parts['Channel'].ShellExtrude(depth=se, flipExtrudeDirection=
        OFF, sketch=mdb.models['CFSSC240EH5'].sketches['__profile__'], sketchOrientation=
        RIGHT, sketchPlane=mdb.models['CFSSC240EH5'].parts['Channel'].faces.findAt((-b, 2, L/2), (1.0, 0.0, 0.0)),
sketchPlaneSide=SIDE1,
        sketchUpEdge=mdb.models['CFSSC240EH5'].parts['Channel'].edges.findAt((-b, 0, (O+2*SL+le)), ))
    del mdb.models['CFSSC240EH5'].sketches['__profile__']
    mdb.models['CFSSC240EH5'].parts['Channel'].Round(
        edgeList=(
            mdb.models['CFSSC240EH5'].parts['Channel'].edges.findAt((-b, (d-2*l-D)/2, L/2), ),
        ),
        radius=sr
    )
elif Z == 2:
    mdb.models['CFSSC240EH5'].ConstrainedSketch(gridSpacing=56.93, name='__profile__',
        sheetSize=2277.22, transform=
        mdb.models['CFSSC240EH5'].parts['Channel'].MakeSketchTransform(
        sketchPlane=mdb.models['CFSSC240EH5'].parts['Channel'].faces.findAt((-b, 0, L/2), (1.0, 0.0, 0.0)),
sketchPlaneSide=SIDE1,
```

```
      sketchUpEdge=mdb.models['CFSSC240EH5'].parts['Channel'].edges.findAt((-b, 0, (O+2*SL+le)), ),
sketchOrientation=RIGHT, origin=(-b, (d/2-l), L/2)))
   mdb.models['CFSSC240EH5'].parts['Channel'].projectReferencesOntoSketch(filter=
      COPLANAR_EDGES, sketch=mdb.models['CFSSC240EH5'].sketches['__profile__'])
   mdb.models['CFSSC240EH5'].sketches['__profile__'].CircleByCenterPerimeter(center=((S+D)/2, 0.0), point1=(S/2,
0.0))
   mdb.models['CFSSC240EH5'].sketches['__profile__'].CircleByCenterPerimeter(center=(-(S+D)/2, 0.0), point1=(-
S/2, 0.0))
   mdb.models['CFSSC240EH5'].parts['Channel'].ShellExtrude(depth=se,
      flipExtrudeDirection=OFF, sketch=mdb.models['CFSSC240EH5'].sketches['__profile__'],
      sketchOrientation=RIGHT, sketchPlane=
      mdb.models['CFSSC240EH5'].parts['Channel'].faces.findAt((-b, 0, L/2), (1.0, 0.0, 0.0)), sketchPlaneSide=SIDE1,
sketchUpEdge=
      mdb.models['CFSSC240EH5'].parts['Channel'].edges.findAt((-b, 0, (O+2*SL+le)), ))
   del mdb.models['CFSSC240EH5'].sketches['__profile__']
   mdb.models['CFSSC240EH5'].parts['Channel'].Round(
      edgeList=(
         mdb.models['CFSSC240EH5'].parts['Channel'].edges.findAt((-b, (d-2*l-D)/2, round((L-S-D)/2 + 0.5),)),
         mdb.models['CFSSC240EH5'].parts['Channel'].edges.findAt((-b, (d-2*l-D)/2, round((L+S+D)/2 + 0.5),))),
      radius=sr)
elif Z == 4:
   mdb.models['CFSSC240EH5'].ConstrainedSketch(gridSpacing=56.93, name='__profile__',
      sheetSize=2277.22, transform=
      mdb.models['CFSSC240EH5'].parts['Channel'].MakeSketchTransform(
      sketchPlane=mdb.models['CFSSC240EH5'].parts['Channel'].faces.findAt((-b, 0, L/2), (1.0, 0.0, 0.0)),
sketchPlaneSide=SIDE1,
      sketchUpEdge=mdb.models['CFSSC240EH5'].parts['Channel'].edges.findAt((-b, 0, (O+2*SL+le)), ),
sketchOrientation=RIGHT, origin=(-b, (d/2-l), L/2)))
   mdb.models['CFSSC240EH5'].parts['Channel'].projectReferencesOntoSketch(filter=
      COPLANAR_EDGES, sketch=mdb.models['CFSSC240EH5'].sketches['__profile__'])
mdb.models['CFSSC240EH5'].sketches['__profile__'].CircleByCenterPerimeter(center=((S+D)/2, 0.0), point1=(S/2,
0.0))    mdb.models['CFSSC240EH5'].sketches['__profile__'].CircleByCenterPerimeter(center=(-(S+D)/2, 0.0),
point1=(-S/2, 0.0))
mdb.models['CFSSC240EH5'].sketches['__profile__'].CircleByCenterPerimeter(center=(1.5*(S+D), 0.0),
point1=((1.5*S+2*D), 0.0))
mdb.models['CFSSC240EH5'].sketches['__profile__'].CircleByCenterPerimeter(center=(-1.5*(S+D), 0.0), point1=(-
(1.5*S+2*D), 0.0))
   mdb.models['CFSSC240EH5'].parts['Channel'].ShellExtrude(depth=se,
      flipExtrudeDirection=OFF, sketch=mdb.models['CFSSC240EH5'].sketches['__profile__'],
      sketchOrientation=RIGHT, sketchPlane=
      mdb.models['CFSSC240EH5'].parts['Channel'].faces.findAt((-b, 0, L/2), (1.0, 0.0, 0.0)), sketchPlaneSide=SIDE1,
sketchUpEdge=
      mdb.models['CFSSC240EH5'].parts['Channel'].edges.findAt((-b, 0, (O+2*SL+le)), ))
   del mdb.models['CFSSC240EH5'].sketches['__profile__']
   mdb.models['CFSSC240EH5'].parts['Channel'].Round(
      edgeList=(
         mdb.models['CFSSC240EH5'].parts['Channel'].edges.findAt(((-b, (d-2*l-D)/2, round((L-S-D)/2)),),),
         mdb.models['CFSSC240EH5'].parts['Channel'].edges.findAt(((-b, (d-2*l-D)/2, round((L+S+D)/2)),),),
         mdb.models['CFSSC240EH5'].parts['Channel'].edges.findAt(((-b, (d-2*l-D)/2, round((L/2-1.5*S-1.5*D)),),),),
         mdb.models['CFSSC240EH5'].parts['Channel'].edges.findAt(((-b, (d-2*l-D)/2, round((L/2+1.5*S+1.5*D)),),),)),
      radius=sr)
else:
```

```
    print("Invalid value of Z")
#Creating Sets
mdb.models['CFSSC240EH5'].parts['Channel'].Set(faces=
    mdb.models['CFSSC240EH5'].parts['Channel'].faces.findAt(((-b,
    d/2, 1.0), (1.0, 0.0, 0.0)), ((-b, d/2, (L-1)),
    (1.0, 0.0, 0.0)), ((-b/2, (d-l), L/2), (0.0, -1.0, 0.0)), ((
    -b/2, -l, L/2), (1.0, 0.0, 0.0)), ((0, (d-l-r-1),
    L/2), (0.0, 1.0, 0.0)), ((0.0, -l/2, L/2), (-1.0,
    0.0, 0.0)), ), name='Channel')
mdb.models['CFSSC240EH5'].parts['Channel'].Set(faces=
    mdb.models['CFSSC240EH5'].parts['Channel'].faces.findAt(((-b, 1.0,
    L/2), ), ((-b, (d-2*l-2*r)/2,3*L/4 ), ), ((-b, (d-2*l-2*r),
    L/4), ), ), name='Channel1')
mdb.models['CFSSC240EH5'].parts['Channel'].Set(faces=
    mdb.models['CFSSC240EH5'].parts['Channel'].faces.findAt(((-b, (d/2-l), (O+0.5*SL)), (1.0, 0.0, 0.0)), ((-b, (d/2-l),
(O+le+1.5*SL)), (1.0,
    0.0, 0.0)), ((-b, (d/2-l), (O+2*le+2.5*SL)), (1.0, 0.0, 0.0)), ((-b, (d/2-l), (O+3*le+3.5*SL)), (1.0, 0.0, 0.0)), ),
name='Rigid')
mdb.models['CFSSC240EH5'].parts['Channel'].Set(faces=
    mdb.models['CFSSC240EH5'].parts['Channel'].faces.findAt(((-r+r*0.7071067811865475244, (d-l-
r)+r*(0.7071067811865475244), L/2), )), name='Corner1')
mdb.models['CFSSC240EH5'].parts['Channel'].Set(faces=
    mdb.models['CFSSC240EH5'].parts['Channel'].faces.findAt(((-(b-r)-r*0.70710678118654752440084 4, (d-l-
r)+r*(0.7071067811865475244), L/2), )), name='Corner2')
mdb.models['CFSSC240EH5'].parts['Channel'].Set(faces=
    mdb.models['CFSSC240EH5'].parts['Channel'].faces.findAt(((-r+r*0.70710678118654752440084 4, -(l-r)-
r*(0.7071067811865475244), L/2), )), name='Corner3')
mdb.models['CFSSC240EH5'].parts['Channel'].Set(faces=
    mdb.models['CFSSC240EH5'].parts['Channel'].faces.findAt(((-(b-r)-r*0.70710678118654752440084 4, -(l-r)-
r*(0.7071067811865475244), L/2), )), name='Corner4')
# mdb.models['CFSSC240EH5'].parts['Channel'].Set(faces=
    # mdb.models['CFSSC240EH5'].parts['Channel'].faces.findAt(((-0.025369, 292.389323, 2333.333333), (-0.991544, -
0.129774, 0.0)), ((-62.389325, 294.97463, 2333.333333),
    # (0.129775, -0.991543, 0.0)), ((-64.97463, -22.389326, 2333.333333), (0.991543, 0.129775, 0.0)), ((-2.610674, -
24.97463, 2333.333333), (-0.129775, 0.991543, 0.0)), ), name='Corner')
#Section
mdb.models['CFSSC240EH5'].HomogeneousShellSection(idealization=NO_IDEALIZATION,
    integrationRule=SIMPSON, material='Channel', name='Channel',
    nodalThicknessField='', numIntPts=5, poissonDefinition=DEFAULT,
    preIntegrate=OFF, temperature=GRADIENT, thickness=1.81, thicknessField='',
    thicknessModulus=None, thicknessType=UNIFORM, useDensity=OFF)
mdb.models['CFSSC240EH5'].HomogeneousShellSection(idealization=NO_IDEALIZATION,
    integrationRule=SIMPSON, material='Rigid', name='Rigid',
    nodalThicknessField='', numIntPts=5, poissonDefinition=DEFAULT,
    preIntegrate=OFF, temperature=GRADIENT, thickness=10.0, thicknessField='',
    thicknessModulus=None, thicknessType=UNIFORM, useDensity=OFF)
mdb.models['CFSSC240EH5'].HomogeneousShellSection(idealization=NO_IDEALIZATION,
    integrationRule=SIMPSON, material='Corner', name='Corner',
    nodalThicknessField='', numIntPts=5, poissonDefinition=DEFAULT,
    preIntegrate=OFF, temperature=GRADIENT, thickness=1.81, thicknessField='',
    thicknessModulus=None, thicknessType=UNIFORM, useDensity=OFF)
# Assigning Section
```

```
# mdb.models['CFSSC240EH5'].parts['Channel'].SectionAssignment(offset=0.0,
    # offsetField='', offsetType=MIDDLE_SURFACE, region=
    # mdb.models['CFSSC240EH5'].parts['Channel'].sets['Corner'], sectionName='Corner',
    # thicknessAssignment=FROM_SECTION)
mdb.models['CFSSC240EH5'].parts['Channel'].SectionAssignment(offset=0.0,
    offsetField='', offsetType=MIDDLE_SURFACE, region=
    mdb.models['CFSSC240EH5'].parts['Channel'].sets['Rigid'], sectionName='Rigid',
    thicknessAssignment=FROM_SECTION)
mdb.models['CFSSC240EH5'].parts['Channel'].SectionAssignment(offset=0.0,
    offsetField='', offsetType=MIDDLE_SURFACE, region=
    mdb.models['CFSSC240EH5'].parts['Channel'].sets['Channel'], sectionName=
    'Channel', thicknessAssignment=FROM_SECTION)
mdb.models['CFSSC240EH5'].parts['Channel'].SectionAssignment(offset=0.0, offsetField='',
    offsetType=MIDDLE_SURFACE, region=
    mdb.models['CFSSC240EH5'].parts['Channel'].sets['Channel1'], sectionName='Channel',
    thicknessAssignment=FROM_SECTION)
mdb.models['CFSSC240EH5'].parts['Channel'].Set(faces=
    mdb.models['CFSSC240EH5'].parts['Channel'].faces.findAt(((-b+0.9*se, (d/2-l),
    L/2-D/2), ), ((-b+0.9*se, (d/2-l), (L/2-S-1.5*D)), ), ((-b+0.9*se,
    (d/2-l), (L/2-2*S-2.5*D)), ), ((-b+0.9*se, (d/2-l), (L/2+S+1.5*D)), ), ((
    -b+0.9*se, (d/2-l), (L/2+2*S+2.5*D)), ), ), name='Set-6')
mdb.models['CFSSC240EH5'].parts['Channel'].SectionAssignment(offset=0.0, offsetField='',
    offsetType=MIDDLE_SURFACE, region=
    mdb.models['CFSSC240EH5'].parts['Channel'].sets['Set-6'], sectionName='Channel',
    thicknessAssignment=FROM_SECTION)
mdb.models['CFSSC240EH5'].parts['Channel'].Set(faces=
    mdb.models['CFSSC240EH5'].parts['Channel'].faces.findAt(((-77.80939, 134.100148,
    2164.83079), ), ((-79.937252, 101.241725, 2255.098663), ), ((-79.937252,
    101.241725, 1850.098663), ), ((-79.937252, 101.241725, 1715.098663), ), ((
    -79.937252, 101.241725, 1985.098663), ), ), name='Set-5')
# mdb.models['CFSSC240EH5'].parts['Channel'].SectionAssignment(offset=0.0, offsetField="
    # , offsetType=MIDDLE_SURFACE, region=
    # mdb.models['CFSSC240EH5'].parts['Channel'].sets['Set-5'], sectionName='Corner',
    # thicknessAssignment=FROM_SECTION)
# Support plate
mdb.models['CFSSC240EH5'].ConstrainedSketch(name='__profile__', sheetSize=500.0)
mdb.models['CFSSC240EH5'].sketches['__profile__'].Line(point1=(0.0, 0.0), point2=(0.0, d-2*r))
mdb.models['CFSSC240EH5'].sketches['__profile__'].VerticalConstraint(addUndoState=
    False, entity=mdb.models['CFSSC240EH5'].sketches['__profile__'].geometry[2])
mdb.models['CFSSC240EH5'].Part(dimensionality=THREE_D, name='WSP', type=
    DISCRETE_RIGID_SURFACE)
mdb.models['CFSSC240EH5'].parts['WSP'].BaseShellExtrude(depth=SL, sketch=
    mdb.models['CFSSC240EH5'].sketches['__profile__'])
mdb.models['CFSSC240EH5'].parts['WSP'].ReferencePoint(point=(0.0, ((d-2*r)/2), (SL/2)))
# Assembly
mdb.models['CFSSC240EH5'].rootAssembly.DatumCsysByDefault(CARTESIAN)
mdb.models['CFSSC240EH5'].rootAssembly.Instance(dependent=ON, name='Channel-1',
    part=mdb.models['CFSSC240EH5'].parts['Channel'])
mdb.models['CFSSC240EH5'].rootAssembly.Instance(dependent=ON, name='WSP-1', part=
    mdb.models['CFSSC240EH5'].parts['WSP'])
mdb.models['CFSSC240EH5'].rootAssembly.instances['WSP-1'].translate(vector=(0.0,
    0.0, 0.0))
```

```
mdb.models['CFSSC240EH5'].rootAssembly.Instance(dependent=ON, name='WSP-2', part=
    mdb.models['CFSSC240EH5'].parts['WSP'])
mdb.models['CFSSC240EH5'].rootAssembly.instances['WSP-2'].translate(vector=(
    0.0, 0.0, 0.0))
mdb.models['CFSSC240EH5'].rootAssembly.Instance(dependent=ON, name='WSP-3', part=
    mdb.models['CFSSC240EH5'].parts['WSP'])
mdb.models['CFSSC240EH5'].rootAssembly.instances['WSP-3'].translate(vector=(
    0.0, 0.0, 0.0))
mdb.models['CFSSC240EH5'].rootAssembly.Instance(dependent=ON, name='WSP-4', part=
    mdb.models['CFSSC240EH5'].parts['WSP'])
mdb.models['CFSSC240EH5'].rootAssembly.instances['WSP-4'].translate(vector=(
    0.0, 0.0, 0.0))
mdb.models['CFSSC240EH5'].rootAssembly.translate(instanceList=('WSP-1', ), vector=(
    -b, -(l-r), O))
mdb.models['CFSSC240EH5'].rootAssembly.translate(instanceList=('WSP-2', ), vector=(
    -b, -(l-r), le+SL+O))
mdb.models['CFSSC240EH5'].rootAssembly.translate(instanceList=('WSP-3', ), vector=(
    -b, -(l-r), 2*le+2*SL+O))
mdb.models['CFSSC240EH5'].rootAssembly.translate(instanceList=('WSP-4', ), vector=(
    -b, -(l-r), 3*le+3*SL+O))
# Materials
mdb.models['CFSSC240EH5'].Material(name='Channel')
mdb.models['CFSSC240EH5'].materials['Channel'].Density(table=((Den, ), ))
mdb.models['CFSSC240EH5'].materials['Channel'].Plastic(table=((Fy, ey), (Fu, eu) ))
mdb.models['CFSSC240EH5'].materials['Channel'].Elastic(table=((E, v), ))
mdb.models['CFSSC240EH5'].Material(name='Corner')
mdb.models['CFSSC240EH5'].materials['Corner'].Elastic(table=((Ec, v), ))
mdb.models['CFSSC240EH5'].materials['Corner'].Plastic(table=((Fy, ey), (Fu, eu) ))
mdb.models['CFSSC240EH5'].Material(name='Rigid')
mdb.models['CFSSC240EH5'].materials['Rigid'].Elastic(table=((Er, v),  ))
mdb.models['CFSSC240EH5'].Material(name='HRS')
mdb.models['CFSSC240EH5'].materials['HRS'].Elastic(table=((Ehrs, v), ))
mdb.models['CFSSC240EH5'].materials['HRS'].Plastic(table=((Fyhrs, ey), ))
# Constrain
mdb.models['CFSSC240EH5'].rootAssembly.Surface(name='SL-M', side1Faces=
    mdb.models['CFSSC240EH5'].rootAssembly.instances['WSP-4'].faces.findAt(((-b, d/2, 3*le+3*SL+O), )))
mdb.models['CFSSC240EH5'].rootAssembly.Surface(name='SR-M', side1Faces=
    mdb.models['CFSSC240EH5'].rootAssembly.instances['WSP-1'].faces.findAt(((-b, d/2, O), )))
mdb.models['CFSSC240EH5'].rootAssembly.Surface(name='LL-M', side1Faces=
    mdb.models['CFSSC240EH5'].rootAssembly.instances['WSP-3'].faces.findAt(((-b, d/2, 2*le+2*SL+O), )))
mdb.models['CFSSC240EH5'].rootAssembly.Surface(name='LR-M', side1Faces=
    mdb.models['CFSSC240EH5'].rootAssembly.instances['WSP-2'].faces.findAt(((-b, d/2, le+SL+O), )))
mdb.models['CFSSC240EH5'].rootAssembly.Surface(name='SL-S', side1Faces=
    mdb.models['CFSSC240EH5'].rootAssembly.instances['Channel-1'].faces.findAt(((-b, d/2, 3*le+4*SL+O-SL/2), )))
mdb.models['CFSSC240EH5'].rootAssembly.Surface(name='SR-S', side1Faces=
    mdb.models['CFSSC240EH5'].rootAssembly.instances['Channel-1'].faces.findAt(((-b, d/2, SL+O-SL/2), )))
mdb.models['CFSSC240EH5'].rootAssembly.Surface(name='LL-S', side1Faces=
    mdb.models['CFSSC240EH5'].rootAssembly.instances['Channel-1'].faces.findAt(((-b, d/2, 2*le+3*SL+O-SL/2), )))
mdb.models['CFSSC240EH5'].rootAssembly.Surface(name='LR-S', side1Faces=
    mdb.models['CFSSC240EH5'].rootAssembly.instances['Channel-1'].faces.findAt(((-b, d/2, le+2*SL+O-SL/2), )))
mdb.models['CFSSC240EH5'].Tie(adjust=ON, master=
    mdb.models['CFSSC240EH5'].rootAssembly.surfaces['SL-M'], name='Constraint-1',
```

```
    positionToleranceMethod=COMPUTED, slave=
    mdb.models['CFSSC240EH5'].rootAssembly.surfaces['SL-S'], thickness=ON,
    tieRotations=ON)
mdb.models['CFSSC240EH5'].Tie(adjust=ON, master=
    mdb.models['CFSSC240EH5'].rootAssembly.surfaces['SR-M'], name='Constraint-2',
    positionToleranceMethod=COMPUTED, slave=
    mdb.models['CFSSC240EH5'].rootAssembly.surfaces['SR-S'], thickness=ON,
    tieRotations=ON)
mdb.models['CFSSC240EH5'].Tie(adjust=ON, master=
    mdb.models['CFSSC240EH5'].rootAssembly.surfaces['LL-M'], name='Constraint-3',
    positionToleranceMethod=COMPUTED, slave=
    mdb.models['CFSSC240EH5'].rootAssembly.surfaces['LL-S'], thickness=ON,
    tieRotations=ON)
mdb.models['CFSSC240EH5'].Tie(adjust=ON, master=
    mdb.models['CFSSC240EH5'].rootAssembly.surfaces['LR-M'], name='Constraint-4',
    positionToleranceMethod=COMPUTED, slave=
    mdb.models['CFSSC240EH5'].rootAssembly.surfaces['LR-S'], thickness=ON,
    tieRotations=ON)
# Creating step and BCs
mdb.models['CFSSC240EH5'].ImplicitDynamicsStep(alpha=DEFAULT, amplitude=RAMP,
    application=QUASI_STATIC, initialConditions=OFF, initialInc=0.05, maxInc=
    0.05, maxNumInc=1000000, minInc=8e-15, name='Step-1', nlgeom=ON, nohaf=OFF,
    previous='Initial', timePeriod=8.0)
mdb.models['CFSSC240EH5'].rootAssembly.Set(name='S-L', referencePoints=(
    mdb.models['CFSSC240EH5'].rootAssembly.instances['WSP-4'].referencePoints[2], ))
mdb.models['CFSSC240EH5'].DisplacementBC(amplitude=UNSET, createStepName='Initial',
    distributionType=UNIFORM, fieldName='', localCsys=None, name='SL', region=
    mdb.models['CFSSC240EH5'].rootAssembly.sets['S-L'], u1=SET, u2=SET, u3=UNSET, ur1=
    UNSET, ur2=UNSET, ur3=SET)
mdb.models['CFSSC240EH5'].rootAssembly.Set(name='S-R', referencePoints=(
    mdb.models['CFSSC240EH5'].rootAssembly.instances['WSP-1'].referencePoints[2], ))
mdb.models['CFSSC240EH5'].DisplacementBC(amplitude=UNSET, createStepName='Initial',
    distributionType=UNIFORM, fieldName='', localCsys=None, name='SR', region=
    mdb.models['CFSSC240EH5'].rootAssembly.sets['S-R'], u1=SET, u2=SET, u3=SET, ur1=
    UNSET, ur2=UNSET, ur3=SET)
mdb.models['CFSSC240EH5'].rootAssembly.Set(name='P-L', referencePoints=(
    mdb.models['CFSSC240EH5'].rootAssembly.instances['WSP-3'].referencePoints[2], ))
mdb.models['CFSSC240EH5'].DisplacementBC(amplitude=UNSET, createStepName='Initial',
    distributionType=UNIFORM, fieldName='', localCsys=None, name='PL', region=
    mdb.models['CFSSC240EH5'].rootAssembly.sets['P-L'], u1=SET, u2=UNSET, u3=UNSET, ur1=
    UNSET, ur2=UNSET, ur3=SET)
mdb.models['CFSSC240EH5'].rootAssembly.Set(name='P-R', referencePoints=(
    mdb.models['CFSSC240EH5'].rootAssembly.instances['WSP-2'].referencePoints[2], ))
mdb.models['CFSSC240EH5'].DisplacementBC(amplitude=UNSET, createStepName='Initial',
    distributionType=UNIFORM, fieldName='', localCsys=None, name='PR', region=
    mdb.models['CFSSC240EH5'].rootAssembly.sets['P-R'], u1=SET, u2=UNSET, u3=UNSET, ur1=
    UNSET, ur2=UNSET, ur3=SET)
mdb.models['CFSSC240EH5'].rootAssembly.Set(name='L-L', referencePoints=(
    mdb.models['CFSSC240EH5'].rootAssembly.instances['WSP-3'].referencePoints[2], ))
mdb.models['CFSSC240EH5'].DisplacementBC(amplitude=UNSET, createStepName='Step-1',
    distributionType=UNIFORM, fieldName='', fixed=OFF, localCsys=None, name=
    'LL', region=mdb.models['CFSSC240EH5'].rootAssembly.sets['L-L'], u1=UNSET, u2=-50.0,
```

```
    u3=UNSET, ur1=UNSET, ur2=UNSET, ur3=UNSET)
mdb.models['CFSSC240EH5'].rootAssembly.Set(name='L-R', referencePoints=(
    mdb.models['CFSSC240EH5'].rootAssembly.instances['WSP-2'].referencePoints[2], ))
mdb.models['CFSSC240EH5'].DisplacementBC(amplitude=UNSET, createStepName='Step-1',
    distributionType=UNIFORM, fieldName='', fixed=OFF, localCsys=None, name=
    'LR', region=mdb.models['CFSSC240EH5'].rootAssembly.sets['L-R'], u1=UNSET, u2=-50.0,
    u3=UNSET, ur1=UNSET, ur2=UNSET, ur3=UNSET)
#MESHING
mdb.models['CFSSC240EH5'].parts['Channel'].seedPart(deviationFactor=0.1,
    minSizeFactor=0.1, size=M)
if d == 200:
    mdb.models['CFSSC240EH5'].parts['Channel'].Set(faces=
        mdb.models['CFSSC240EH5'].parts['Channel'].faces.findAt(
            ((-0.02537, 182.389328, 2666.666667), ),
            ((-62.389325, 184.97463, 2666.666667), ),
            ((-64.97463, -12.389326, 2666.666667), ),
            ((-2.610674, -14.97463, 2666.666667), )),
        name='Corner')
    mdb.models['CFSSC240EH5'].parts['Channel'].deleteMesh(regions=
        mdb.models['CFSSC240EH5'].parts['Channel'].faces.findAt(
            ((-65.0, 45.401398, 2480.87321), ),
            ((-65.0, 117.333333, 3816.666667), ),
            ((-65.0, 117.333333, 3383.333333), ),
            ((-65.0, 117.333333, 2616.666667), ),
            ((-65.0, 117.333333, 1416.666667), ),
            ((-65.0, 117.333333, 983.333333), ),
            ((-65.0, 117.333333, 216.666667), ),
            ((-65.0, 117.333333, 100.0), ),
            ((0.0, 174.0, 2666.666667), ),
            ((-0.02537, 182.389328, 2666.666667), ),
            ((-22.666667, 185.0, 2666.666667), ),
            ((-62.389325, 184.97463, 2666.666667), ),
            ((-65.0, 52.666667, 3900.0), ),
            ((-64.97463, -12.389326, 2666.666667), ),
            ((-42.333333, -15.0, 2666.666667), ),
            ((-2.610674, -14.97463, 2666.666667), ),
            ((0.0, -8.0, 2666.666667), )),
        )
mdb.models['CFSSC240EH5'].parts['Channel'].setMeshControls(algorithm=MEDIAL_AXIS,
        elemShape=QUAD, regions=
        mdb.models['CFSSC240EH5'].parts['Channel'].faces.findAt(
            ((-65.0, 45.401398, 2480.87321), ),
            ((-65.0, 117.333333, 3816.666667), ),
            ((-65.0, 117.333333, 3383.333333), ),
            ((-65.0, 117.333333, 2616.666667), ),
            ((-65.0, 117.333333, 1416.666667), ),
            ((-65.0, 117.333333, 983.333333), ),
            ((-65.0, 117.333333, 216.666667), ),
            ((-65.0, 117.333333, 100.0), ),
            ((0.0, 174.0, 2666.666667), ),
            ((-0.02537, 182.389328, 2666.666667), ),
            ((-22.666667, 185.0, 2666.666667), ),
```

```
        ((-62.389325, 184.97463, 2666.666667), ),
        ((-65.0, 52.666667, 3900.0), ),
        ((-64.97463, -12.389326, 2666.666667), ),
        ((-42.333333, -15.0, 2666.666667), ),
        ((-2.610674, -14.97463, 2666.666667), ),
        ((0.0, -8.0, 2666.666667), )),
      )
mdb.models['CFSSC240EH5'].parts['Channel'].seedEdgeByNumber(constraint=FINER,
      edges=mdb.models['CFSSC240EH5'].parts['Channel'].edges.findAt(
        ((-0.228361, 183.14805, 4000.0), ),
        ((-63.14805, 184.771639, 4000.0), ),
        ((-64.771639, -13.14805, 4000.0), ),
        ((-1.85195, -14.771639, 4000.0), )),
      number=9)
elif d == 300:
   mdb.models['CFSSC240EH5'].parts['Channel'].Set(faces=
      mdb.models['CFSSC240EH5'].parts['Channel'].faces.findAt(
        ((-0.025369, 277.389323, 2666.666667), ),
        ((-77.389325, 279.97463, 2666.666667), ),
        ((-79.97463, -17.389326, 2666.666667), ),
        ((-2.610674, -19.97463, 2666.666667), )),
      name='Corner')
   mdb.models['CFSSC240EH5'].parts['Channel'].deleteMesh(regions=
      mdb.models['CFSSC240EH5'].parts['Channel'].faces.findAt(
        ((-80.0, 59.204196, 2475.953125), ),
        ((-80.0, 179.0, 3816.666667), ),
        ((-80.0, 179.0, 3383.333333), ),
        ((-80.0, 179.0, 2616.666667), ),
        ((-80.0, 179.0, 1416.666667), ),
        ((-80.0, 179.0, 983.333333), ),
        ((-80.0, 179.0, 216.666667), ),
        ((-80.0, 179.0, 100.0), ),
        ((0.0, 265.666667, 2666.666667), ),
        ((-0.025369, 277.389323, 2666.666667), ),
        ((-27.666667, 280.0, 2666.666667), ),
        ((-77.389325, 279.97463, 2666.666667), ),
        ((-80.0, 81.0, 3900.0), ),
        ((-79.97463, -17.389326, 2666.666667), ),
        ((-52.333333, -20.0, 2666.666667), ),
        ((-2.610674, -19.97463, 2666.666667), ),
        ((0.0, -11.333333, 2666.666667), )),
      )    mdb.models['CFSSC240EH5'].parts['Channel'].setMeshControls(algorithm=MEDIAL_AXIS,
      elemShape=QUAD, regions=
      mdb.models['CFSSC240EH5'].parts['Channel'].faces.findAt(
        ((-80.0, 59.204196, 2475.953125), ),
        ((-80.0, 179.0, 3816.666667), ),
        ((-80.0, 179.0, 3383.333333), ),
        ((-80.0, 179.0, 2616.666667), ),
        ((-80.0, 179.0, 1416.666667), ),
        ((-80.0, 179.0, 983.333333), ),
        ((-80.0, 179.0, 216.666667), ),
        ((-80.0, 179.0, 100.0), ),
```

```
            ((0.0, 265.666667, 2666.666667), ),
            ((-0.025369, 277.389323, 2666.666667), ),
            ((-27.666667, 280.0, 2666.666667), ),
            ((-77.389325, 279.97463, 2666.666667), ),
            ((-80.0, 81.0, 3900.0), ),
            ((-79.97463, -17.389326, 2666.666667), ),
            ((-52.333333, -20.0, 2666.666667), ),
            ((-2.610674, -19.97463, 2666.666667), ),
            ((0.0, -11.333333, 2666.666667), )),
        )
mdb.models['CFSSC240EH5'].parts['Channel'].seedEdgeByNumber(constraint=FINER,
        edges=mdb.models['CFSSC240EH5'].parts['Channel'].edges.findAt(
            ((-0.228361, 278.14805, 4000.0), ),
            ((-78.14805, 279.771639, 4000.0), ),
            ((-79.771639, -18.14805, 4000.0), ),
            ((-1.85195, -19.771639, 4000.0), )),
        number=9)
else:
    print("Invalid value of d")
mdb.models['CFSSC240EH5'].parts['Channel'].seedEdgeByNumber(constraint=FINER,
    edges=mdb.models['CFSSC240EH5'].parts['Channel'].edges.findAt(((-b, (d/2-l+D/2),
    (L/2+S/2+D/2)), ), ((-b, (d/2-l-D/2), (L/2-S/2-D/2)), ), ((-b, (d/2-l+D/2), (L/2+1.5*S+1.5*D)), ), ((-b, (d/2-l-D/2),
    (L/2-1.5*S-1.5*D)), ), ), number=50)
mdb.models['CFSSC240EH5'].parts['Channel'].deleteSets(setNames=('Set-5', 'Set-6'))
mdb.models['CFSSC240EH5'].parts['Channel'].regenerate()
mdb.models['CFSSC240EH5'].parts['Channel'].generateMesh()
mdb.models['CFSSC240EH5'].parts['WSP'].seedPart(deviationFactor=0.1, minSizeFactor=
    0.1, size=Mp)
mdb.models['CFSSC240EH5'].parts['WSP'].generateMesh()
#JOB
mdb.models['CFSSC240EH5'].rootAssembly.regenerate()
mdb.Job(atTime=None, contactPrint=OFF, description='', echoPrint=OFF,
    explicitPrecision=SINGLE, getMemoryFromAnalysis=True, historyPrint=OFF,
    memory=90, memoryUnits=PERCENTAGE, model='CFSSC240EH5', modelPrint=OFF,
    multiprocessingMode=DEFAULT, name='CFSSC240EH5', nodalOutputPrecision=SINGLE,
    numCpus=8, numDomains=8, numGPUs=0, queue=None, resultsFormat=ODB, scratch=
    '', type=ANALYSIS, userSubroutine='', waitHours=0, waitMinutes=0)
mdb.models['CFSSC240EH5'].parts['Channel'].regenerate()
# Generating input files
mdb.jobs['CFSSC240EH5'].writeInput(consistencyChecking=OFF)
```